Metal Organic Frameworks for Gas-phase Capacitive Sensing

Sachdeva, Sumit

DOI
10.4233/uuid:5ada7892-3836-440e-ac58-451a45524ae0

Publication date
2017

Document Version
Final published version

Citation (APA)
Sachdeva, S. (2017). *Metal Organic Frameworks for Gas-phase Capacitive Sensing*. [Dissertation (TU Delft), Delft University of Technology]. https://doi.org/10.4233/uuid:5ada7892-3836-440e-ac58-451a45524ae0

Metal Organic Frameworks for Gas-phase Capacitive Sensing

Sumit Sachdeva

Metal Organic Frameworks for Gas-phase Capacitive Sensing

Proefschrift

ter verkrijging van de graad van doctor
aan de Technische Universiteit Delft,
op gezag van de Rector Magnificus Prof. Ir. K. Ch. A. M. Luyben,
voorzitter van het College voor Promoties,
in het openbaar te verdedigen op

maandag 27 maart 2017 om 15:00 uur

door

Sumit SACHDEVA
Master of Science in Biochemical Engineering
at Delft University of Technology
geboren te New Delhi, India

This dissertation has been approved by the

promotors: Prof. dr. E.J.R. Sudhölter and Prof. dr. J. Gascon

copromotor: Dr.ir. L.C.P.M. de Smet

Composition of the doctoral committee:

Rector Magnificus	Chairperson
Prof. dr. E.J.R. Sudhölter	Delft University of Technology, promotor
Prof. dr. J. Gascon	Delft University of Technology, promotor
Dr.ir. L.C.P.M. de Smet	Wageningen University & Research, copromotor

Independent members:

Prof. dr. B. Dam	Delft University of Technology
Prof. dr. U. Staufer	Delft University of Technology
Prof. dr. R. Ameloot	KU Leuven, Belgium
Dr. F. Widdershoven	NXP Semiconductors
Prof. dr. F. Kapteijn	Delft University of Technology (reserve)

This research work was financially supported by NanoNextNL, a micro and nanotechnology innovation consortium of the Government of the Netherlands and 130 partners from academia and industry. More information on www.nanonextnl.nl.

Printed by: Ridderprint BV

ISBN 978-94-6186-797-1

An electronic version of this dissertation is available at http://repository.tudelft.nl/.

Table of Contents

Chapter 1

Introduction

1.1. Chemical Sensing

Chemical sensors play an important role in industry for various applications such as detection of toxic gases, process and quality control, medical diagnostics and environmental monitoring[1-2]. In contrast to physical sensors, which focus on the detection of physical parameters such as temperature and pressure, chemical sensors are made for the (often) quantitative detection of specific molecular or ionic analytes. Most of the existing chemical detection techniques are expensive, bulky and have a high energy consumption[1, 3]. The advancements in nanotechnology and the concomitant miniaturization make the fabrication of low energy consuming sensor devices possible at low cost[1-2]. The basic principle of a chemical sensing process is shown in Figure 1.

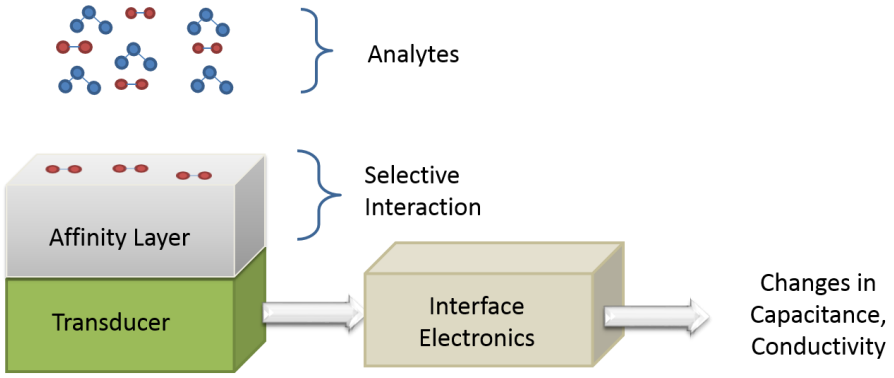

Figure 1. *Schematic representation of the chemical sensing principle. Selective interaction of the analytes with the affinity layer present on the sensor device are transduced and monitored as changes in parameters such as capacitance, mass, conductivity.*

A sensor device consists of a transducer platform connected with an affinity layer which interacts selectively and sensitively to certain analytes in the external environment. This affinity interaction results in changes in the physical properties of the affinity layer. The transducer platform is able to convert these changes into measurable parameters, including the refractive index, conductivity, capacitance, mass, stress, and temperature. The output

signal of the transducer can then be amplified by the underlying electronics. Besides electrical or optical output signals, also acoustic, thermal or mechanical signals are possible[2, 4].

With the low cost and ease of mass fabrication in conjunction with semiconductor technologies, chemical sensors with an electrical output signal have gained a great deal of attention[3]. Most of the commercially available chemical sensor devices utilize metal oxides as the affinity layer, because of their high sensitivity for a range of analytes[5-7]. Usually SnO_2, TiO_2, ZnO, CuO, In_2O_3, WO_3 are used as the metal oxide layer in these chemiresistive devices[8]. However, there exist still challenges to improve selectivity, to reduce cross-sensitivity and to reduce the operation temperature of such chemical sensors[5, 9]. Even though novel and promising approaches such as temperature modulation[9], application of metal doping[10] and pattern recognition in case of multi-array chemical sensors[11] have been applied to improve the selectivity of these metal-oxide sensor devices, there is also a challenge to study other materials as affinity layer, making use at room temperature possible.

Of interest for such applications are affinity layers based on polymers[12]. The uptake of certain analytes change the conductance and dielectric properties of the polymer layer. In general, such chemical sensors can function at room temperature and they show a higher sensitivity and lower fabrication cost compared to the metal oxide-bases sensors. However, polymer-based sensors can still be improved regarding selectivity, reversibility and drift[1]. In addition, new functional materials like carbon nanomaterials (carbon nanotubes, graphene)[13-16], mesoporous silica[17], zeolites[18-19] and also Metal-Organic Frameworks[19] (MOFs), are being investigated for their affinity properties in chemical sensors. In this thesis, the use of MOFs as affinity component has been investigated.

1.2. Metal Organic Frameworks as Component in Affinity Layers

MOFs are hybrid materials composed of metal ions coordinatively linked with organic ligands to form highly porous and crystalline frameworks[20-22]. A wide-range of metal ions and organic ligands can be chosen, forming crystalline materials with different structures and functions. Because of their

selective gas adsorption properties these MOFs find application in catalysis[23], gas storage[24], gas separation[25], drug delivery[26] and sensing[27].

The majority of the sensing studies with MOFs made use of the fact that, upon gas adsorption in the porous MOF structure, the luminescence properties are effected[27-28]. Many studies have been reported using such photo-luminescent MOFs for the detection of alcohols, gases or volatile compounds (like for example NH_3, H_2S, N,N-dimethylformamide (DMF), H_2O, CO_2), ionic species and also for explosives[28]. However, most of these studies are done with bulk material, rather than being integrated with transducer devices. For such an integration, it is required to synthesize the MOF affinity layer as a (very) thin film in direct contact with the transducer element. This will be discussed in more detail in the following section.

Next to these luminescence based sensors, also other optical methods such as interferometry and localized surface plasmon resonance have been applied to transduce the change of physical properties of well-known MOFs like CuBTC and ZIF-8[27]. Other transduction techniques such as Quartz Crystal Microbalance (QCM), Surface Acoustic Wave (SAW), Micro-cantilever probe and Kelvin probe have also been applied successfully in MOF-based sensor devices[29-33]. Finally, transduction via electrical impedance, conductance and capacitance of changing physical properties of MOF affinity layers have shown the potential of MOFs for arriving at sensitive and selective chemical sensors[34-35].

1.3. Fabrication of MOF Thin Films

A variety of techniques have been developed to grow thin films of MOFs in a controlled way on substrates such as a metal, metal oxide, alumina, silicon, glass[27, 36-37]. Most commonly used is a technique based on the exposure of the pre-functionalized substrate to a solution containing the ingredients for the desired MOF synthesis at a given temperature[36]. Such a method is, however, limited if harsh reaction conditions are needed in combination with delicate small electrical transducers.

Alternatively, techniques like liquid-phase epitaxial growth of MOFs and Langmuir-Blodgett deposition of MOFs have also been used to grow

preferentially-oriented MOF layers in a layer-by-layer approach[37]. Such layers usually have a thickness in the nanometer range and are very well suited for growth on a variety of substrates. Recent developments in vapor phase deposition to grow ultrathin MOF films are promising for integration with microelectronics[38-39]. Quartz Crystal Microbalance (QCM) and Localized Surface Plasmon Resonance (LSPR) spectroscopic studies on these thin MOF films have clearly demonstrated the sensing capabilities of the MOF affinity layers[40-41].

In order to grow thicker MOF layers on metal substrates in a controlled way, electrochemical synthesis is a well suitable method[42-44]. This method can be adapted to synthesize MOF thin films on metal surfaces by anodic dissolution and cathodic deposition techniques[42-43, 45]. Since electrodeposition techniques are established processes in wet fabrication procedures in the microelectronics industry, such MOF synthesis procedures can easily be integrated with the current processing techniques. Commonly, anodic dissolution is used for the MOF synthesis and deposition utilizing anodes as the metal ion source in combination with the organic ligands present in the electrolyte solution. This process is well suited for Cu-based MOFs, since they nucleate fast, and their deposition can be carried out on a variety of different substrate morphologies, including flat plates and meshes[46-47]. Multiple parameters such as applied current, voltage, temperature, solvent/water ratio, electrolyte type and concentration can be varied to find the optimal conditions for the fabrication of MOF thin films[47-48].

Since most of the synthetic procedures have been developed to synthesize MOFs as bulk material, there is also a need to integrate MOFs with transducer devices post-synthetically. Inspiration is obtained from the use of mixed matrix membranes (MMM) incorporating MOF particles for selective gas separations[49-50]. Such composite membranes can be deposited on transducer devices. Methods such as spin coating, drop casting, inkjet printing, electrospraying, dip coating have been developed for such depositions[12, 51]. Like in gas separations, the composite membranes may show different sensitivity and selectivity properties due to the presence of the polymer which remain to be explored.

1.4. Transducer Devices

The proper choice of the transducer is of importance. The transducer is able to convert the change of physical properties of the affinity layer into an output signal. For electrical read out, Field-Effect Transistors (FETs) and Interdigitated Electrodes (IDEs) are good choices and their low-cost fabrication and ease of integration with the microelectronic fabrication methods offer a significant advantage.

In particular, IDEs are promising. They belong to the class of planar electrodes having often an interdigitated structure of two comb-like electrodes (Figure 2)[52-53]. Such IDEs are simple and can be made at low cost. They are able to detect accurately changes in resistance, capacitance, and impedance[52-55]. IDEs can be easily made on a variety of different inert supports, including glass, quartz, silicon and polymers. This offers a wide flexibility towards subsequent integration with different affinity layers.

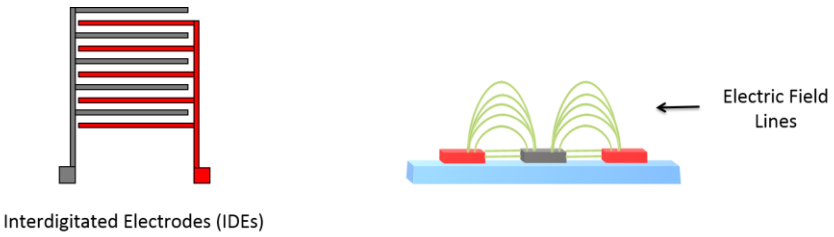

Figure 2. *Schematic representation of the comb-like structure (left, top-view) in Interdigitated Electrodes (IDEs). The side-view (right) of the IDEs illustrates the pattern of the electric field lines (in green) present in the external environment upon the application of a fixed voltage and frequency.*

The planar nature of the comb-shaped microelectrodes in the IDE structure allows for a large area for interaction with the external environment. Depending on the exact dimensions of the IDE structure, the electrical field lines extend in the direction perpendicular to the IDE plane. For optimal performance, the affinity layer should have such a thickness that the electrical field lines are fully embedded. Since the electrical field lines also extend to the IDE substrate, an additional constant parasitic contribution is obtained.

1.5. MOF-IDE Sensor Devices

Integration of the MOF-based affinity layers and IDE transducers leads to chemical sensor devices showing sensitivity and selectivity towards the detection of certain analytes in the external environment as determined by the changing properties of the affinity layer. Typically, the conductance and capacitance will change. Chemical sensors made by the drop casting of MOFs such as CuBDC, ZIF-67, NH_2-MIL-125(Ti), $Cu_3(HITP)_2$, $Ni_3(HITP)_2$ on IDEs have shown the capabilities of such sensor devices[34-35, 56-57]. The sensitivity of these chemical sensors is determined by the partitioning of the analyte to the affinity layer. The higher the affinity, the lower the analyte concentration in the external environment that can be monitored. The lower detection limit is, in addition, determined by the smallest change of electrical properties of the affinity layer, which can be registered by the transducer. This, in turn, is determined by the precise structure and dimensions of the IDE. Selectivity of these chemical sensors is determined by the ratio of partitioning of the different analytes. The larger the difference in partitioning, the higher the selectivity. Both sensitivity and selectivity can be tuned by the choice of MOF in combination with the polymer matrix (if any). The reproducibility of the response to analytes is in part dependent on the reversibility of the partitioning processes.

1.6. Thesis Outline

The main objective of this thesis is to investigate Metal-Organic Frameworks (MOFs) as components of the affinity layer for gas-phase sensing, with special emphasis on the integration with capacitive transduction elements, including Interdigitated Electrodes (IDEs) and the selectivity. The studied methodologies for the device fabrication were the *in-situ* electrochemical synthesis of MOFs on electrode surfaces (Chapters 2 and 3) and the deposition of MOF-containing polymer coatings on the transducer (Chapter 4 and 5).

Chapter 1 describes the basic principle of chemical sensors and the current status of the chemical sensing. It introduces also Metal-Organic Frameworks as the active component in the affinity layer. Different methods for

fabrication of thin MOF (-containing) layers on planar transducers (IDEs) are described. A summary is presented on the current state of MOF-based chemical sensors.

Chapter 2 describes a comparative study of copper-based MOFs (CuBTC and CuTATB) synthesized electrochemically as bulk powder on flat copper surfaces. The surface-grown MOF and the obtained bulk material showed differences in morphology and functional properties for CuTATB (containing the 4,4',4''-s-TriAzine-2,4,6-triyl-TriBenzoic acid organic linker) as confirmed with the structural refinement studies.

Chapter 3 presents a sensing study of methanol and water in the vapor phase using electrochemically grown CuBTC on custom-made copper based IDEs. Response time and reversibility were determined and the absorption behavior was simulated using a Langmuir model. Experimental sensing results and simulations were compared.

Chapter 4 describes a method to utilize NH_2-MIL-53(Al) MOF-Matrimid® polymer composite films as the affinity layer for capacitive sensor devices. The transducer applied was a meander-patterned device. Changes in the electrical properties of the sensing layer towards exposure of methanol vapors were monitored by impedance spectroscopy. The various methanol vapor concentrations were generated in our home-built gas-mixing system. The addition of MOF particles to the polymer showed an enhancement of the overall sensor response compared to the pure Matrimid® polymer.

Chapter 5 describes an in-depth study of NH_2-MIL-53(Al) MOF-Matrimid® polymer composites on IDEs. Different MOF-polymer weight fractions were investigated. The sensor response was studied towards exposure to different

alcohols and water vapors. Cross-sensitivity studies applying water and methanol vapor mixtures were performed to study both kinetic aspects of these sensors as well as their Langmuir adsorption behavior.

References

[1] X. Liu, S. Cheng, H. Liu, S. Hu, D. Zhang, H. Ning, *Sensors* **2012**, *12*, 9635.

[2] K. Cammann, U. Lemke, A. Rohen, J. Sander, H. Wilken, B. Winter, *Angewandte Chemie International Edition in English* **1991**, *30*, 516-539.

[3] S.-W. Chiu, K.-T. Tang, *Sensors* **2013**, *13*, 14214.

[4] J. Janata, *Principles of chemical sensors*, Springer Science & Business Media, **2009**.

[5] D. R. Miller, S. A. Akbar, P. A. Morris, *Sensors and Actuators B: Chemical* **2014**, *204*, 250-272.

[6] E. Comini, C. Baratto, I. Concina, G. Faglia, M. Falasconi, M. Ferroni, V. Galstyan, E. Gobbi, A. Ponzoni, A. Vomiero, D. Zappa, V. Sberveglieri, G. Sberveglieri, *Sensors and Actuators B: Chemical* **2013**, *179*, 3-20.

[7] Y.-F. Sun, S.-B. Liu, F.-L. Meng, J.-Y. Liu, Z. Jin, L.-T. Kong, J.-H. Liu, *Sensors* **2012**, *12*, 2610.

[8] N. Ramgir, N. Datta, M. Kaur, S. Kailasaganapathi, A. K. Debnath, D. K. Aswal, S. K. Gupta, *Colloids and Surfaces A: Physicochemical and Engineering Aspects* **2013**, *439*, 101-116.

[9] R. Gosangi, R. Gutierrez-Osuna, *Sensors and Actuators B: Chemical* **2013**, *185*, 201-210.

[10] G. De, R. Kohn, G. Xomeritakis, C. J. Brinker, *Chemical Communications* **2007**, 1840-1842.

[11] D.-S. Lee, J.-K. Jung, J.-W. Lim, J.-S. Huh, D.-D. Lee, *Sensors and Actuators B: Chemical* **2001**, *77*, 228-236.

[12] H. Bai, G. Shi, *Sensors* **2007**, *7*, 267.

[13] E. Llobet, *Sensors and Actuators B: Chemical* **2013**, *179*, 32-45.

[14] D. Jariwala, V. K. Sangwan, L. J. Lauhon, T. J. Marks, M. C. Hersam, *Chemical Society Reviews* **2013**, *42*, 2824-2860.

[15] S. Basu, P. Bhattacharyya, *Sensors and Actuators B: Chemical* **2012**, *173*, 1-21.

[16] F. R. Baptista, S. A. Belhout, S. Giordani, S. J. Quinn, *Chemical Society Reviews* **2015**, *44*, 4433-4453.

[17] T. Wagner, S. Haffer, C. Weinberger, D. Klaus, M. Tiemann, *Chemical Society Reviews* **2013**, *42*, 4036-4053.

[18] X. Xu, J. Wang, Y. Long, *Sensors* **2006**, *6*, 1751.

[19] D. J. Wales, J. Grand, V. P. Ting, R. D. Burke, K. J. Edler, C. R. Bowen, S. Mintova, A. D. Burrows, *Chemical Society Reviews* **2015**, *44*, 4290-4321.

[20] G. Ferey, *Chemical Society Reviews* **2008**, *37*, 191-214.

[21] A. U. Czaja, N. Trukhan, U. Muller, *Chemical Society Reviews* **2009**, *38*, 1284-1293.

[22] H. Furukawa, K. E. Cordova, M. O'Keeffe, O. M. Yaghi, *Science* **2013**, *341*.

[23] J. Lee, O. K. Farha, J. Roberts, K. A. Scheidt, S. T. Nguyen, J. T. Hupp, *Chemical Society Reviews* **2009**, *38*, 1450-1459.

[24] Y. He, W. Zhou, G. Qian, B. Chen, *Chemical Society Reviews* **2014**, *43*, 5657-5678.

[25] S. Qiu, M. Xue, G. Zhu, *Chemical Society Reviews* **2014**, *43*, 6116-6140.

[26] P. Horcajada, T. Chalati, C. Serre, B. Gillet, C. Sebrie, T. Baati, J. F. Eubank, D. Heurtaux, P. Clayette, C. Kreuz, J.-S. Chang, Y. K. Hwang, V. Marsaud, P.-N. Bories, L. Cynober, S. Gil, G. Ferey, P. Couvreur, R. Gref, *Nat Mater* **2010**, *9*, 172-178.

[27] L. E. Kreno, K. Leong, O. K. Farha, M. Allendorf, R. P. Van Duyne, J. T. Hupp, *Chemical Reviews* **2012**, *112*, 1105-1125.

[28] Z. Hu, B. J. Deibert, J. Li, *Chemical Society Reviews* **2014**, *43*, 5815-5840.

[29] V. Stavila, A. A. Talin, M. D. Allendorf, *Chemical Society Reviews* **2014**, *43*, 5994-6010.

[30] H. Yamagiwa, S. Sato, T. Fukawa, T. Ikehara, R. Maeda, T. Mihara, M. Kimura, *Scientific Reports* **2014**, *4*, 6247.

[31] P. Davydovskaya, R. Pohle, A. Tawil, M. Fleischer, *Sensors and Actuators B: Chemical* **2013**, *187*, 142-146.

[32] I. Stassen, B. Bueken, H. Reinsch, J. F. M. Oudenhoven, D. Wouters, J. Hajek, V. Van Speybroeck, N. Stock, P. M. Vereecken, R. Van Schaijk, D. De Vos, R. Ameloot, *Chemical Science* **2016**, *7*, 5827-5832.

[33] A. Venkatasubramanian, J.-H. Lee, V. Stavila, A. Robinson, M. D. Allendorf, P. J. Hesketh, *Sensors and Actuators B: Chemical* **2012**, *168*, 256-262.

[34] C. Sapsanis, H. Omran, V. Chernikova, O. Shekhah, Y. Belmabkhout, U. Buttner, M. Eddaoudi, K. Salama, *Sensors* **2015**, *15*, 18153.

[35] M. G. Campbell, D. Sheberla, S. F. Liu, T. M. Swager, M. Dincă, *Angewandte Chemie International Edition* **2015**, *54*, 4349-4352.

[36] D. Zacher, O. Shekhah, C. Woll, R. A. Fischer, *Chemical Society Reviews* **2009**, *38*, 1418-1429.

[37] A. Bétard, R. A. Fischer, *Chemical Reviews* **2012**, *112*, 1055-1083.

[38] I. Stassen, M. Styles, G. Grenci, H. V. Gorp, W. Vanderlinden, S. D. Feyter, P. Falcaro, D. D. Vos, P. Vereecken, R. Ameloot, *Nat Mater* **2016**, *15*, 304-310.

[39] I. Stassen, D. De Vos, R. Ameloot, *Chemistry – A European Journal* **2016**, *22*, 14452-14460.

[40] L. Heinke, M. Tu, S. Wannapaiboon, R. A. Fischer, C. Wöll, *Microporous and Mesoporous Materials* **2015**, *216*, 200-215.

[41] D. Bradshaw, A. Garai, J. Huo, *Chemical Society Reviews* **2012**, *41*, 2344-2381.

[42] N. Campagnol, T. R. C. Van Assche, M. Li, L. Stappers, M. Dinca, J. F. M. Denayer, K. Binnemans, D. E. De Vos, J. Fransaer, *Journal of Materials Chemistry A* **2016**, *4*, 3914-3925.

[43] H. Al-Kutubi, J. Gascon, E. J. R. Sudhölter, L. Rassaei, *ChemElectroChem* **2015**, *2*, 462-474.

[44] W.-J. Li, M. Tu, R. Cao, R. A. Fischer, *Journal of Materials Chemistry A* **2016**, *4*, 12356-12369.

[45] M. Li, M. Dincă, *Journal of the American Chemical Society* **2011**, *133*, 12926-12929.

[46] T. R. C. Van Assche, G. Desmet, R. Ameloot, D. E. De Vos, H. Terryn, J. F. M. Denayer, *Microporous and Mesoporous Materials* **2012**, *158*, 209-213.

[47] A. Martinez Joaristi, J. Juan-Alcañiz, P. Serra-Crespo, F. Kapteijn, J. Gascon, *Crystal Growth & Design* **2012**, *12*, 3489-3498.

[48] T. R. C. Van Assche, N. Campagnol, T. Muselle, H. Terryn, J. Fransaer, J. F. M. Denayer, *Microporous and Mesoporous Materials* **2016**, *224*, 302-310.

[49] B. Seoane, J. Coronas, I. Gascon, M. E. Benavides, O. Karvan, J. Caro, F. Kapteijn, J. Gascon, *Chemical Society Reviews* **2015**, *44*, 2421-2454.

[50] G. Dong, H. Li, V. Chen, *Journal of Materials Chemistry A* **2013**, *1*, 4610-4630.

[51] Y. Diao, L. Shaw, Z. Bao, S. C. B. Mannsfeld, *Energy & Environmental Science* **2014**, *7*, 2145-2159.

[52] N. F. Sheppard, R. C. Tucker, C. Wu, *Analytical Chemistry* **1993**, *65*, 1199-1202.

[53] J. Staginus, I. M. Aerts, Z.-y. Chang, G. C. M. Meijer, L. C. P. M. de Smet, E. J. R. Sudhölter, *Sensors and Actuators B: Chemical* **2013**, *184*, 130-142.

[54] J. Yun, G. Kang, Y. Park, H. W. Kim, J.-J. Cha, J.-H. Lee, *Sensors and Actuators B: Chemical* **2016**, *237*, 984-991.

[55] S. H. Hyun, D. K. Park, A. Kang, S. Kim, D. Kim, Y. M. Shin, J.-J. Song, W. S. Yun, *Applied Physics Letters* **2016**, *108*, 093101.

[56] E.-X. Chen, H. Yang, J. Zhang, *Inorganic Chemistry* **2014**, *53*, 5411-5413.

[57] Y. Zhang, Y. Chen, Y. Zhang, H. Cong, B. Fu, S. Wen, S. Ruan, *Journal of Nanoparticle Research* **2013**, *15*, 2014.

Chapter 2

Control of Interpenetration of Copper-based MOFs on Supported Surfaces by Electrochemical Synthesis

This chapter is based on the following publication:

S. Sachdeva, A. Pustovarenko, E. J. R. Sudholter, F. Kapteijn, L. C. P. M. de Smet, J. Gascon, *CrystEngComm* **2016**, *18*, 4018-4022.

Abstract

A study of a copper-based Metal-Organic Framework (MOF) synthesized by an electrochemical route is presented. Morphological and adsorption properties of the MOF synthesized as bulk powder and on supported copper surfaces were investigated. Differences in these properties and structural refinement studies indicate that when 4,4',4''-s-Triazine-2,4,6-triyl-tribenzoic acid (H_3TATB) is used as linker interpenetration can be prevented when the structure is grown on a surface.

2.1. Introduction

Metal-organic Frameworks (MOFs) are porous, crystalline materials comprised of metal ions coordinatively linked with organic ligands[1-3]. The high porosity and structural versatility of these materials have attracted research towards many potential applications, including gas separation[4], gas storage[5], drug delivery[6], catalysis[7] and sensing[8]. Some of these applications require MOFs to be grown as thin films[9] with a maximum pore volume available for selective gas interactions.

Another interesting aspect about MOF chemistry lays in the principle of isoreticular design, which was introduced by Yaghi[10]. Typically, the first step within this concept involves figuring out the reaction conditions that lead to the formation of a particular tecton with corresponding connectivity. Then control over the formation of similar MOFs becomes possible by simply changing the size of the organic linker while keeping the same connectivity[11]. This can further allow systematic control over pore size and functionality of MOFs. Such a powerful approach has however a number of limitations, the most important being the fact that the use of longer organic linkers may lead to network interpenetration, with the corresponding loss in porosity[2, 12-13].

In spite of the importance of interpenetration for the final application opportunities of MOFs, only a few studies have been reported on the control of this phenomenon[13]. The general approach in most cases relies on changing reaction conditions[14], solvent removal[15] or by using a template[16], while, to the best of our knowledge, only one study deals with the control of interpenetration during surface growth[17]. In this case, interpenetration is suppressed by using liquid-phase epitaxy on an organic template, resulting in a controlled layer-by-layer growth preventing interpenetration.

Over the last few decades, several approaches have been developed for the positioning of MOFs on different surfaces[18]. Pioneered by BASF for the continuous production of MOF crystals[19], electrochemical synthesis allows the metal salt-free synthesis of MOFs. The principle relies on supplying the metal ion by anodic dissolution to a synthesis solution of the organic linker in an electrolyte. The production of MOF coatings on electrodes is another attractive feature of electrochemistry[20-23]. In previous years, we, among

others, have demonstrated that it is possible to synthesize high-quality coatings of MOF structures such as HKUST-1 on the surface of Cu electrodes. In short, the high concentration of Cu ions near the surface of the electrode upon application of voltage favors formation of the MOF on the electrode. Recently, we optimized the process in terms of MOF growth over the electrode surface by using a pulsed current for a limited number of cycles[20].

Building on our previous works on electrochemical synthesis of Cu-based MOFs, we report a simple, fast and controlled way of limiting framework interpenetration in a framework isoreticular with the well-known HKUST-1. In order to investigate the interpenetration process, we performed the electrochemical synthesis of Cu paddlewheel MOFs using benzene-1,3,5-tricarboxylic acid (H_3BTC) and 4,4′,4″-s-Triazine-2,4,6-triyl-tribenzoic acid (H_3TATB) as organic linkers (Fig. S1 (page 31)). The MOFs were synthesized under optimized synthesis conditions by an electrochemical route. Hereafter, these MOFs will be referred as CuBTC and CuTATB respectively. CuBTC is a well-characterized MOF[24] and it has been chosen as reference material as there should be no interpenetration due to the small size of the linker.

The syntheses of CuBTC and CuTATB were carried out in an electrochemical cell in a 96% ethanol solution. Conditions were tuned in such a way that all of these MOFs could be synthesized both as bulk powder and as surface-supported films on copper electrodes (see Section 2.2 for experimental details). After synthesis, these materials were filtered and washed with ethanol to remove the excess unreacted linker and electrolyte before being dried at 100°C. In a second step, the electrolyte concentration and the number of current cycles were modified to obtain uniform, crack-free layers on the surface.

2.2. Experimental Details

All chemicals were purchased from Sigma Aldrich as used as received. The electrode used were made from 99.9% pure copper. The electrodes were inserted between 2 PTFE plates, which only allowed a small square opening (6.26 mm × 6.26 mm) to be in contact with the synthesis solution. The potentiostat used was an AUTOLAB PGSTAT302N.

Scanning Electron Microscopy (SEM) images were obtained with a JEOL JSM 6010LA setup. N_2 and CO_2 sorption analysis were carried out in a Micromeritics instrument Tristar II. The samples were pre-treated before measurement by outgassing under vacuum at a temperature of 393 K for 16 hrs.

The powder X-ray diffraction measurements were performed on a Bruker D8-Advance diffractometer operated in Bragg-Brentano geometry, equipped with a Co-Kα source (λ = 1.78897 Å). The diffraction data for MOFs found in bulk were collected over an angle range from 5° to 62° and for MOFs samples obtained on the electrode surface from 2° to 80° with a step width of 0.02° and scan speed of 0.2°/s.

2.1.1. Electrochemical synthesis of Copper MOFs

Synthesis of MOFs as bulk powder

200 mg of linker (H_3BTC or H_3TATB) and 25 mg of electrolyte (MTBS) were dissolved in 8 mL of 96% ethanol. The solution was mixed in a home-built, Teflon electrochemical cell (~10 mL, see literature for details of larger version of this cell[20]) at either room temperature or 70°C for high-temperature synthesis with two copper electrodes spaced 2.4 mm apart. Constant current of 1 mA was applied for 10 h to obtain the material in solution. The material was then filtered and washed with ethanol overnight at 75°C. The material was then filtered again and dried at 100°C for 2 h.

Synthesis of MOFs as surface supported film

100 mg of linker (H_3BTC or H_3TATB) and 25 mg of electrolyte (MTBS) were dissolved in 8 mL of 96% ethanol. The solution was mixed in the electrochemical cell at room temperature with two electrodes, copper mesh as anode and copper electrode as cathode, which were spaced 2.4 mm apart. Cyclic pulses of 2 mA/5 s and 0 mA /5 s (or 1 mA/5s and 0 mA/5s) were applied for 12 cycles (60 s of current). The meshes were washed with ethanol at room temperature overnight and dried at 100°C for 2 h

Optimization procedure for surface growth

3.15 g of H_3BTC and different concentrations of MTBS (155-623 mg, i.e. 0.5-2 mmol) were dissolved in 100 mL of 96% ethanol. The solution was mixed in the electrochemical cell at room temperature with two copper electrodes spaced 3 cm apart with a circular opening of 25 mm in contact with solution (area 4.9 cm^2). Cyclic pulses of 50 mA/5 s and 0 mA/5 s were applied to keep the current density constant with other experiments. Different pulse cycles were applied to obtain the crack-free uniform layer. The meshes were washed with ethanol overnight and dried at 100°C for 2 h.

2.3. Results and Discussion

The crystalline nature of CuBTC and CuTATB was determined by powder X-ray diffraction with cobalt as X-ray source. The diffraction pattern of synthesized CuBTC was similar to patterns simulated from the crystal structure and as reported from the literature[20] (Fig. S2 (page 32)). Known MOF structures built of copper metal centres and H_3TATB as a linker did not show resemblance with the synthesized CuTATB[25-26], but resembled a highly interpenetrated polymeric structure based on copper and 4,4′,4″-Benzene-1,3,5-triyl-tris(benzoic acid) (H_3BTB), reported by Walton et. al[27]. Furthermore, based on this known CuBTB structure, the isostructurality of CuTATB was confirmed by Rietveld refinement showing only slight differences in the unit cell dimensions (Fig. 1, Table S1 (page 34)).

Thus, the CuTATB framework consists of a 2D polymeric network built from copper paddlewheel units, linked in an alternated manner by the two carboxylate groups of the TATB ligand (Fig. 2). One of them is protonated and points out of the 2D polymeric layer, being involved in hydrogen bonding with the parallel-laid network, forming a 3D architecture (Fig. 2c). By using simplified building units for this 3D structure (as illustrated in Fig. S4 (page 35)) shows that the network can be described as a 3,4-connected binodal net of ***sur*** topological type and expressed by a $(6^2.8^2.10^2)(6^2.8)_2$ Schläfli symbol[28]. Furthermore, the network structure of CuTATB consists of four highly interpenetrated simple nets where each net is symmetry-equivalent and related to other by translations [100] and by inversion (Fig. S5 (page 31)). All

the interpenetration nets have the topology of ***sur*** net and the interpenetration type belongs to a rare class IIIa (for details see supporting information)[29].

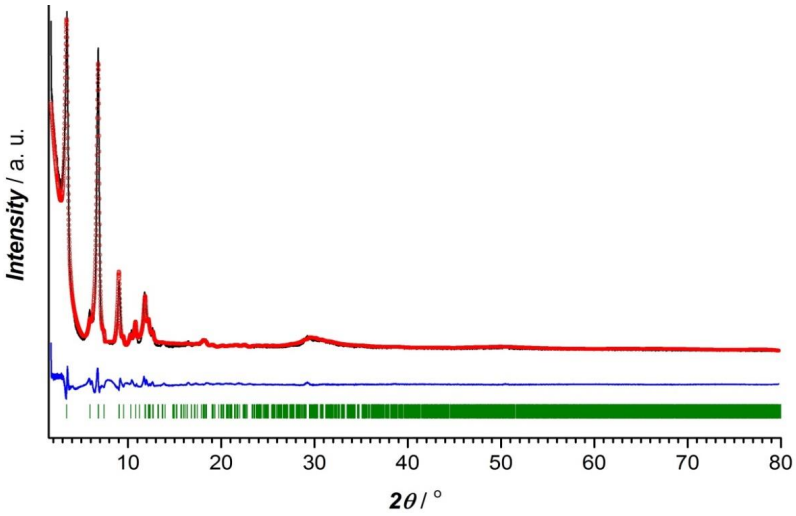

Figure 1. *Rietveld refinement plot for the CuTATB MOF obtained in bulk. The experimental data are presented as black line, the calculated data by red circles and difference as blue line. The Bragg positions of the peaks are represented as green sticks.*

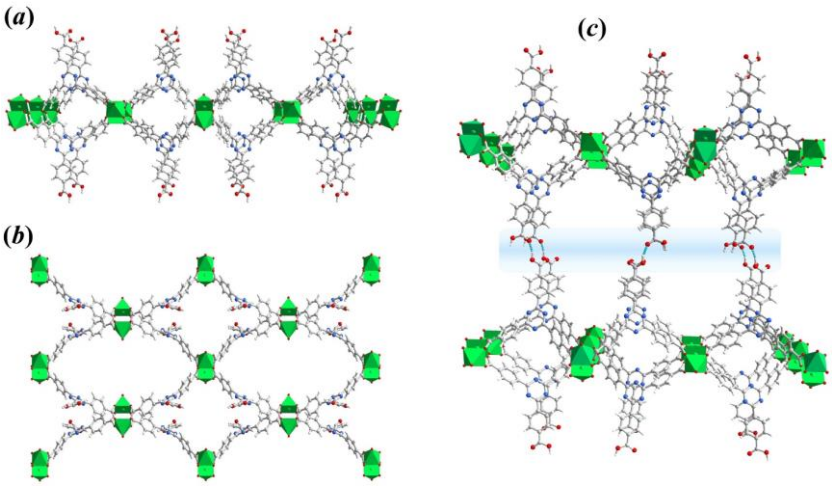

Figure 2. *Two-dimensional framework structure of bulk CuTATB MOF obtained by Rietveld refinement: (a) view along b-crystallographic direction and (b) along a-axis,*

and (c) Three-dimensional arrangement of 2D-layers expended via hydrogen bonding (blue region).

MOF films were synthesized on copper electrode surfaces including copper meshes. Powder XRD patterns for CuTATB coated electrodes exhibits a single detectable peak at $2\theta = 6.42^{\circ}$ that does not match with the sample obtained in bulk (Fig. S6 (page 37)). Additionally, similar patterns were obtained even when the synthesis was carried out with higher number of cycles. It was observed that during the electrochemical synthesis of CuTATB, a thin layer of MOF was formed on the copper mesh in the first seconds of the synthesis. This further resulted in the formation of islands at various nucleation sites as reported recently[30]. As the intergrowth of the deposited MOF layer takes place, these islands can detach from the surface. This detachment can also have self-limiting effect on thickness of the deposited layer. Thus, these processes result in layers of similar thickness of MOFs even when the synthesis was carried out with higher number of cycles (up to 200 cycles). In order to identify the structure of the MOF directly grown on the Cu surface, this surface was scratched off and analysed by XRD (Fig. S6 (page 37)). A comparison of experimental XRD patterns with simulated ones for CuBTC and CuTATB (here compared to the previously reported PCN-6 MOF)[25] was performed. The reflection at $2\theta = 6.42^{\circ}$ corresponds well with the most intense (202) diffraction of the PCN-6 structure (Fig. S6 (page 37)). Correspondingly, the crystal structure of CuTATB consists of a 3D network of the cage-type architecture and possesses large accessible voids (Fig. 3a-b).

However, compared to the non-interpenetrated (PCN-6') framework, the free accessible volumes of the cages of the low-interpenetrated form of the PCN-6 structure reduces by a factor of about 1.5,[26] as a result of the interpenetration of two equivalent frameworks (Fig. 3c). Following a previously used consideration for the bulk framework simplification (Fig. S4a-b (page 35)), the network of CuTATB grown on the electrode surface (PCN-6) is a 3,4-connected binodal net of twisted boracite topological type (***tbo***) and expressed by a $(6^2.8^2.10^2)_3(6^3)_4$ Schläfli symbol[28]. Moreover, the network structure consists of two equivalent symmetry nets, which are interpenetrated[29] (Fig. S7 (page 38)).

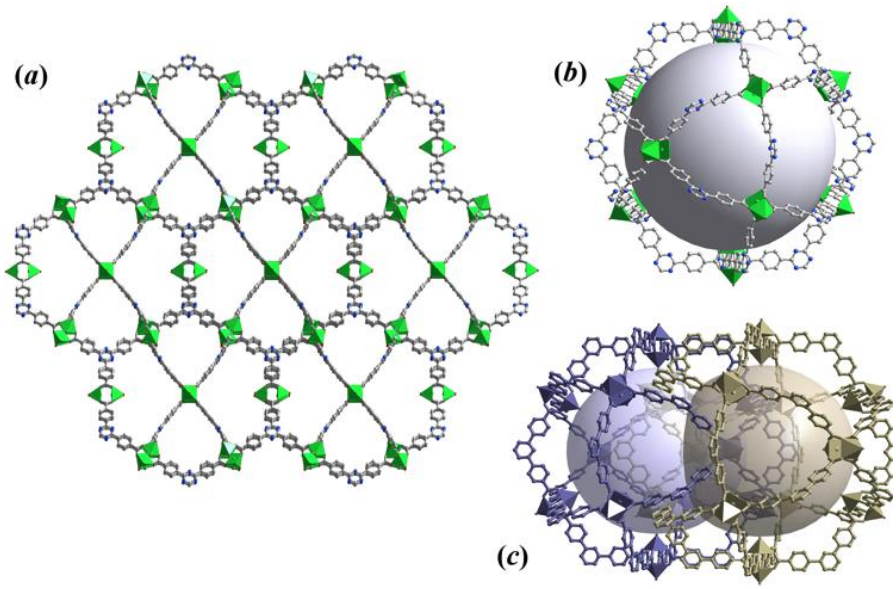

Figure 3. *a) The 3D framework structure of CuTATB MOF grown on the electrode surface, (b) visualization of the cage of non-interpenetrated CuTATB MOF (PCN-6'), and (c) arrangement of voids within the interpenetrated structure of PCN-6. All structures were obtained based on reported studies*[25-26].

Further characterization of these materials was carried out using scanning electron microscopy (SEM). Synthesized powder samples of CuTATB with constant current synthesis showed needle-like structures (Figs. 4a-b). The obtained material also showed a wide particle size distribution where the length varied from nanometres to a few micrometres. When the material was synthesized on the supported surfaces, a different morphology of the material was observed. By using a square-wave electrical current for the electrochemical growth of copper-based MOFs, concentration polarization near the surface of the metal electrode can be controlled. This leads to a good MOF coverage on the electrode surface (Fig. 4c) due to a fast nucleation process.

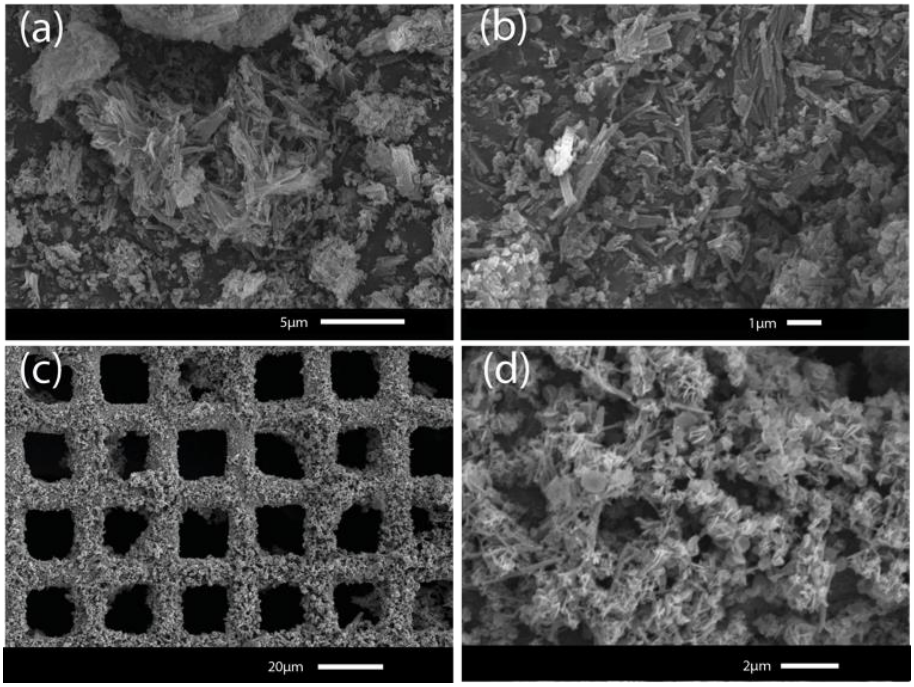

Figure 4. *Scanning Electron Microscope pictures of CuTATB synthesized as bulk powder (a and b), and grown on a copper mesh (c and d).*

To further investigate the differences in the bulk powder MOFs and MOFs grown on surface in terms of porosity, gas adsorption studies were performed. The reference CuBTC MOF displayed a similar isotherm and BET surface area (~1300 m^2/g) as reported in the literature[16] (Fig. S9 (page 40)). Figure 5a and 5b shows the N_2 adsorption isotherms at 77 K of CuTATB measured as bulk powder and as a deposited layer on several copper meshes. The isotherm indicates a microporous nature of CuTATB (Fig. 5a). The BET area and Langmuir area of CuTATB, calculated from N_2 adsorption isotherm, were found to be approximately 570 m^2/g and 740 m^2/g, respectively. The porosity of the material was also observed to be close to the reported material with H_3BTB synthesized solvothermally[27]. Further, in case of CuTATB, the amount of N_2 adsorbed per mole of copper in the MOF was similar to that of CuBTC (Fig. S9 (page 40)).

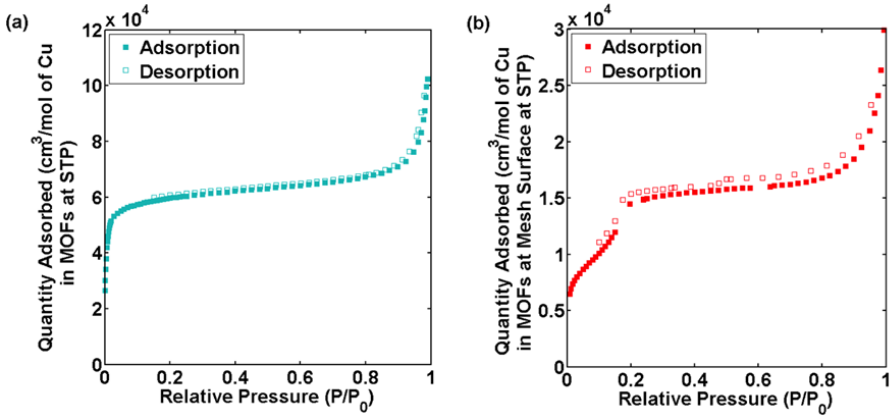

Figure 5. *N_2 sorption isotherms of CuTATB, synthesized as bulk powder (a) and obtained from multiple electrochemically modified copper meshes (b).*

In contrast, the N_2 adsorption isotherm of CuTATB deposited on a copper mesh shows a completely different shape (Fig. 5b). Even though the exact mass of the deposited material could not be calculated (although roughly estimated by measuring the mass change of electrode), the N_2 adsorption isotherm shows a two-step shape (Fig. 5b), indicating a clear difference in the structure of CuTATB synthesized on the surface. This is also supported by the XRD pattern of the MOF on the mesh as discussed earlier (Fig. S6 (page 37)). Further, the cage structure in the molecular network, which arises from controlling interpenetration in the structure, supports the two-step adsorption.

The results obtained so far indicate that there are differences in properties of CuTATB on surface growth with respect to the powder samples. This can be attributed to interpenetration in these large linkers in powder form. The interpenetration in these samples can be rationalized by the following. In order to minimize the energy in the larger networks in these MOFs due to bulky linkers (i.e. H_3TATB), the free void space in the material is filled by the units of the framework, which can lead to interpenetration[13]. This interpenetration also affects the sorption behaviour[15]. A similar two-step behavior for N_2 adsorption as shown in Figure 5 for CuTATB has been reported earlier for other materials as well on the control of interpenetration in the framework[15, 31]. Moreover, other MOFs based on copper metal and

H_3TATB or H_3BTB as similar organic linker have also shown interpenetration, resulting in materials like PCN-6[25-26] and MOF-14[10] respectively. Non-interpenetrated alternatives of PCN-6 and MOF-14, PCN-6'[16, 26] and MOF-143[32] were also synthesized by modification of synthesis conditions. It should be noted that the electrochemically synthesized powder MOF did not show any resemblance with these MOFs. That can be attributed to a reduced solubility of the linkers in ethanol. In order to increase the solubility, the synthesis process was also carried out at 70°C. It resulted in the formation of MOFs with similar properties as the RT-prepared MOFs.

During the electrochemical synthesis, the generation of a high density of metal ions allows the formation of small crystals that end up in the solution. With the use of a pulsed current, the generation of these copper ions is controlled, which results in the growth of MOF on the surface, as the fast nucleation rate of copper MOFs allows crystallization taking place on the electrode surface layer. Further, molecular reorientation of organic ligands near the copper surface can modify the morphological and structural characteristics of the formed MOF[33-34]. This controlled generation of copper ions, molecular reorientation of organic ligands near copper surface and hence the growth kinetics by electrochemical synthesis can affect the interpenetration in the formed MOFs.

2.4. Conclusions

Copper-based Metal-Organic Frameworks (MOFs) were prepared by electrochemical synthesis using an elongated linker with similar geometry to that of benzene 1,3,5-tricarboxylic acid (H_3BTC). Our results demonstrate clear differences in the properties of the MOF grown in the bulk and the MOF grown on the surface of the electrodes. These differences can be attributed to the observation that growth on the surface prevents the interpenetration of the MOF network.

References

[1] M. D. Allendorf, V. Stavila, *CrystEngComm* **2015**, *17*, 229-246.

[2] H. Furukawa, K. E. Cordova, M. O'Keeffe, O. M. Yaghi, *Science* **2013**, *341*.

[3] S. L. James, *Chemical Society Reviews* **2003**, *32*, 276-288.

[4] T. Rodenas, I. Luz, G. Prieto, B. Seoane, H. Miro, A. Corma, F. Kapteijn, F. X. Llabrés i Xamena, J. Gascon, *Nat Mater* **2015**, *14*, 48-55.

[5] L. J. Murray, M. Dinca, J. R. Long, *Chemical Society Reviews* **2009**, *38*, 1294-1314.

[6] P. Horcajada, T. Chalati, C. Serre, B. Gillet, C. Sebrie, T. Baati, J. F. Eubank, D. Heurtaux, P. Clayette, C. Kreuz, J.-S. Chang, Y. K. Hwang, V. Marsaud, P.-N. Bories, L. Cynober, S. Gil, G. Ferey, P. Couvreur, R. Gref, *Nat Mater* **2010**, *9*, 172-178.

[7] J. Gascon, A. Corma, F. Kapteijn, F. X. Llabrés i Xamena, *ACS Catalysis* **2013**, *4*, 361-378.

[8] L. E. Kreno, K. Leong, O. K. Farha, M. Allendorf, R. P. Van Duyne, J. T. Hupp, *Chemical Reviews* **2011**, *112*, 1105-1125.

[9] A. Bétard, R. A. Fischer, *Chemical Reviews* **2011**, *112*, 1055-1083.

[10] B. Chen, M. Eddaoudi, S. T. Hyde, M. O'Keeffe, O. M. Yaghi, *Science* **2001**, *291*, 1021-1023.

[11] M. G. Goesten, F. Kapteijn, J. Gascon, *CrystEngComm* **2013**, *15*, 9249-9257.

[12] O. M. Yaghi, *Nat Mater* **2007**, *6*, 92-93.

[13] H.-L. Jiang, T. A. Makal, H.-C. Zhou, *Coordination Chemistry Reviews* **2013**, *257*, 2232-2249.

[14] J. Zhang, L. Wojtas, R. W. Larsen, M. Eddaoudi, M. J. Zaworotko, *Journal of the American Chemical Society* **2009**, *131*, 17040-17041.

[15] S. B. Choi, H. Furukawa, H. J. Nam, D.-Y. Jung, Y. H. Jhon, A. Walton, D. Book, M. O'Keeffe, O. M. Yaghi, J. Kim, *Angewandte Chemie International Edition* **2012**, *51*, 8791-8795.

[16] S. Ma, D. Sun, M. Ambrogio, J. A. Fillinger, S. Parkin, H.-C. Zhou, *Journal of the American Chemical Society* **2007**, *129*, 1858-1859.

[17] O. Shekhah, H. Wang, M. Paradinas, C. Ocal, B. Schupbach, A. Terfort, D. Zacher, R. A. Fischer, C. Woll, *Nat Mater* **2009**, *8*, 481-484.

[18] P. Falcaro, R. Ricco, C. M. Doherty, K. Liang, A. J. Hill, M. J. Styles, *Chemical Society Reviews* **2014**, *43*, 5513-5560.

[19] U. Mueller, M. Schubert, F. Teich, H. Puetter, K. Schierle-Arndt, J. Pastre, *Journal of Materials Chemistry* **2006**, *16*, 626-636.

[20] A. M. Joaristi, J. Juan-Alcaniz, P. Serra-Crespo, F. Kapteijn, J. Gascon, *Cryst Growth Des* **2012**, *12*, 3489-3498.

[21] U. Mueller, H. Puetter, M. Hesse, M. Schubert, H. Wessel, J. Huff, M. Guzmann, U.S. Patent No. 8,163,949, **2012**.

[22] R. Ameloot, L. Stappers, J. Fransaer, L. Alaerts, B. F. Sels, D. E. De Vos, *Chemistry of Materials* **2009**, *21*, 2580-2582.

[23] I. Stassen, M. Styles, T. Van Assche, N. Campagnol, J. Fransaer, J. Denayer, J.-C. Tan, P. Falcaro, D. De Vos, R. Ameloot, *Chemistry of Materials* **2015**, *27*, 1801-1807.

[24] S. S.-Y. Chui, S. M.-F. Lo, J. P. H. Charmant, A. G. Orpen, I. D. Williams, *Science* **1999**, *283*, 1148-1150.

[25] D. Sun, S. Ma, Y. Ke, D. J. Collins, H.-C. Zhou, *Journal of the American Chemical Society* **2006**, *128*, 3896-3897.

[26] J. Kim, S.-T. Yang, S. B. Choi, J. Sim, J. Kim, W.-S. Ahn, *Journal of Materials Chemistry* **2011**, *21*, 3070-3076.

[27] B. Mu, F. Li, K. S. Walton, *Chemical Communications* **2009**, 2493-2495.

[28] V. A. Blatov, A. P. Shevchenko, D. M. Proserpio, *Cryst Growth Des* **2014**, *14*, 3576-3586.

[29] I. A. Baburin, V. A. Blatov, L. Carlucci, G. Ciani, D. M. Proserpio, *Journal of Solid State Chemistry* **2005**, *178*, 2452-2474.

[30] N. Campagnol, T. Van Assche, L. Stappers, J. F. M. Denayer, K. Binnemans, D. E. De Vos, J. Fransaer, *ECS Transactions* **2014**, *61*, 25-40.

[31] S. Bureekaew, H. Sato, R. Matsuda, Y. Kubota, R. Hirose, J. Kim, K. Kato, M. Takata, S. Kitagawa, *Angewandte Chemie International Edition* **2010**, *49*, 7660-7664.

[32] H. Furukawa, Y. B. Go, N. Ko, Y. K. Park, F. J. Uribe-Romo, J. Kim, M. O'Keeffe, O. M. Yaghi, *Inorganic Chemistry* **2011**, *50*, 9147-9152.

[33] J. V. Barth, J. Weckesser, N. Lin, A. Dmitriev, K. Kern, *Appl Phys A* **2003**, *76*, 645-652.

[34] S. Stepanow, T. Strunskus, M. Lingenfelder, A. Dmitriev, H. Spillmann, N. Lin, J. V. Barth, C. Wöll, K. Kern, *The Journal of Physical Chemistry B* **2004**, *108*, 19392-19397.

Control of Interpenetration of Copper-based MOFs on Supported Surfaces by Electrochemical Synthesis

Supporting Information

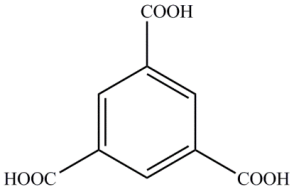

(a)

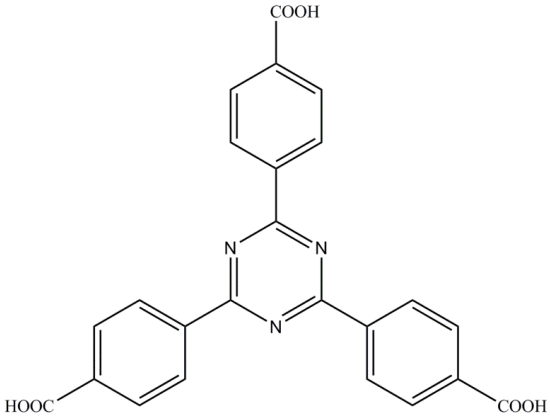

(b)

Figure S1*. Molecular structures of the two linkers used in the study:H_3BTC (a) and H_3TATB (b).*

2.5. Powder X-ray diffraction, refinement and structural details for MOFs obtained in bulk and surface-supported.

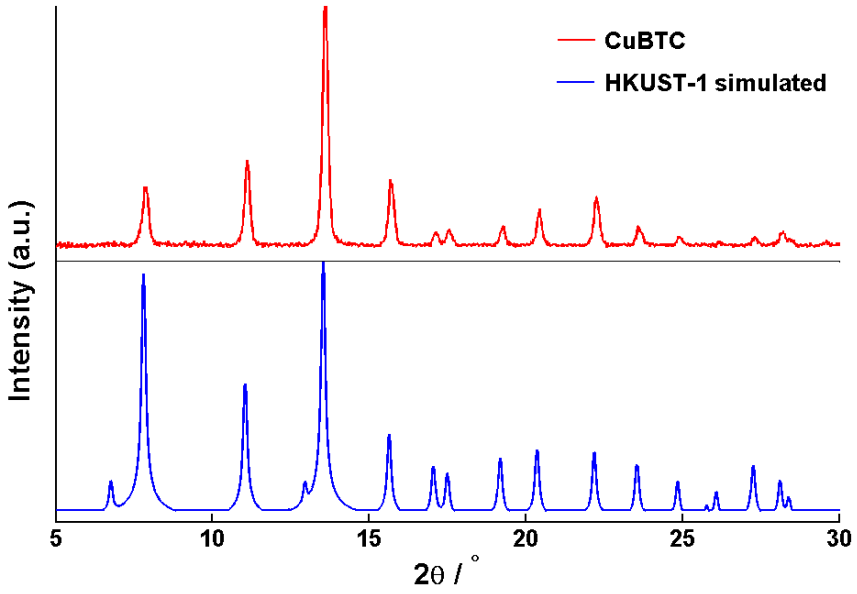

Figure S2. *Comparison of XRD patterns of CuBTC obtained in bulk (experimental) and HKUST-1 (simulated).*

Rietveld refinement of CuTATB obtained in bulk has been performed with EXPO2014[1], by which zero offset, scale factor, eight background terms and profile parameters as a PearsonVII function were refined.

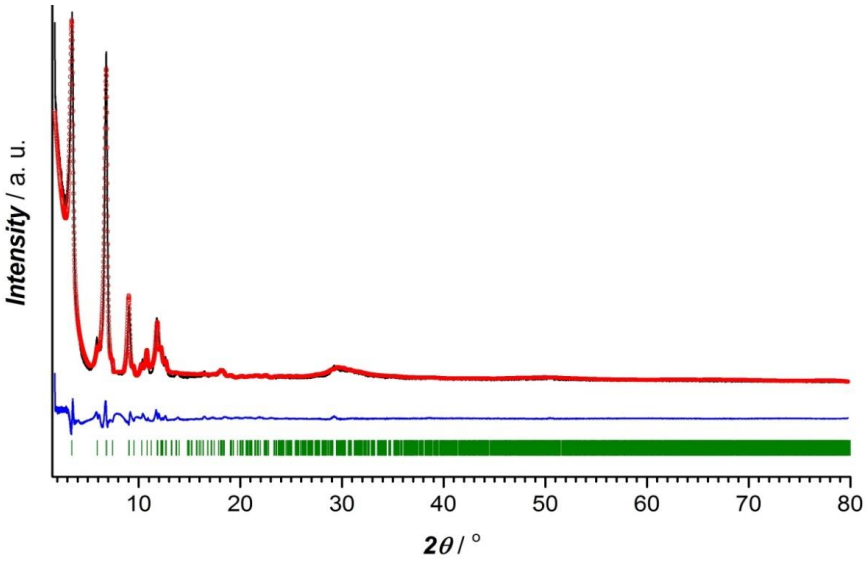

Figure S3*. Rietveld refinement plot for CuTATB MOF obtained in bulk. The experimental data are presented as black solid line, the calculated data by red circles and difference as blue solid line. The Bragg positions of the peaks are represented as green sticks.*

Table S1. *Unit cell parameters for CuTATB (obtained in bulk) determined by Rietveld refinement of experimental XRD pattern and compared with CuBTB [2]*

Compound	CuTATB	CuBTB
Formula	C_{100} H_{57} Cu_4 N_{12} O_{28}	C_{456} H_{308} Cu_{16} O_{142}
FW / g·mol^{-1}	2128.78	9075.84
Crystal system	Orthorhombic	Orthorhombic
Space group	*Pbcm*	*Pbcm*
a / Å	29.9203(20)	28.0524(17)
b / Å	17.3963(9)	14.8658(9)
c / Å	34.5860(17)	28.7818(18)
α / °	90	90
V / Å^3	18002.2(10)	12002.6(13)
Z	4	1
R_1,[i] wR_2[ii]	9.290, 12.917	–

[i] $R_P = \Sigma_i |y_{i,o} - y_{i,c}| / \Sigma_i |y_{i,o}|$; [ii] $R_{wp} = \left[\Sigma_i w_i (y_{i,o} - y_{i,c})^2 / \Sigma_i w_i (y_{i,o})^2\right]^{1/2}$

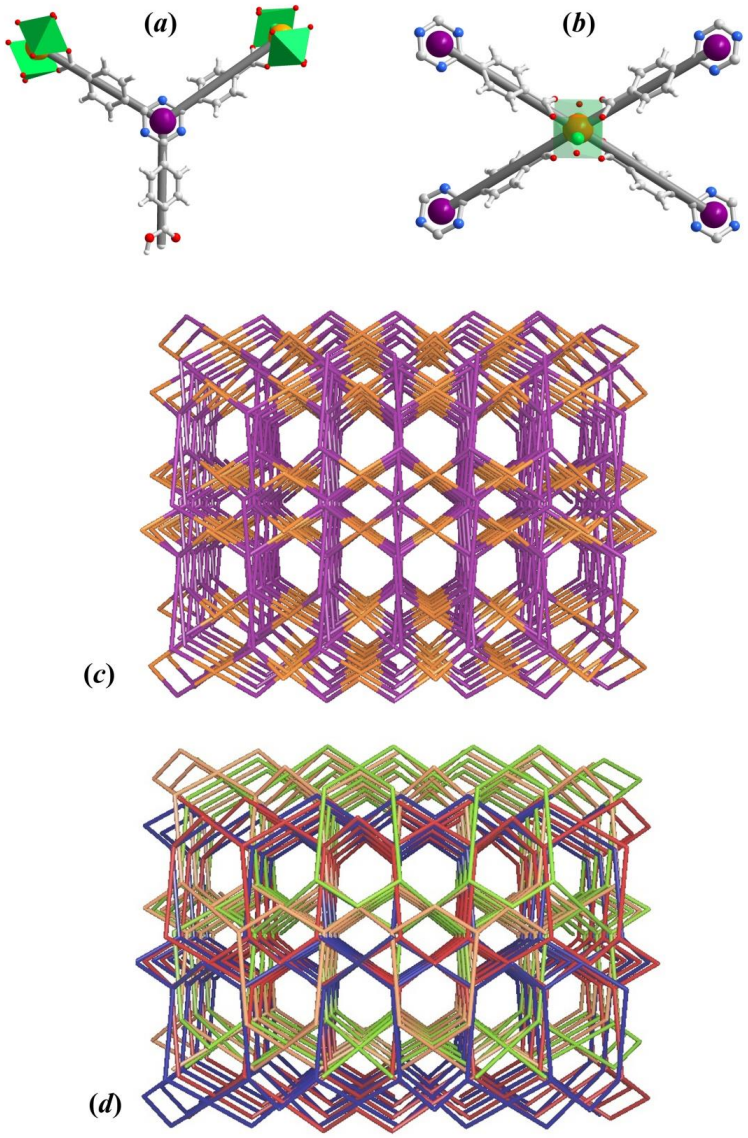

Figure S4. *Simplification of CuTATB structural units: (a) TATB tripod linker represented as a 3-connected node; (b) paddlewheel cupper unit represented as a 4-connected node. (c) Topological view of CuTATB highly interpenetrated net where 3-c nodes of TATB are drawn as violet centers and 4-c nodes of dimeric copper unit as orange centers. (d) The four-component interpenetration in CuTATB polymeric network where each independent polymeric frame is binodal 3,4-connected of sur topological type (each independent net is drawn with different color).*

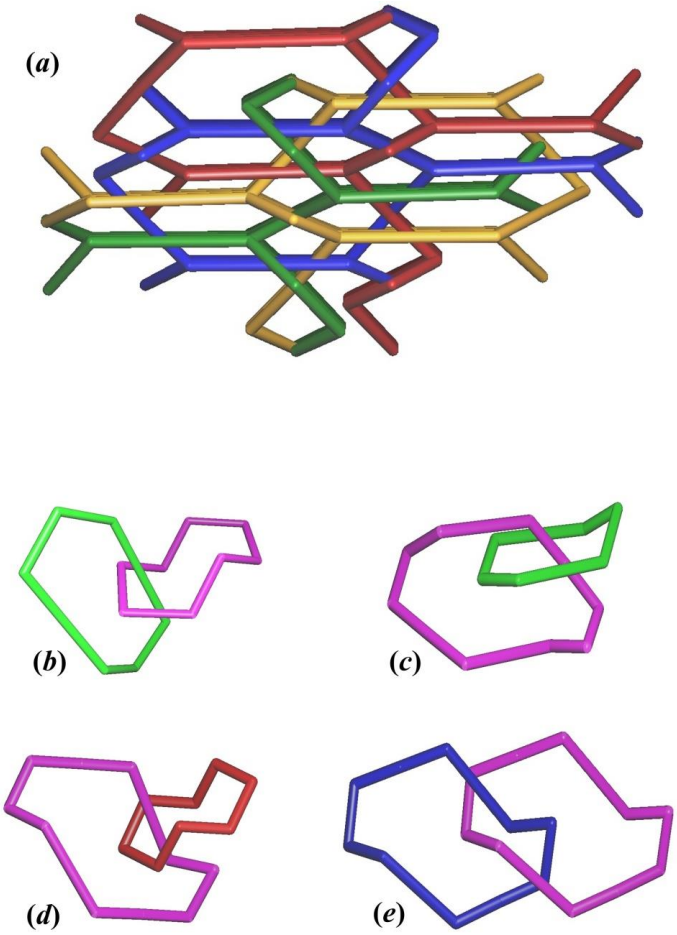

Figure S5. *(a) Four interpenetrated nets forming array of CuTATB which show four different links (knots) of Hopf type between closed circles: (b) 6-membered (green) and 8-membered (magenta); (c) 8-membered (green) and 8-membered (magenta); (d) 8-membered (red) and 10-membered (magenta); (e) 10-membered (blue) and 10-membered (magenta)*

Topological analyses of CuTATB structures have been performed using ToposPro software package[3]. All the interpenetration nets have the topology of ***sur***-type net and the interpenetration type belongs to a rare class IIIa[4]. As

shown in Fig. S5, the interpenetration of four equivalent ***sur***-nets realized by four kinds of interwoven rings (Hopf links): six- and eight-membered rings (b); eight- and eight-membered rings (c); ten- and eight-membered rings (d); ten- and ten-membered rings (e).

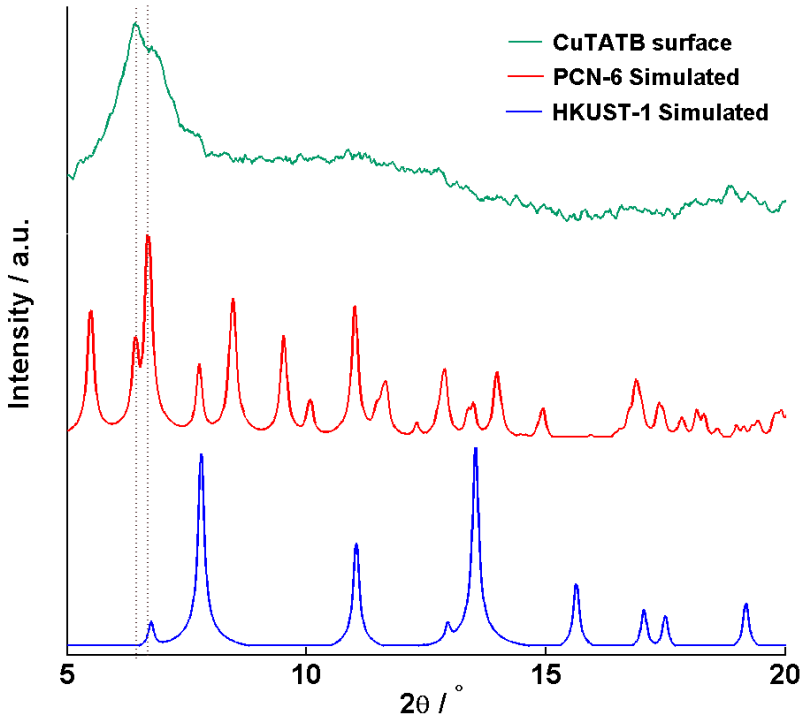

Figure S6. *Comparison of the pattern of CuTATB scratched from the electrode surface (green) and simulated patterns of PCN-6 structure (red) and HKUST-1 (blue). The dashed lines indicate the most intense peak of the measured spectrum.*

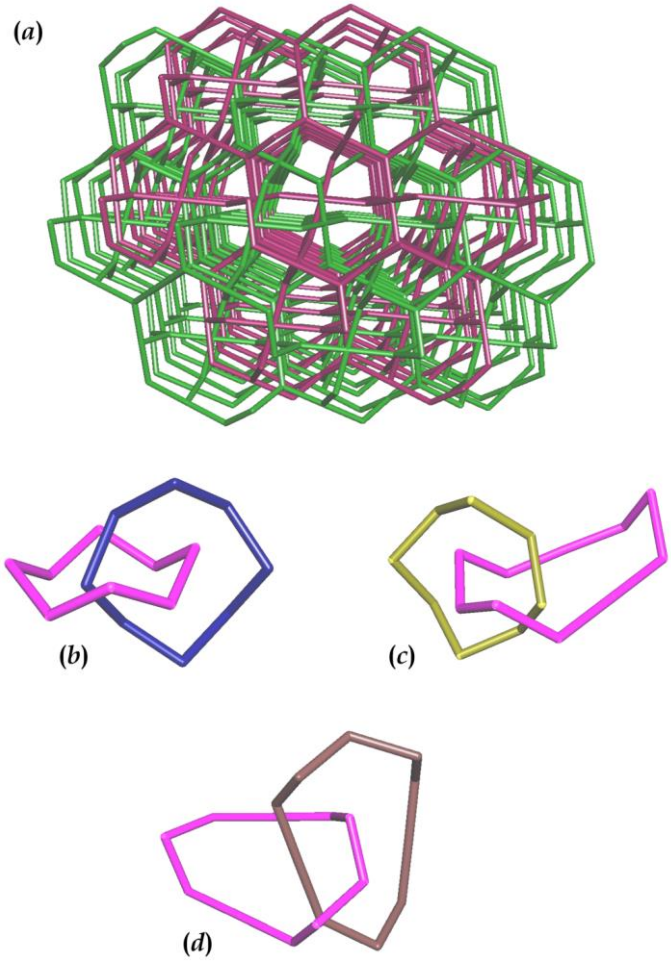

Figure S7*. (a) Two interpenetrated nets of* ***tbo****-type forming array of CuTATB, which show three different links (knots) of Hopf type between closed circles: (b) 8-membered (blue) and 8-membered (magenta); (c) 8-membered (yellow) and 10-membered (magenta); (d) 10-membered (brown) and 10-membered (magenta).*

Topological analysis of CuTATB structure grown on the electrode surface has been performed using ToposPro software package[3]. All the interpenetration nets have the topology of ***tbo***-type net and the interpenetration type belongs to a class IIa[4]. As shown in Fig. S7, the interpenetration of two equivalent ***tbo***-nets realized by three kinds of interweaved rings (Hopf links): eight- and eight-membered rings (b); eight- and ten-membered rings (c); ten- and ten-membered rings (d).

2.6. SEM images of CuBTC grown on copper mesh

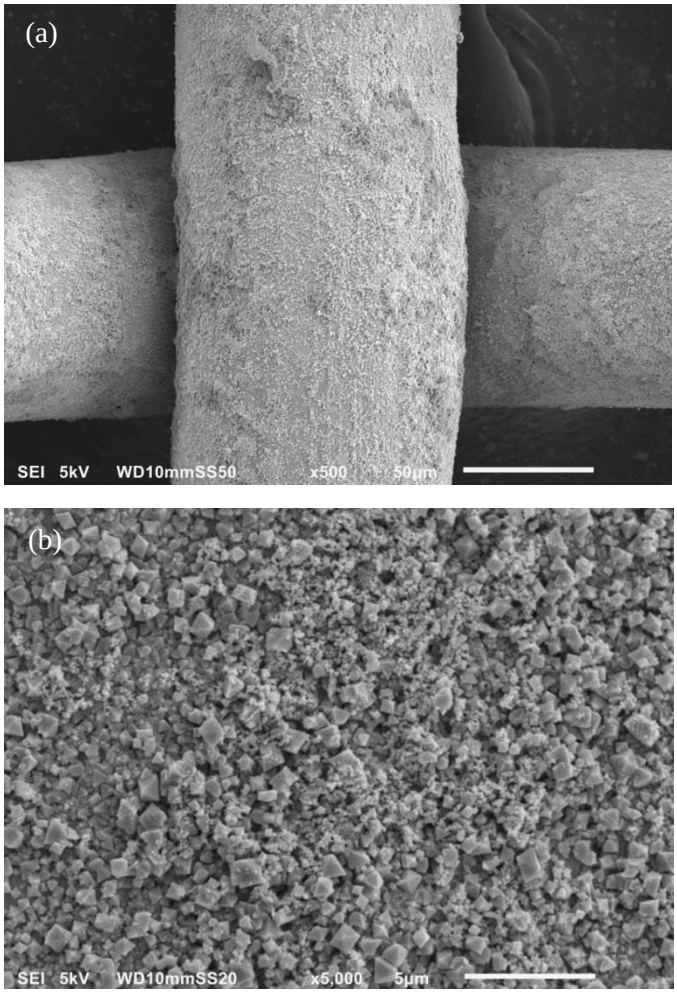

Figure S8. *SEM micrographs of CuBTC grown on the surface of a copper mesh at different magnifications: ×500 (a) and ×5000 (b).*

2.7. Sorption studies of electrochemically-grown MOFs

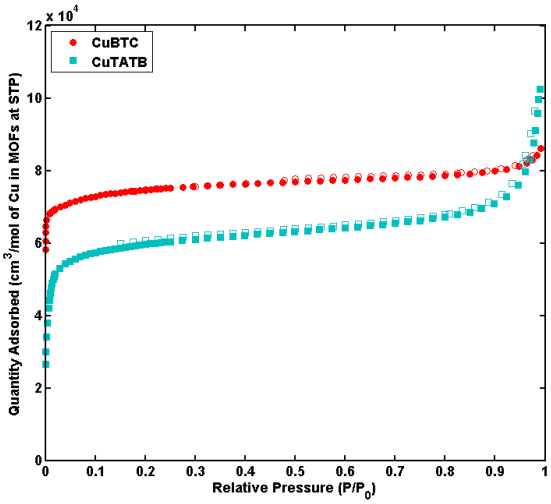

Figure S9. *N_2 sorption isotherm (at 77 K) of CuBTC (red) and CuTATB (blue) synthesized as bulk powder.*

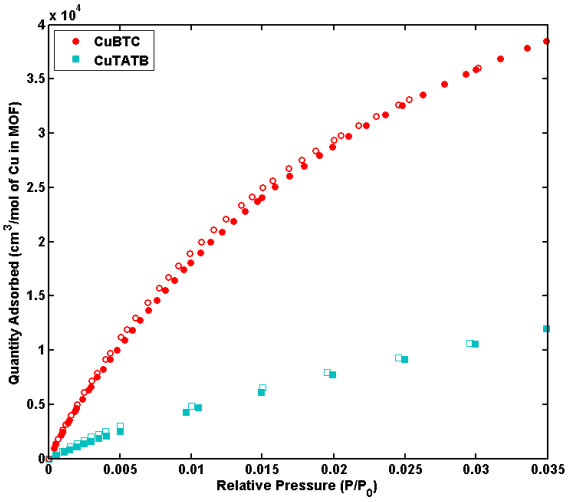

Figure S10. *CO_2 sorption isotherm of bulk CuBTC (red) and CuTATB (blue) measured at 273 K.*

References

[1] A. Altomare, C. Cuocci, C. Giacovazzo, A. Moliterni, R. Rizzi, N. Corriero, A. Falcicchio, *Journal of Applied Crystallography* **2013**, *46*, 1231-1235.

[2] B. Mu, F. Li, K. S. Walton, *Chemical Communications* **2009**, 2493-2495.

[3] V. A. Blatov, A. P. Shevchenko, D. M. Proserpio, *Cryst Growth Des* **2014**, *14*, 3576-3586.

[4] I. A. Baburin, V. A. Blatov, L. Carlucci, G. Ciani, D. M. Proserpio, *Journal of Solid State Chemistry* **2005**, *178*, 2452-2474.

Chapter 3

Sensitive and Reversible Detection of Methanol and Water Vapor by *in-situ* Electrochemically Grown CuBTC MOFs on Interdigitated Electrodes

This chapter is based on the following work:

S. Sachdeva, M.R. Venkatesh, B. El Mansouri, J. Wei, A. Bossche, F. Kapteijn, G. Q. Zhang, J. Gascon, L.C.P.M. de Smet, E.J.R. Sudhölter, submitted to *Small*

Abstract

This study describes the in-situ electrochemical growth of CuBTC MOFs, as an affinity layer, directly on custom-fabricated Cu InterDigitated Electrodes (IDEs), acting as a transducer. Crystalline 5-7 μm thick CuBTC layers were grown on IDEs consisting of 100 electrodes with a width and a gap of both 50 μm and a height of 6-8 μm. These capacitive sensors were exposed to methanol and water vapor at 30 °C. The affinities showed to be completely reversible with higher affinity towards water compared to methanol. For exposure to 1000 ppm methanol, a fast response was observed with a capacitance change of 5.57 pF at equilibrium. The capacitance increase in time followed diffusion-controlled kinetics (k = 2.9 mmol $s^{-0.5}g^{-1}_{CuBTC}$). The observed capacitance change with methanol concentration followed a Langmuir adsorption isotherm, with a value for the equilibrium affinity K_e = 174.8 bar^{-1}. A volume fraction f_{MeOH} = 0.038, is occupied upon exposure to 1000 ppm of methanol. The thin CuBTC affinity layer on the Cu-IDEs shows fast, reversible, and sensitive response to methanol and water vapor, enables quantitative detection in the range of 100-8000 ppm.

3.1. Introduction

Recent advances in the microelectronics industry have resulted in the development of miniaturized transduction devices for accurate, real-time detection of various analytes. Such systems require, in addition, affinity layers for the introduction of sensitive, selective and reversible interactions with the analytes to be detected[1-2]. While most of the commercially available sensors utilize metal-oxides as affinity layers, there is interest for extending the range of affinity materials to reduce cross-sensitivity and to lower energy consumption[3-4]. Recent studies have focused on utilizing Metal-Organic Frameworks (MOFs) as affinity layer materials, because of their high porosity, selective gas adsorption properties and tunability[5-7]. MOFs belong to the class of hybrid materials and are composed of coordinatively linked metal ions or clusters via organic ligands to form porous crystalline frameworks[6, 8]. *Hitherto*, most of the sensing studies with MOFs were carried out using the material as a bulk powder, i.e. by monitoring the change of luminescence properties upon analyte binding[5, 9]. Only a few studies have appeared on post-synthetically deposited MOFs on a transducer surface, able to transform the interactions with the analyte into changes of conductivity or dielectric properties[10-12]. The layer-by-layer deposition method has also been used to make thin films of MOFs on the surface of transducers[13-15]. While all these multiple-step approaches illustrate well the attractiveness of using MOFs as selective affinity layers for sensor devices, their further applicability will benefit from developments that shorten the fabrication process of the MOF coatings[16-17].

An interesting approach to grow MOF films directly on metal (transducer) surfaces in a fast and controllable way makes use of anodic dissolution of the metal ions in the presence of the organic linkers[18-21]. Such an electrochemical deposition procedure can be easily integrated with semiconductor processing techniques[22-23]. Recently, we have shown the possibility to grow Cu-MOFs as uniform films on flat Cu electrodes by applying cyclic current pulses[24-25]. In this study, we have investigated the electrochemical growth of Cu-MOFs on interdigitated Cu electrodes as sensors and their ability to detect methanol and water vapor at room temperature. The interdigitated electrode (IDE) structure allows capacitive detection[26-27] of the affinity process. IDEs can easily be fabricated, are compatible with CMOS

technology and are able to operate at room temperature allowing for a low power consumption[26, 28].

3.2. Experimental Details:

All chemicals were purchased from Sigma Aldrich and used as received. The device fabrication was carried out in a clean-room environment. Scanning Electron Microscopy (SEM) micrographs were acquired at different magnifications using a JEOL JSM 6360 microscope and a Nova NanoSEM™ (for cross-sectional images). The powder X-Ray Diffraction (pXRD) patterns of IDEs with and without MOF deposition were recorded using the Bruker D8 Advance diffractometer with Co-$K\alpha$ radiation (λ = 1.788897 Å).

3.2.1. Device Fabrication

The copper (Cu) interdigitated electrode (IDE) devices were fabricated on a p-type Silicon substrate (100) with a thickness of 300 µm. The fabrication process is summarized schematically in Figure S1 (page 62). First, a 500 nm thick Si_3N_4 layer was deposited by low pressure chemical vapour deposition (LPCVD) at 850 °C followed by the deposition of 300 nm adhesion layer of Titanium Nitride (TiN) using a TRIKON SIGMA sputter coater. A Cu-seed layer of a 300 nm thick was deposited on top of the TiN layer in a similar fashion. IDEs were patterned using an AZ960 positive photo-resist by photo-lithography for 60 s using a contact aligner. After the IDE patterning, the wafers were developed using AZ400K for ~120 s. The Cu electrodes were then electroplated in the non-patterned region containing Cu seed layer by applying a current of 1 A for 900 s using the MECO electroplating equipment. After electroplating, the photo-resist was stripped by using acetone and iso-propanol. The exposed Cu seed layer and TiN layer (below the photo-resist patterns) were removed by first immersing the wafer to a solution of 5 g $Na_2S_2O_8$ in a mixture of 1.25 mL H_2SO_4 (96%) and 500 mL distilled water for 20 minutes to remove the Cu seed layer followed by dipping the wafer to a solution containing 25 mL NH_4OH (25%), 100 mL H_2O_2 (30%) and 100 mL distilled water for removing the TiN layer. After the fabrication, the wafer was diced and wire-bonded for external electrical connections. These devices are then used for electrochemical growth of MOFs.

Alternatively, IDE patterning was done using negative photo-resist AZ Nlof 2020 by lithography. The patterned devices were developed using MF322 developer for ~120 s before electroplating. The photoresist was stripped using NMP at 70 °C.

3.2.2. Electrochemical Synthesis of MOFs

Electrochemical synthesis of the MOFs was carried out as described previously[24]. 100 mg organic linker (H_3BTC or H_3TATB) and 25 mg electrolyte Methyl-TriButylammonium methyl Sulfate (MTBS) were dissolved in 8 mL 96 vol.% ethanol. The solution was mixed in the 10 mL electrochemical cell at room temperature. The MOF synthesis over the IDEs was carried out in a two-electrode system by using both electrodes of IDEs as anode (by electrically shorting) with a copper plate as the cathode. Cyclic pulses of current with 6 mA/5 s and 0 mA /5 s were applied for 5 min using an Autolab potentiostat PGSTAT302N. After the MOF growth, the devices were washed in the ethanol solution overnight at room temperature and dried at 100 °C for 2 h.

3.2.3. Finite element analysis of the IDEs

Finite element analysis of the IDEs structure was carried out using the simulation environment of COMSOL Multiphysics to predict the behavior of the devices over MOF growth and during methanol sensing. The geometry of the IDEs was defined with a width, W and a gap, G of 50 µm each and all the calculations were done over half of the spatial wavelength (λ) and estimated for the complete IDE with $N = 100$ electrodes.

The following equations were used to calculate the charge density (ρ), electric field ($\overrightarrow{E}$), electric displacement field ($\vec{D}$), work done (W_e) and capacitance (C) of the devices across the surface (S) before and after the growth of CuBTC[29]:

$$\rho = -\nabla \varepsilon_0 \varepsilon_r \nabla V \quad (1)$$

$$\vec{D} = \varepsilon_0 \varepsilon_r \vec{E} \quad (2)$$

$$W_e = \int_S (\vec{D} \cdot \vec{E}) dS \quad (3)$$

$$C = \frac{2}{V^2} \int_S W_e dS \quad (4)$$

3.2.4. Sensing Measurements

Sensing measurements of the coated and non-coated devices were carried out at a frequency of 20 kHz and a voltage of 0.1 V using a HP 4284A precision LCR meter. The frequency was chosen as 20 kHz to reduce the noise and parasitic in the measurement. The devices were kept in a custom-built gas mixing and sensing equipment[12] at $30 \pm 0.05\,°C$. During the measurements, a continuous stream of dry N_2 was passed over the devices at a flow rate of 200 mL/min using Mass Flow Controllers (MFCs) and perturbations in the form of different analytes (methanol or water) were introduced after a stable base-line was established.

The vapors of methanol or water were introduced by first passing dry N_2 through a series of two bubblers containing the analyte to generate a saturated stream of vapors and then diluting it with a parallel stream of dry N_2. The saturated concentration of the analyte was calculated using the Antoine equation[30-31]:

$$\mathrm{Log}P = A - \frac{B}{T+C} \quad (5)$$

Where P is the saturated vapor pressure of the analyte and T is the temperature of the bubbler. A, B and C are the analyte-dependent constants.

After the stabilization and equilibration of the capacitive signal during the measurements, the devices were recovered to the baseline by replacing the stream of N_2 and methanol (or water) with dry N_2.

3.3. Results and Discussion

The IDEs were fabricated on *p*-type silicon substrates by photolithography using two different procedures with either positive or negative photoresist to pattern the IDE structures (Figs. 1, S1 (page 62), Section 3.2). Next, Cu was electroplated utilizing a pre-sputtered 300 nm Cu seed layer as cathode to obtain the planar electrodes with varying widths (W) and gaps (G) ranging from 5 to 50 μm (Figs. 1(i), 1(ii), 1(iii)). For our study, we have

used the IDEs with W=G=50 μm and a number of electrodes (N) of 100, to ensure a good coverage of the MOF and to prevent electrical shortcuts which might arise at smaller G. Since the total capacitance is a linear function of N, it was set at the indicated value to enhance the overall sensitivity. The height of the produced Cu electrodes was 6-8 μm, as determined by cross-sectional Scanning Electron Microscopy (SEM, Figure 1(iv)) and by Dektak profilometry (Figure S2 (page 63), Supporting Information). The spatial wavelength[32-33] (λ) of the IDE device is defined by:

$$\lambda = 2\,(W + G) \tag{6}$$

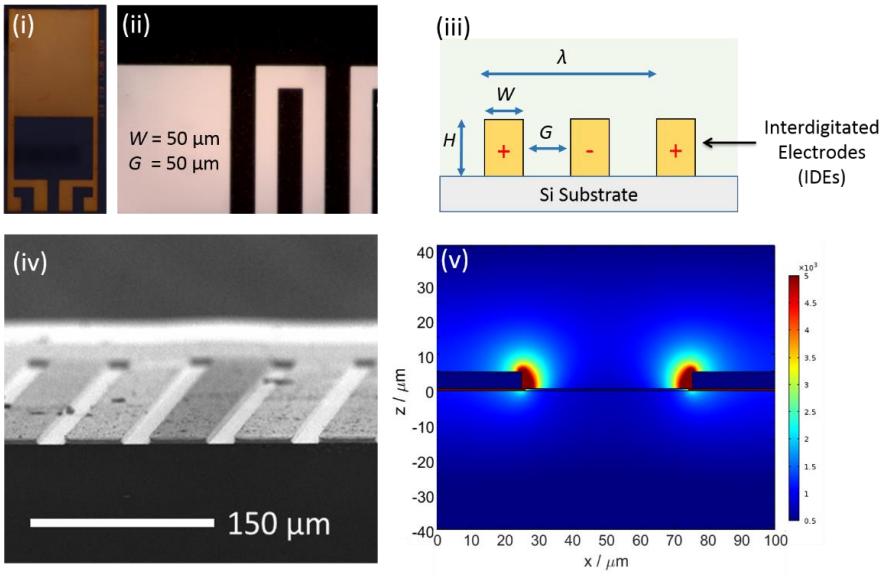

Figure 1. *Fabricated devices with Interdigitated Electrodes (IDEs). (i) optical image of the fabricated IDE with 4 bond pads in the end for external connections and (ii) optical image of a region of the IDEs with electrodes (represented by black regions) with width (W) and gap (G) of each 50 μm. (iii) schematic of the device illustrating the dimensions (width (W), gap (G) and height (H) of the electrodes) and spatial wavelength (λ) of the device. (iv) SEM image of the IDEs width of 50 μm and gap of 20 μm captured at 6° angle view and (v) figure indicating the distribution and*

electrical field strength (V/m) calculated across x and z dimensions. Color map indicates a distribution from the weakest (in blue) to the strongest (in red) field strength (V/m).

The sensitivity of the IDE transducer to detect changes in the capacitance of the affinity layer increases with a smaller value of λ. We have performed theoretical calculations of the electric field properties and the capacitance of our IDE structures making use of COMSOL Multiphysics[29] for a configuration of two electrodes (half spatial wavelength (λ)). The total capacitance was estimated by multiplying the resulting modeled capacitance with (N-1) = 99, to yield a (N-1) × $C_{\text{electrode}}$. The width (W) and gap (G) of the IDE structure were both set to 50 µm in COMSOL[29] and the height of the electrodes was set to 6 µm and 3 µm, to simulate the situation before and after the MOF growth process, respectively (Experimental Details, Section 3.2.3).

From Figure 1(v), it can be seen that the field strength remains strongest underneath the substrate. However, it is not accessible for the analyte and is regarded as the constant substrate contribution. Also, about 75 % of the field lines are found at a distance z, as measured perpendicular to the electrode surface, of < 40 µm. Near the edges of the electrodes (*i.e.* region between x = 0-25 µm and x = 75-100 µm in Figure 1(v); red colored) the maximal electrical field strength was found (other than the contribution through the substrate). A capacitance of 132 pF was calculated for IDE with W=G=50 µm and N = 100. Experimentally, the capacitance of the IDE was 3940 ± 0.017 pF at 20 kHz (Figure S3 (page 63), Supporting Information). The observed larger capacitance compared to the calculated capacitance is due to the parasitic contributions from the substrate and the wire bonding (~3000 pF; see Supporting Information, Section 2).

The Cu IDEs were used to electrochemically grow thin films of the well-known CuBTC MOF[34-35]. It consists of a Cu paddlewheel framework formed from three Cu ions coordinated with two benzene-1,3,5-tricarboxylate (BTC) ligands[34]. CuBTC has affinity for small-size gases and volatile organic components (VOCs), making it a potential candidate for application as

affinity layer on our IDEs[36-38]. We have grown CuBTC electrochemically on the Cu IDE structures with a Cu counter-electrode (cathode) in a 10 mL electrochemical cell containing a H_3BTC solution in 96 vol.% ethanol (Experimental Details, Section 3.2.2). Cyclic pulses of the current (6 mA for 5 s followed by no current for 5 s) were applied for 5 min[24]. This resulted in the deposition of crystalline materials on the IDE structure. By X-Ray diffraction (XRD), the formation of CuBTC was confirmed (Figure 2(i))[34, 39].

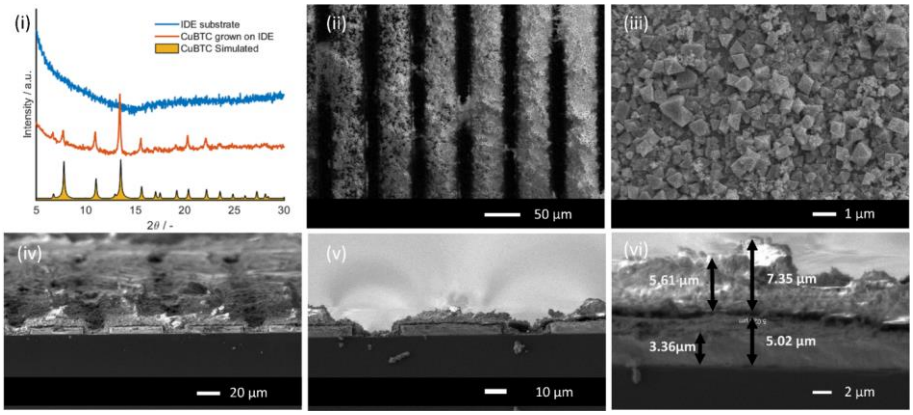

Figure 2*. (i) Comparison of the XRD pattern for the IDEs with (red) and without (blue) CuBTC layer with the simulated pattern of CuBTC. (ii), (iii) SEM images of CuBTC grown over the electrodes. (iv), (v) and (vi) cross-sectional SEM of a coated IDE indicating a clear separation between the CuBTC layer and the electrodes.*

The crystalline layer completely covered the electrodes and showed a thickness of 5-7 µm as deduced from SEM micrographs (Figs. 2 and S4 (page 65), Supporting Information). Cracks in the CuBTC layers were observed and also some crystallite detachment if the pulses were applied during a longer time period (7.5 min). This is most likely due to induced mechanical stress by the partial dissolution of the copper finger-electrodes and the concomitant formation of CuBTC[19] (Figure S5 (page 66), Supporting Information). The thickness of the IDE electrodes was reduced from 6-8 µm to 3-5 µm (Figs. 2(vi), S2 (page 63)). Due to this electrochemical deposition process of CuBTC (ε_r=1.7)[40-41], the device configuration is changed (Figure S6 (page 66), Supporting Information),

resulting in a slight decrease of the calculated capacitance from ~132 pF to ~122 pF as a combined result of reduction in electrode thickness and growth of a higher dielectric layer (Figure S7 (page 67), Supporting Information).

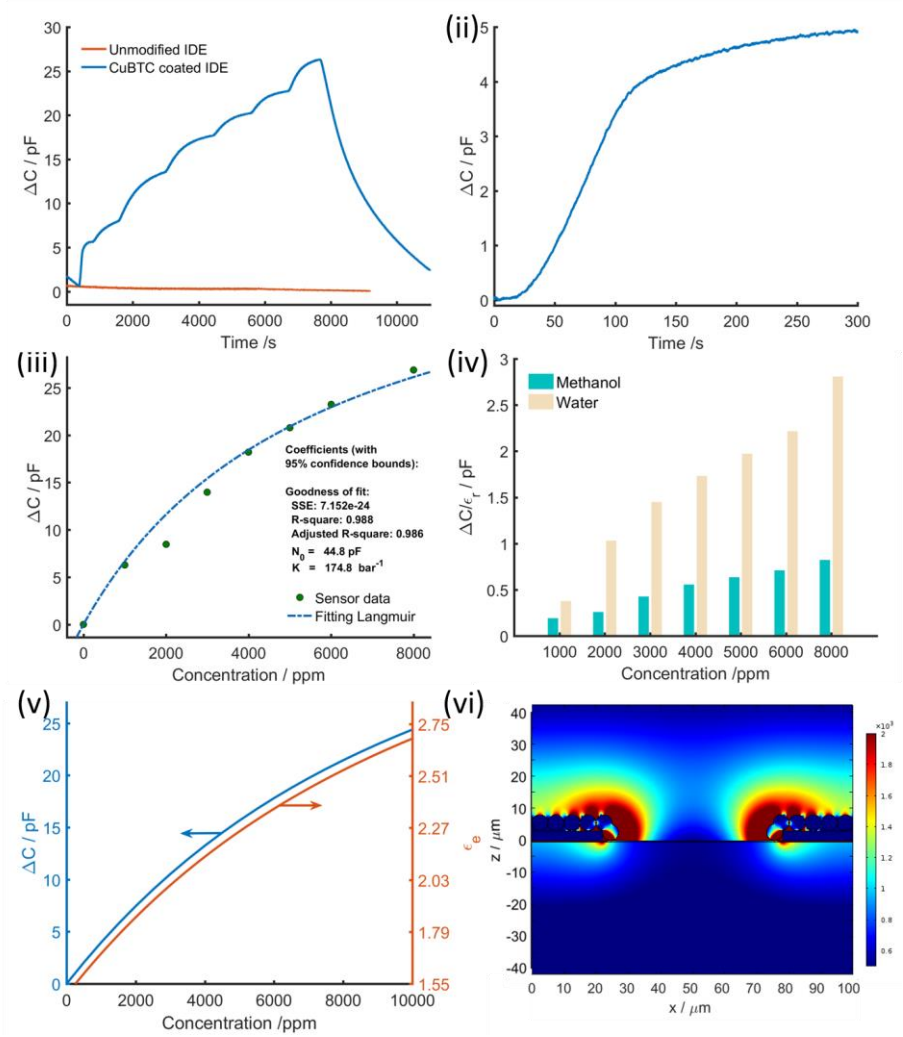

Figure 3*. (i) Capacitive response of unmodified IDE (red) and CuBTC-coated IDE (blue) towards methanol. (ii) Capacitive response vs time of CuBTC-coated IDE towards 1000 ppm of methanol vapour. (iii) Quantitative behavior of the sensor device towards methanol vapor and the Langmuir model fit. (iv) Comparison between the response towards methanol and water vapour normalized with respect to*

the dielectric constants of analyte. (v) Estimated dielectric constant(red) and capacitive change(blue) of these devices with methanol concentration as deduced by finite element analysis. (vi) Simulated distribution of the electric field strength, —E— over the IDE geometry. Color map indicates a distribution from the weakest (blue) to the strongest (red) field strength (V/m).

These CuBTC-modified IDEs were exposed to different concentrations of methanol and water vapor present in a nitrogen carrier gas at 30 °C in a custom-built gas mixing and sensing equipment system described previously[12]. The capacitance changes were determined by using impedance spectroscopy at a constant frequency of 20 kHz. In Figure 3(i), a capacitive response of 5-25 pF is shown upon the exposure to 1000-8000 ppm of methanol at a constant flow rate of 200 mL/min, in contrast to the unmodified IDE that showed no response. The response of the modified device to methanol vapor was completely reversible. The desorption time is longer than the adsorption time, reflecting the so-called 'favorable' methanol isotherm.

The capacitive response started a few seconds after applying the methanol and starts to approach equilibration value in 120-150 s (Figure 3(ii)). Such response is comparable with the metal-oxide based methanol sensors[42] and clearly reflects the presence of the thin CuBTC layer with its high porosity (having a BET surface area of ~1300 m^2/g and a pore volume of ~0.73 cm^3/g)[43]. In contrast, a coating of NH_2-MIL-53(Al) MOF blended in a Matrimid® polymeric matrix, shows a ~12 times slower response[12]. This slower response is the result of the presence of the polymer, which acts as a diffusion barrier[12].

Next, this capacitive increase in time for the situation, where 1000 ppm of methanol vapor was applied, was further analyzed to understand the role of pore diffusion in the methanol sensing. At these concentrations of the methanol, the methanol adsorption takes place mostly at the open-metal sites of CuBTC framework[43] which have a cage diameter of 9 Å with pore window between 3.5 – 4.6 Å. With a kinetic diameter of 3.6 Å, diffusion of methanol within CuBTC framework can significantly affect the adsorption process and hence the sensor response. Such intra-particle diffusion plays a

dominant role in the adsorption processes, if the uptake and hence the sensor response is directly proportional with the square root of the time ($t^{0.5}$) as described below[44-45] (Equation 7, Supporting information, Section 5):

$$\Delta C = k_{\mathrm{p}} t^{0.5} + I \qquad (7)$$

where ΔC is the change in capacitance at time t, k_{p} is the rate constant and I is the intercept representing the boundary layer effects. Figure S8 (page 68, Supporting information) shows that the relation between ΔC and $t^{0.5}$ can be divided into three regimes. Initial section of very small increase in capacitance ($t^{0.5} < 4\ s^{0.5}$) can be accounted for the equilibration of the measurement chamber due to the presence of large dead-volume (400-450 mL). It is followed by the linear regime of the response indicating the dominance of the intraparticle diffusion in the adsorption process. The rate constant (k_{p}) for this diffusion controlled process was determined to be 0.648 pF $s^{-0.5}$ with R^2 of 0.9958. The third section represent the equilibrium stage ($t^{0.5} > 9\ s^{0.5}$) where decrease in the concentration gradient slows down the diffusion process.

The capacitance response, (ΔC) in the measured methanol concentration range was further related to the concentration of methanol in the CuBTC affinity layer near the transducer by applying a Langmuir isotherm model as indicated in Figure 3(iii) and described by Equation 8:

$$\frac{\Delta C}{C_{\mathrm{s}}} = \frac{K_{\mathrm{e}} c_{\mathrm{m}}}{1 + K_{\mathrm{e}} c_{\mathrm{m}}} = \frac{q}{q_{\mathrm{s}}} = \theta \qquad (8)$$

where C_{s}, K_{e}, c_{m}, q_{s} indicate the saturation capacitance, affinity constant, concentration of methanol in the measurement chamber and saturated amount of methanol adsorbed, respectively. K_{e} and C_{s} were determined to be 174.8 bar^{-1} and ~44.8 pF by non-linear least square fitting of Equation 8 to the experimental sensor response. Even though C_{s} indicates that the adsorption capacity is still far from saturation, extrapolation to higher concentration has to be done carefully as multiple-site adsorption and pore filling in CuBTC can result in deviations from Langmuir behavior[43]. Based on these parameters, the amount of methanol adsorbed for applying a 1000

ppm concentration was estimated to be ~2.9 mmol/g of CuBTC (corresponding to 5.57 pF capacitive change and q_s = ~0.02 mol/g)[46]. These estimated adsorbed amount (2.9 mmol/g-11.6 mmol/g) for the applied methanol concentration range (1000-8000 ppm) were well in correspondence with the literature[43]. Utilizing the amount of the methanol adsorbed, the diffusion rate constant was also recalculated as 0.29 mmol $s^{-0.5}g^{-1}_{CuBTC}$. Furthermore, changes in the volume fraction (f) of methanol inside the pores of CuBTC was also calculated on exposure to different concentrations of methanol vapor with the assumption of a Langmuir behavior of adsorption (Supporting information, Section 6, Figure S9 (page 69)). For 1000 ppm of methanol in N_2, f_{MeOH} was calculated to be 0.038.

With an accuracy of our equipment (HP 4284A LCR meter) in the fF range, the sensitivity of the devices is clearly indicated by changes of 5 pF/1000 ppm of methanol. Our CuBTC-modified IDEs were also exposed to different concentrations of water vapor and the results were compared with the responses observed to methanol (Figure 3(iv)). The responses were therefore corrected for the differences of dielectric constants of methanol and water by dividing the observed capacitance change by the respective dielectric constants ($\varepsilon_{r,\ methanol}$ = 32.7, $\varepsilon_{r,\ water}$ = 78). Clearly, the affinity of the CuBTC towards water vapor is much stronger than the observed affinity to methanol. This observation confirms earlier studies[36]. However, the response time was longer towards water than methanol ($\tau_{0.5,\ water}$ = ~480 s (data not shown), $\tau_{0.5,\ methanol}$ = ~85 s). For lower methanol concentrations (~100 ppm) similar results related to reversibility and reproducibility were found (Figs. S10-S13 (page 71-72), Supporting information, Section 7).

The methanol adsorption by the CuBTC framework also changes the effective local dielectric constant (ε_e). This ε_e was approximated utilizing the Bruggeman effective medium approximation[47] which is based on changes in the volumetric fraction(f) (Supporting information, Section 6). The relative static dielectric constant of CuBTC[40] (in vacuum) was assumed to be ε_r = 1.7. It can be seen in Figure 3(v) that the calculated ε_e roughly increases from ~1.5 to ~2.7 on exposure from 0 to 8000 ppm of methanol (ε_r = 32.7). The calculated capacitance (by finite element modeling) for these dielectric

constant changes indicated correspondence with the measured capacitance changes confirming the role of changes in local polarity on the adsorption of polar molecules like methanol. Finally, the simulated electric field strength of these MOF-modified electrodes indicated a slight decrease with this increase of ε_r to 2.7 (Figure 3(vi), S14-S15 (page 73-74), Supporting information).

3.4. Conclusions

In summary, we have demonstrated successfully the feasibility of electrochemical grown CuBTC MOFs on Cu IDEs. These devices show a fast response (120-150 s to approach equilibrium for methanol sensing), are sensitive and have reversible sensing properties useful for the quantitative detection of methanol and water vapor in the 100-8000 ppm range. The time-dependent responses were successfully simulated by the diffusion controlled kinetics. Equilibrium capacitive responses also followed the Langmuir adsorption model with an affinity constant of 174 bar^{-1} for methanol concentrations up to 8000 ppm. Comparative sensing studies with methanol and water indicated higher sensitivity towards water due to its stronger affinity to the CuBTC. Theoretical estimations of the local dielectric constants by application of the Bruggeman approximation, indicated that on the exposure to different methanol vapor concentrations (0-8000 ppm), the relative dielectric constant of partially filled CuBTC increases from ~1.5 to ~2.7 as a result of the uptake of methanol. The calculated capacitance changes correlate well with the experimentally observed data, supporting our applied methods. In conclusion, we have shown that CuBTC MOFs can be formed *in situ* electrochemically on micro-structured copper IDEs in a fast and easy way. These devices act as fast, reversible and sensitive sensors for the quantitative detection of methanol and water vapor in the range of 100 to 8000 ppm. With ability to measure near room temperature and possibility to synthesize MOFs with enhanced selectivity, this study can be a useful step towards developing MOF-based sensor devices.

References

[1] C. Hagleitner, A. Hierlemann, D. Lange, A. Kummer, N. Kerness, O. Brand, H. Baltes, *Nature* **2001**, *414*, 293-296.

[2] X.-J. Huang, Y.-K. Choi, *Sensors and Actuators B: Chemical* **2007**, *122*, 659-671.

[3] D. R. Miller, S. A. Akbar, P. A. Morris, *Sensors and Actuators B: Chemical* **2014**, *204*, 250-272.

[4] Y.-F. Sun, S.-B. Liu, F.-L. Meng, J.-Y. Liu, Z. Jin, L.-T. Kong, J.-H. Liu, *Sensors* **2012**, *12*, 2610.

[5] F.-Y. Yi, D. Chen, M.-K. Wu, L. Han, H.-L. Jiang, *ChemPlusChem* **2016**, *81*, 675-690.

[6] D. J. Wales, J. Grand, V. P. Ting, R. D. Burke, K. J. Edler, C. R. Bowen, S. Mintova, A. D. Burrows, *Chemical Society Reviews* **2015**, *44*, 4290-4321.

[7] I. Stassen, B. Bueken, H. Reinsch, J. F. M. Oudenhoven, D. Wouters, J. Hajek, V. Van Speybroeck, N. Stock, P. M. Vereecken, R. Van Schaijk, D. De Vos, R. Ameloot, *Chemical Science* **2016**, *7*, 5827-5832.

[8] A. U. Czaja, N. Trukhan, U. Muller, *Chemical Society Reviews* **2009**, *38*, 1284-1293.

[9] Z. Hu, B. J. Deibert, J. Li, *Chemical Society Reviews* **2014**, *43*, 5815-5840.

[10] M. G. Campbell, D. Sheberla, S. F. Liu, T. M. Swager, M. Dincă, *Angewandte Chemie* **2015**, *127*, 4423-4426.

[11] S. Achmann, G. Hagen, J. Kita, I. Malkowsky, C. Kiener, R. Moos, *Sensors* **2009**, *9*, 1574.

[12] S. Sachdeva, D. Soccol, D. J. Gravesteijn, F. Kapteijn, E. J. R. Sudhölter, J. Gascon, L. C. P. M. de Smet, *ACS Sensors* **2016**.

[13] H. Gliemann, C. Wöll, *Materials Today* **2012**, *15*, 110-116.

[14] L. Heinke, M. Tu, S. Wannapaiboon, R. A. Fischer, C. Wöll, *Microporous and Mesoporous Materials* **2015**, *216*, 200-215.

[15] C. Sapsanis, H. Omran, V. Chernikova, O. Shekhah, Y. Belmabkhout, U. Buttner, M. Eddaoudi, K. Salama, *Sensors* **2015**, *15*, 18153.

[16] H. K. Arslan, O. Shekhah, J. Wohlgemuth, M. Franzreb, R. A. Fischer, C. Wöll, *Advanced Functional Materials* **2011**, *21*, 4228-4231.

[17] I. Stassen, M. Styles, G. Grenci, H. V. Gorp, W. Vanderlinden, S. D. Feyter, P. Falcaro, D. D. Vos, P. Vereecken, R. Ameloot, *Nat Mater* **2016**, *15*, 304-310.

[18] W.-J. Li, M. Tu, R. Cao, R. A. Fischer, *Journal of Materials Chemistry A* **2016**, *4*, 12356-12369.

[19] N. Campagnol, T. R. C. Van Assche, M. Li, L. Stappers, M. Dinca, J. F. M. Denayer, K. Binnemans, D. E. De Vos, J. Fransaer, *Journal of Materials Chemistry A* **2016**, *4*, 3914-3925.

[20] I. Stassen, M. Styles, T. Van Assche, N. Campagnol, J. Fransaer, J. Denayer, J.-C. Tan, P. Falcaro, D. De Vos, R. Ameloot, *Chemistry of Materials* **2015**, *27*, 1801-1807.

[21] B. Van de Voorde, R. Ameloot, I. Stassen, M. Everaert, D. De Vos, J.-C. Tan, *Journal of Materials Chemistry C* **2013**, *1*, 7716-7724.

[22] M. Beidaghi, Y. Gogotsi, *Energy & Environmental Science* **2014**, *7*, 867-884.

[23] G. Oskam, J. G. Long, A. Natarajan, P. C. Searson, *Journal of Physics D: Applied Physics* **1998**, *31*, 1927.

[24] S. Sachdeva, A. Pustovarenko, E. J. R. Sudholter, F. Kapteijn, L. C. P. M. de Smet, J. Gascon, *CrystEngComm* **2016**, *18*, 4018-4022.

[25] A. Martinez Joaristi, J. Juan-Alcañiz, P. Serra-Crespo, F. Kapteijn, J. Gascon, *Crystal Growth & Design* **2012**, *12*, 3489-3498.

[26] N. F. Sheppard, R. C. Tucker, C. Wu, *Analytical Chemistry* **1993**, *65*, 1199-1202.

[27] U. Altenberend, F. Molina-Lopez, A. Oprea, D. Briand, N. Bârsan, N. F. De Rooij, U. Weimar, *Sensors and Actuators B: Chemical* **2013**, *187*, 280-287.

[28] Y. Lu, J. Li, J. Han, H. T. Ng, C. Binder, C. Partridge, M. Meyyappan, *Chemical Physics Letters* **2004**, *391*, 344-348.

[29] P. Oikonomou, A. Salapatas, K. Manoli, K. Misiakos, D. Goustouridis, E. Valamontes, M. Sanopoulou, I. Raptis, G. P. Patsis, *Procedia Engineering* **2011**, *25*, 423-426.

[30] C. L. Yaws, *The Yaws handbook of vapor pressure: Antoine coefficients*, Gulf Professional Publishing, **2015**.

[31] G. W. Thomson, *Chemical Reviews* **1946**, *38*, 1-39.

[32] R. Igreja, C. J. Dias, *Sensors and Actuators A: Physical* **2004**, *112*, 291-301.

[33] R. Igreja, C. J. Dias, *Sensors and Actuators B: Chemical* **2006**, *115*, 69-78.

[34] S. S.-Y. Chui, S. M.-F. Lo, J. P. H. Charmant, A. G. Orpen, I. D. Williams, *Science* **1999**, *283*, 1148-1150.

[35] T. R. C. Van Assche, G. Desmet, R. Ameloot, D. E. De Vos, H. Terryn, J. F. M. Denayer, *Microporous and Mesoporous Materials* **2012**, *158*, 209-213.

[36] S. Calero, P. Gómez-Œlvarez, *The Journal of Physical Chemistry C* **2015**, *119*, 467-472.

[37] P. Davydovskaya, A. Ranft, B. V. Lotsch, R. Pohle, *Analytical Chemistry* **2014**, *86*, 6948-6958.

[38] M. S. Hosseini, S. Zeinali, M. H. Sheikhi, *Sensors and Actuators B: Chemical* **2016**, *230*, 9-16.

[39] A. Vishnyakov, P. I. Ravikovitch, A. V. Neimark, M. Bülow, Q. M. Wang, *Nano Letters* **2003**, *3*, 713-718.

[40] K. Zagorodniy, G. Seifert, H. Hermann, *Applied Physics Letters* **2010**, *97*, 251905.

[41] E. Redel, Z. Wang, S. Walheim, J. Liu, H. Gliemann, C. Wöll, *Applied Physics Letters* **2013**, *103*, 091903.

[42] P. P. Sahay, R. K. Nath, *Sensors and Actuators B: Chemical* **2008**, *134*, 654-659.

[43] T. R. C. Van Assche, T. Duerinck, J. J. Gutiérrez Sevillano, S. Calero, G. V. Baron, J. F. M. Denayer, *The Journal of Physical Chemistry C* **2013**, *117*, 18100-18111.

[44] R. Subramanian, V. Lakshminarayanan, *Electrochimica Acta* **2000**, *45*, 4501-4509.

[45] F.-C. Wu, R.-L. Tseng, R.-S. Juang, *Chemical Engineering Journal* **2009**, *153*, 1-8.

[46] Y. Wu, H. Chen, J. Xiao, D. Liu, Z. Liu, Y. Qian, H. Xi, *ACS Applied Materials & Interfaces* **2015**, *7*, 26930-26940.

[47] K. Lazarova, B. Georgieva, M. Spasova, T. Babeva, *Journal of Physics: Conference Series* **2014**, *558*, 012042.

Sensitive and Reversible Detection of Methanol and Water Vapor by *in-situ* Electrochemically Grown CuBTC MOFs on Interdigitated Electrodes

Supporting Information

1. *Device Fabrication*

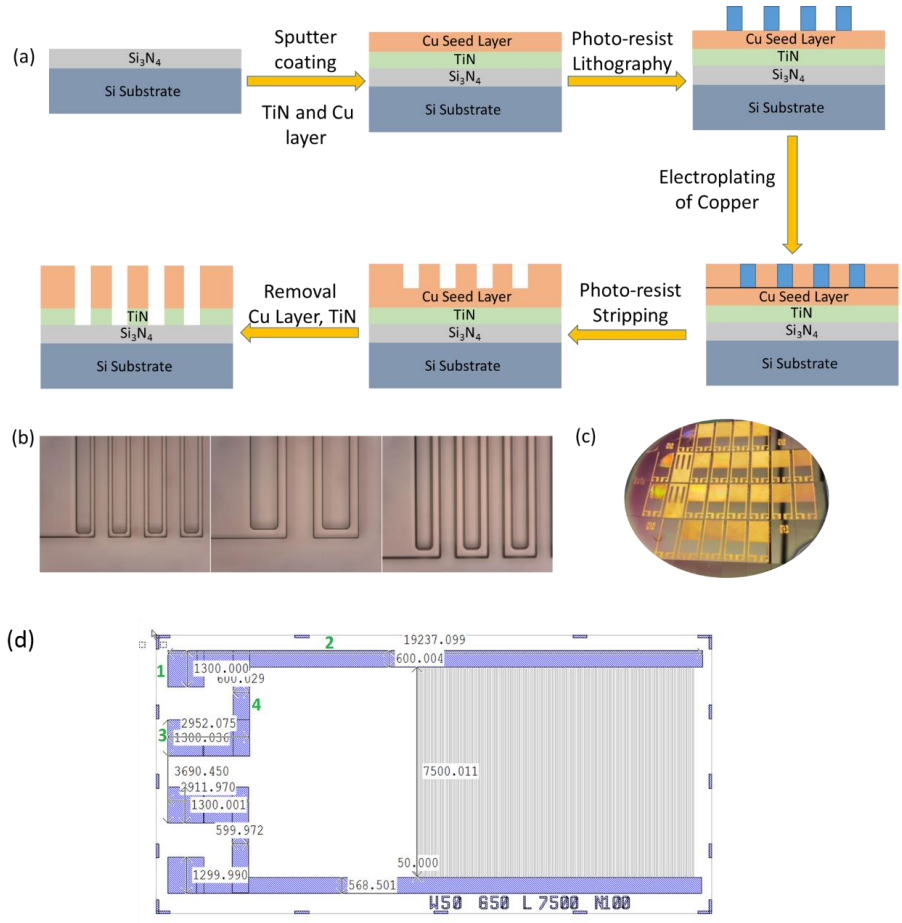

Figure S1. *(a) Schematic of the fabrication process for the Cu-interdigitated electrode devices. (b) Lithographic pattern of the Cu-IDE structure. (c) Optical image of the fabricated devices (d) Cu IDE layout with dimensions in µm indicating width (W) and gap (G) of 50 µm each and number of electrodes (N) of 100.*

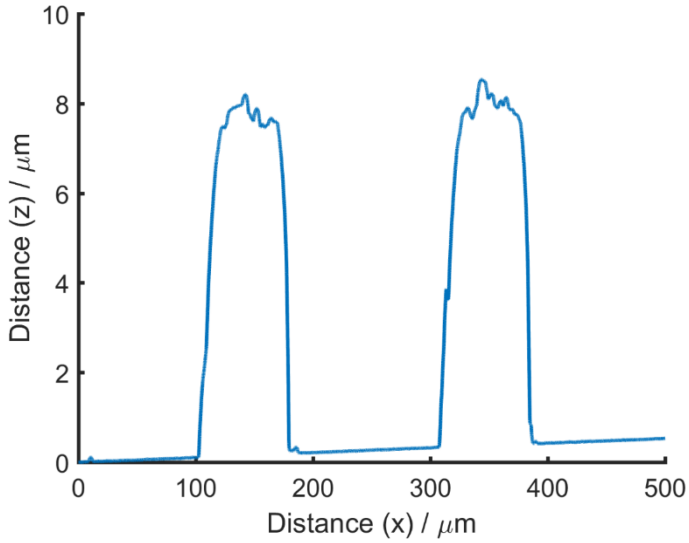

Figure S2. *DEKTAK 8 profilometer data of the reference points (width of 80 μm and gap of 130 μm) on the bare IDE with a width = 50 μm, a gap = 20 μm and a height of 7-8 μm. The measurement was done over the reference points (not over the electrodes) in IDE structure to avoid damage to the device.*

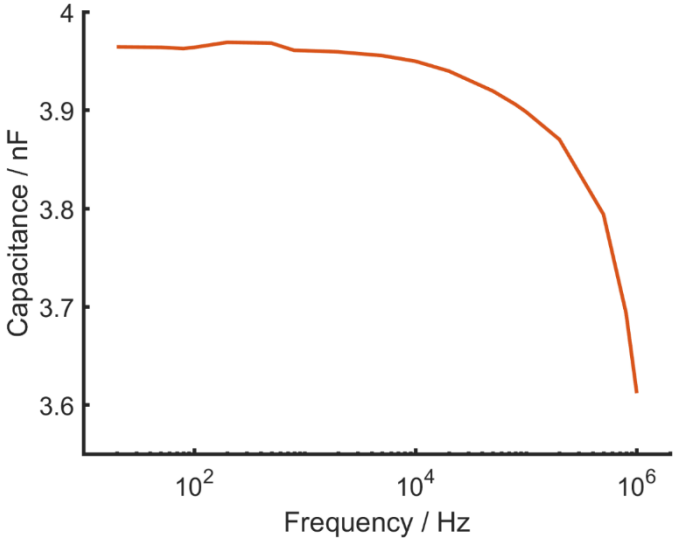

Figure S3. *Measured capacitance of the non-coated IDE with width and gap of 50 μm each at different frequencies.*

2. Calculation of the parasitic contribution of the devices

Parasitic contribution in the IDE structure is mainly introduced by the substrate and can be approximated using the following standard capacitance equation:

$$C = \frac{\varepsilon_0 \varepsilon_r A}{t} \tag{9}$$

where ε_r is the dielectric constant of Si_3N_4 layer ($\varepsilon_r = 9.7$) and A is the area and the t (= 500 nm) is the thickness of the electrode regions. There are 4 components in the IDE structure which contribute for the capacitance in parallel to the capacitance of the IDE structure (labeled 1-4 in Figure S1d). These components are classified as (1) Square bond pads (0.2932 nF), (2) Side electrode lines (1.8677 nF), (3) 2nd Bond Pad (0.666 nF) and (4) Connecting electrode line (0.2083 nF). The total parasitic contribution from both finger electrodes was calculated to be 3.06 nF. The difference between the calculated capacitance with the measured capacitance can be attributed to the parasitic from the soldered wiring.

3. Electrochemical synthesis of CuBTC

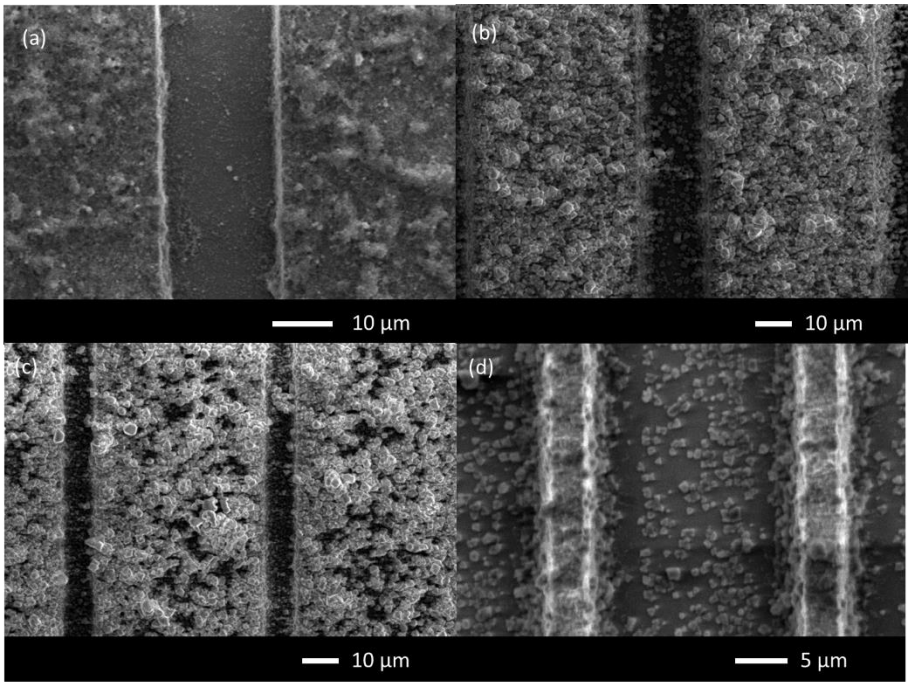

Figure S4. *Electrochemical synthesis of CuBTC over IDEs prepared with negative photoresist and different dimensions. SEM micrograph of (a) a bare IDE, (b) CuBTC coated device with width and gap of 50 µm and 20 µm, respectively, (c) the coated IDEs with width and gap of 50 µm and 10 µm, respectively and (d) the coated IDEs the width and gap of 5 µm and 20 µm, respectively.*

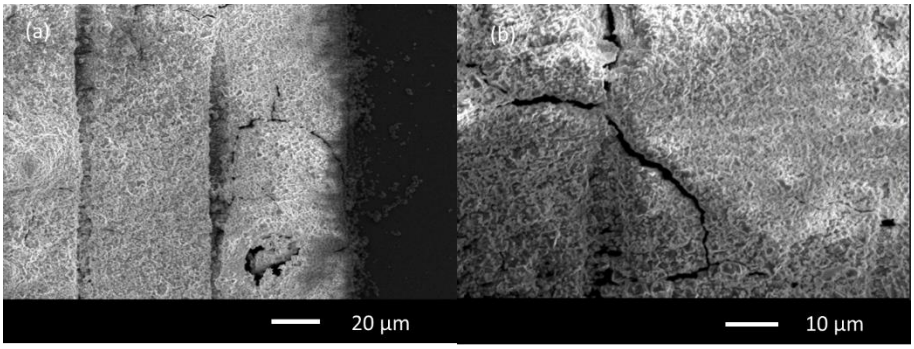

Figure S5. *SEM micrographs indicating crack formation in the CuBTC layer over synthesis for longer duration (7.5 min). (a) and (b) show two different regions of a CuBTC-coated IDE at different magnifications.*

4. Electrical characterization after MOF deposition

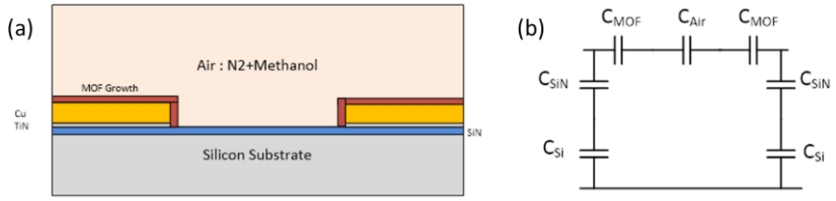

Figure S6*. (a) Schematic of the IDEs representing the IDE device after the MOF growth. (b) Equivalent circuit for the device with capacitive contribution from both the MOF layer and air.*

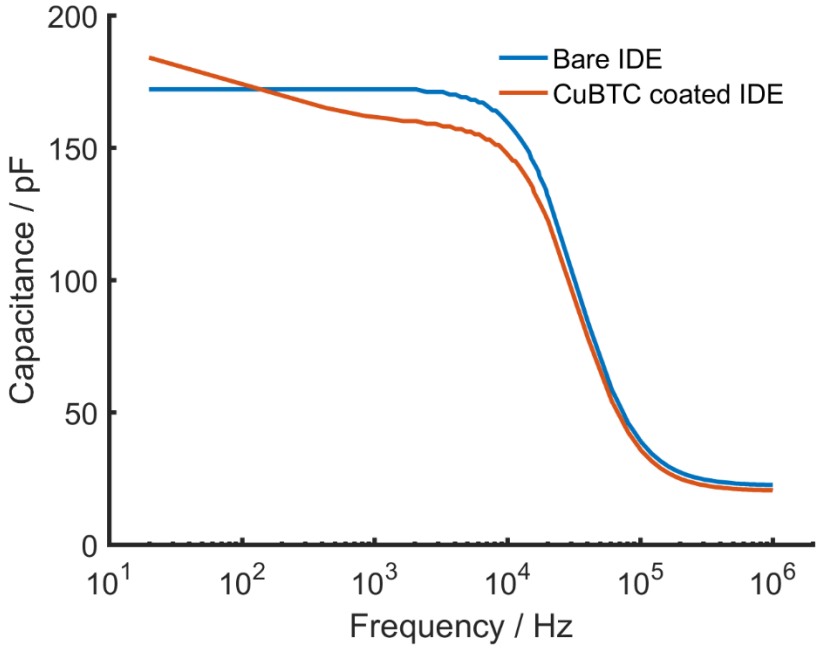

Figure S7*. Calculated capacitance for bare IDE and CuBTC-coated IDE with width and gap of 50 µm each over the frequency range of 20 Hz to 1 MHz.*

5. *Kinetic analysis for the CuBTC coated sensor devices*

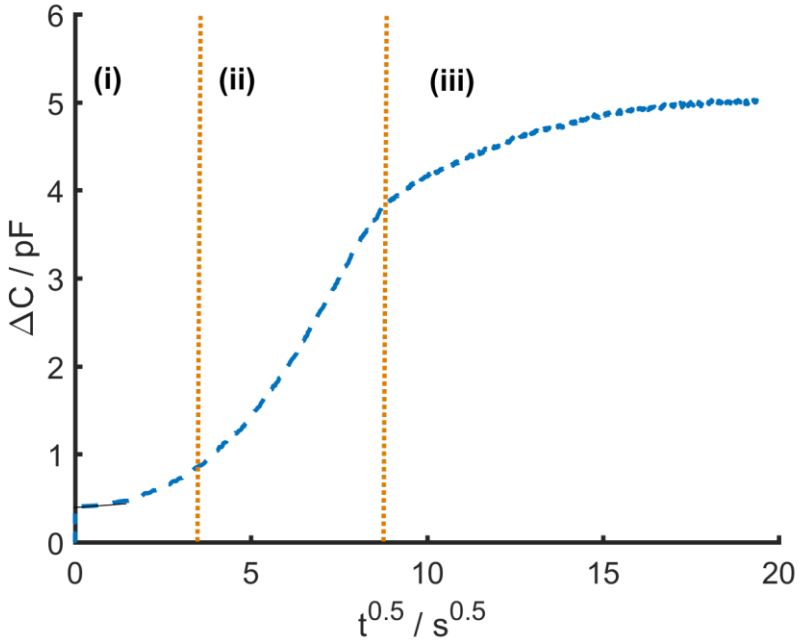

Figure S8*. Observed capacitive response of CuBTC coated IDE towards methanol represented as a function of* $t^{0.5}$ *to correlate with the Intraparticle diffusion-limited kinetic model. (i) accounts for the evolution to the steady state in the measurement chamber, (ii) represents the diffusion-controlled regime and (iii) denotes the equilibrium stage.*

6. Theoretical estimation of changes in the dielectric constant

In order to estimate the changes in the dielectric constant of the layer, first the amount of the MOF deposited on the IDEs was estimated based on the measured thickness across the dimensions of the electrode.

$$m_{\mathrm{CuBTC}} = (V_{\mathrm{CuBTC+IDE}} - V_{\mathrm{IDE}}) \times \rho \qquad (10)$$

Where m_{CuBTC} is the mass of the CuBTC deposited on top of the electrodes, $V_{\mathrm{CuBTC+IDE}}$ is the total volume of the coated IDEs and V_{IDE} represents the volume of the electrodes.

Assuming the Langmuir behaviour in the measured concentration range, the total number of moles of methanol adsorbed inside the pores of MOF was estimated utilizing the parameters listed in Table S1. This amount of methanol was then converted into volume fraction with the assumption of rigid MOF structure and replacement of air by methanol.

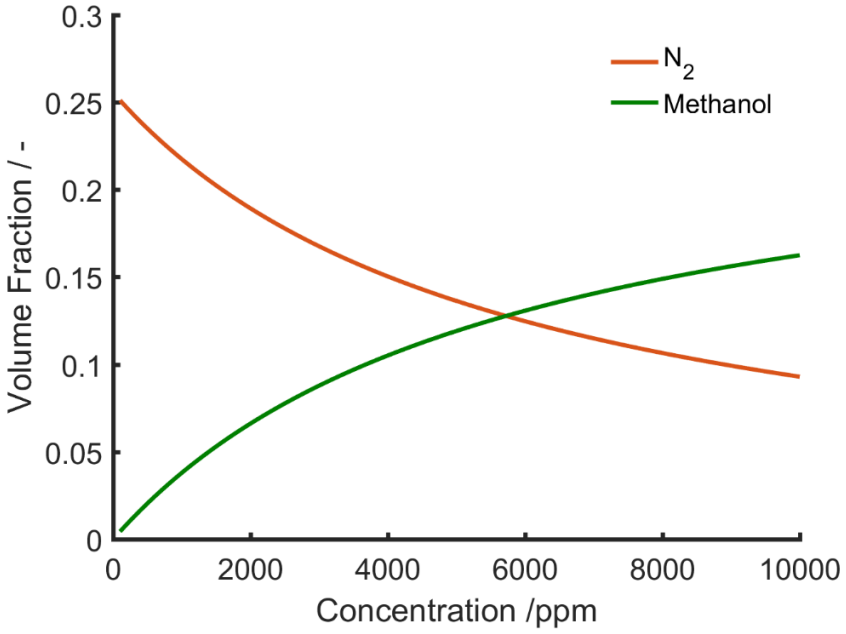

Figure S9. *Changes in the volume fraction of methanol and N_2 in the pores of MOF over the exposure to different concentrations of methanol.*

For a porous structure like present in CuBTC, the effective dielectric constant (ε_e) can be approximated utilizing the Bruggeman effective medium approximation[1] based on these changes in the volumetric fraction(f):

$$f_{CuBTC}\left(\frac{\varepsilon_{CuBTC}-\varepsilon_e}{\varepsilon_{CuBTC}+2\varepsilon_e}\right)+f_{N_2}\left(\frac{\varepsilon_{N_2}-\varepsilon_e}{\varepsilon_{N_2}+2\varepsilon_e}\right)+f_{MeOH}\left(\frac{\varepsilon_{MeOH}-\varepsilon_e}{\varepsilon_{MeOH}+2\varepsilon_e}\right)=0 \quad (11)$$

$$f_{CuBTC}+f_{N_2}+f_{MeOH}=1 \quad (12)$$

All the parameters used for the calculations are listed in Table S1. The static dielectric constant of CuBTC[2] (without air) was assumed to be 1.7.

Table S1. *Parameters used for calculation of the dielectric constant.*

Parameters	**Value**
P_{atm}	101325 Pa
R	8.3145 m^3Pa/K mol
Temperature	303 K
Number of electrodes (N)	100
Length of the electrode	7.5e-3 m
Width of the electrode	46e-6 m
Thickness of the electrode	3e-6 m
Length of the electrode with MOF	7.5e-3 m
Width of the electrode with MOF	56e-6 m
Thickness of the electrode with MOF	8e-6 m
Saturation amount of MeOH	0.64 g/g
K, equilibrium constant	174.8 bar^{-1}
Bulk Density of CuBTC[a]	0.35 g/cm^3
Pore Volume of CuBTC[3]	0.731 cm^3/g
Dielectric Constant of CuBTC[2]	1.7
Dielectric Constant of Methanol	32.7
Dielectric Constant of air	1

[a]Data from Sigma Aldrich

7. *Additional sensing studies of CuBTC-coated devices*

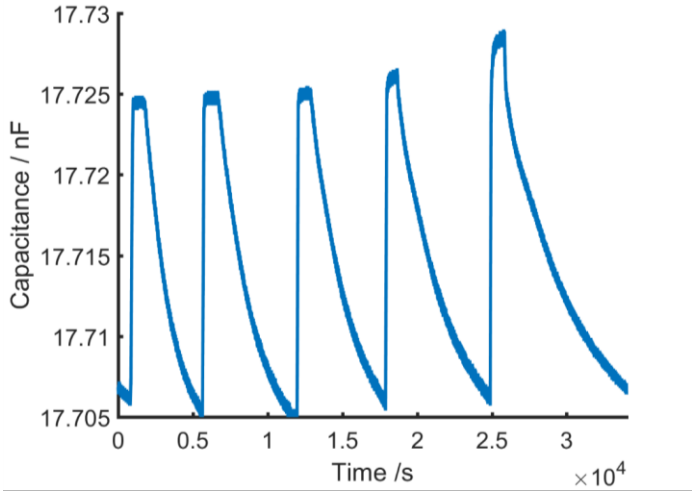

Figure S10. *Capacitive response of a CuBTC-coated IDE with a width and a gap of 50 µm each prepared with negative photoresist towards methanol. From left to right, the reversible steps of the capacitive response indicate adsorption and desorption of 1000, 2000, 3000, 5000 and 8000 ppm of methanol respectively.*

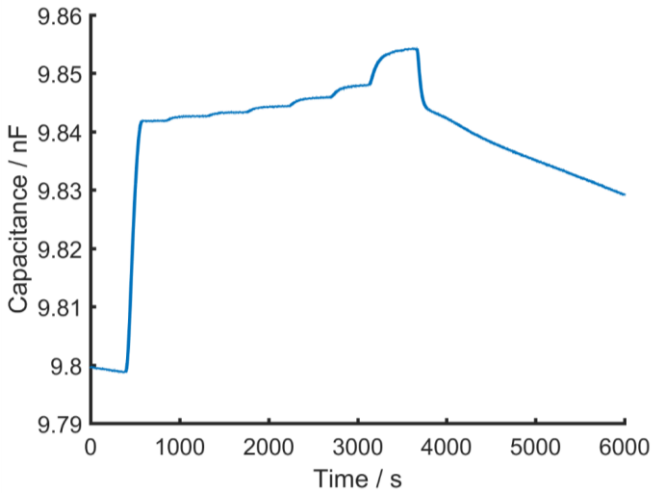

Figure S11. *Capacitive response of CuBTC coated IDE with a width of 5 µm and a gap of 50 µm prepared with negative photoresist. The steps, from left to right, indicate the response to the change in concentration of methanol from 1000, 2000,*

3000, 4000, 5000, 6000 and 8000 ppm respectively. The decrease in capacitance at t ≥ ~3700 indicates the response over removal of methanol from the dry N_2

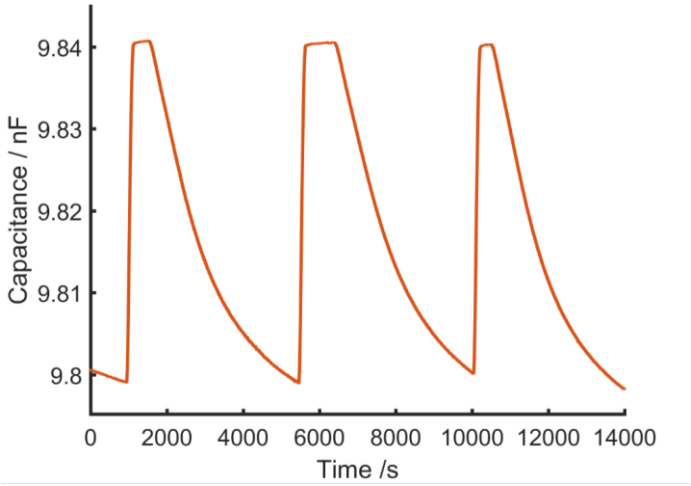

Figure S12. *Repeatability study of CuBTC-coated devices (width 5 µm and gap 50 µm) over the exposure to 1000 ppm of methanol.*

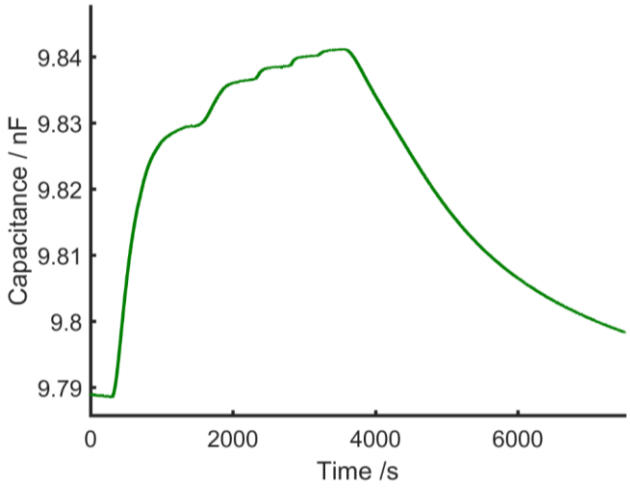

Figure S13*. Capacitive response of CuBTC-coated IDE (width 5 µm and gap 50 µm) prepared with negative photoresist over exposure to the steps of 100, 300, 500, 1000 and 2000 ppm of methanol respectively (from left to right).*

8. Theoretical calculations of changes in electric field strength

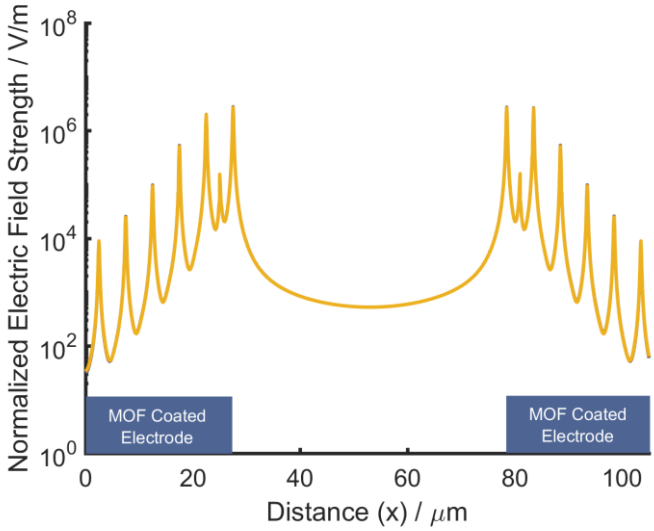

Figure S14. *Distribution of the electrical field strength across the x-axis over the IDEs in a geometry of half-spatial wavelength. (λ/2).*

The changes in the dielectric constant over changes in the methanol concentration also result in changes in the electric field. A higher dielectric constant lead to a slight reduction in the electric field strength due to increase in the charge storage (Figure S15 (page 74)).

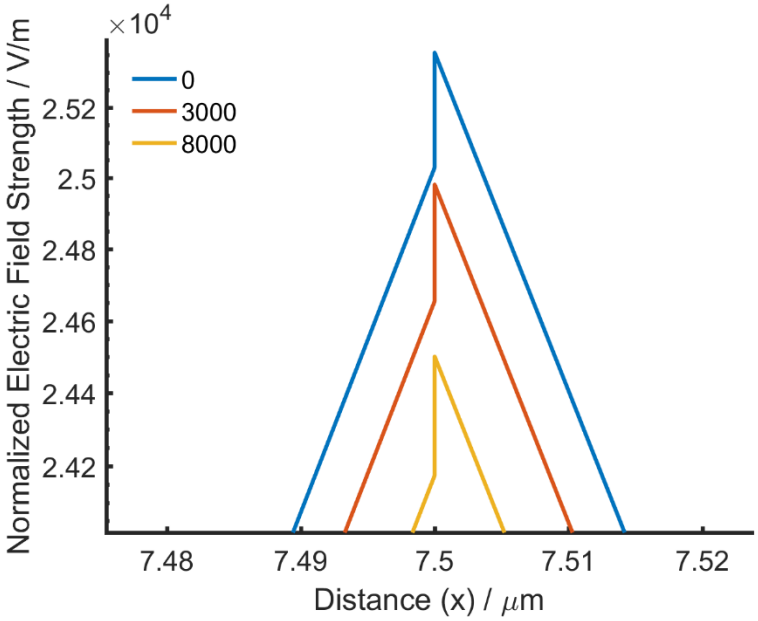

***Figure S15**. Distribution of the electrical field strength at a localized position over the increase in concentration of methanol (0-8000 ppm).*

9. Sensing investigation of CuTATB coated devices

Sensor devices were also prepared with an alternative Cu-based MOF, CuTATB[1] to demonstrate the flexibility of the electrochemical deposition of MOFs (Figure S16). Sensing studies with these devices on the exposure to methanol also indicated the reversible behavior. The response sensitivity for CuTATB-coated devices was observed to be lower compared with that for CuBTC with capacitive change of ~0.3 pF and ~5.5 pF, respectively over exposure to 1000 ppm of methanol. Even though these devices require further investigation, this behavior can be attributed to the hydrophobic nature of the linker (H_3TATB) and the partially interpenetrated framework[4].

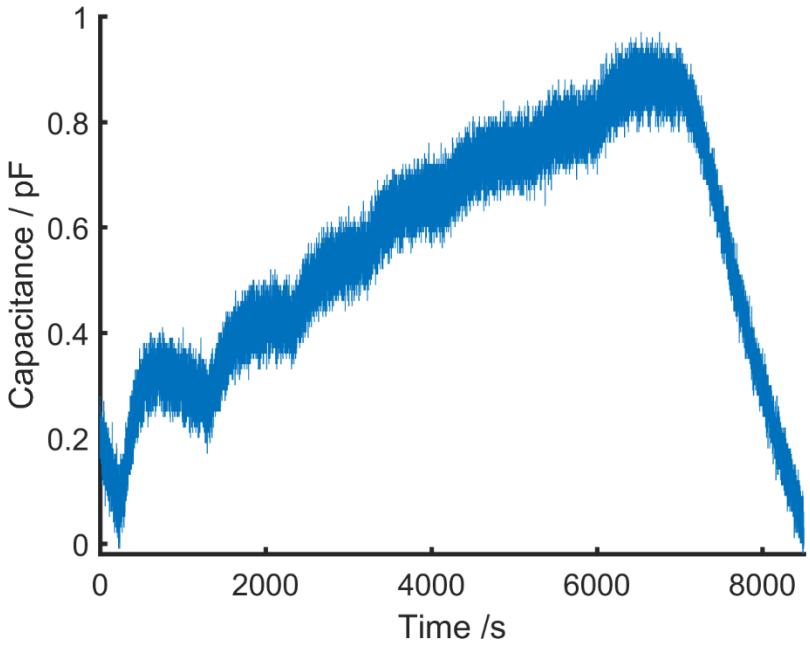

Figure S16. *Capacitive response of CuTATB coated device (with a width and a gap of 50 µm) towards different concentrations of methanol. The steps indicate response over exposure to 1000, 2000, 3000, 4000, 5000, 6000 and 8000 ppm of methanol respectively (from left to right).*

References:

[1] K. Lazarova, B. Georgieva, M. Spasova, T. Babeva, *Journal of Physics: Conference Series* **2014**, *558*, 012042.

[2] K. Zagorodniy, G. Seifert, H. Hermann, *Applied Physics Letters* **2010**, *97*, 251905.

[3] T. R. C. Van Assche, T. Duerinck, J. J. Gutiérrez Sevillano, S. Calero, G. V. Baron, J. F. M. Denayer, *The Journal of Physical Chemistry C* **2013**, *117*, 18100-18111.

[4] S. Sachdeva, A. Pustovarenko, E. J. R. Sudholter, F. Kapteijn, L. C. P. M. de Smet, J. Gascon, *CrystEngComm* **2016**, *18*, 4018-4022.

Chapter 4

Polymer-Metal Organic Framework Composite Films as Affinity Layer for Capacitive Sensor Devices

This chapter is based on the following publication:

S. Sachdeva, D. Soccol, D. J. Gravesteijn, F. Kapteijn, E. J. R. Sudhölter, J. Gascon, L. C. P. M. de Smet, *ACS Sensors* 2016, 1, 1188–1192.

Abstract

We report a simple method for sensor development using polymer-MOF composite films. Nanoparticles of NH_2-MIL-53(Al) dispersed in a Matrimid® polyimide were applied as a thin film on top of capacitive sensor devices with planar electrodes. These drop-cast films act as an affinity layer. Sensing studies carried out with methanol vapor using impedance spectroscopy demonstrate that the presence of MOF enhances the overall response and lowers the detection limit compared to MOF-free polymer films and bare devices. This can be understood by additional changes of the local polarity of the composite films due to higher adsorption of methanol by the porous MOF particles. We expect that this work will stimulate the design of composite polymeric affinity layers for a range of analytes by a proper choice of dispersed MOF particles.

4.1. Introduction

Metal-Organic Frameworks (MOFs) are porous crystalline materials comprising metal nodes coordinated to organic moieties[1-2]. The selective gas adsorption, structural tunability and high porosity of MOFs suggest a high potential for chemical sensing applications[3-4]. Changes in the physical, chemical or electrical properties of these upon the—ideally specific—interaction with an analyte can be used for detection purposes[5]. Most of the current methods for MOF-based sensing devices are focused on utilizing changes in their luminescent properties and were performed on just MOF powders rather than on real devices[6-7]. On the other hand, only a few studies have been reported focusing on using MOFs for gas detection using electrical detection methods[8-9]. One of the main reasons for the rather slow pace of development in this area is the lack of synthetic methods to integrate MOFs with transducers in a compatible and cost-effective manner[10].

Recent advances show possibilities of the formation of electrically conductive MOF thin films, in which the change of conductance upon analyte uptake is measured[5, 11-13]. Also, studies focusing conductive 2D MOF structures for chemiresistive sensing have clearly shown the potential of MOF materials in sensor applications[14-15]. However, only a limited number of building blocks with a high charge mobility through the MOF scaffold have resulted so far in a very small number of suitable 2D structures[11, 16]. In general, 3D MOFs have insulating electrical properties[13]. In view of these issues, instead of detection of changes in the electrical conductance, detection of changes in the electrical capacitance is likely a more promising transduction method. In such systems, MOF particles can be dispersed in a polymeric matrix on top of (interdigitated) electrodes.

In membrane separation processes, the incorporation of MOFs and other (nano)particles in polymer matrices has shown to improve the separation properties[17-18]. The presence of an organic linker in MOFs makes them suitable for application in polymer matrices, and these mixed matrix membranes (MMMs) show selective and enhanced gas permeability[17].

In this study, we report a simple method for sensor development using polymer-MOF composite films. These films act as a selective affinity layer

that can be easily deposited onto electrical capacitance transducers. Use of a polymer-based system allows an easy integration and is compatible with existing fabrication techniques currently applied in the microelectronics industry[19-21]. Moreover, use of these composite materials allows the utilization of the gas permeability and adsorption properties of the composite films for the detection of a range of analytes. The affinity of a MOF for a specific gas will lead to changes in the electrical properties of the coated layer, which can be monitored *in-situ*.

To enable easy integration with the microelectronic industry, the transducer devices were made from a typical 140 nm CMOS (CMOS14)[22] platform. In more detail, the devices were processed using photo-lithography techniques to obtain planar aluminum (Al) electrodes on top. These planar electrodes were patterned as 4 parallel meandering lines with 0.52 µm wide lines (W) with a spacing of 1 µm (G) (Figure 1a, S2 (page 97), Section 4.2.3). The presence of 4 parallel meander lines allows electric field lines to exist between any pair of oppositely charged electrodes upon application of an electrical voltage difference (Figure 1a, S3 (page 98)). These field lines get modified due to the presence of an affinity layer as a result of changes in local polarity and the dielectric constant. Analytical studies indicate that maximum sensitivity towards changes in surrounding is observed with affinity layer thickness above half of the spatial wavelength λ of the device ($\lambda=2(W+G)$),[23-24] which is just over 3 µm in this case. Affinity layer thicknesses (10 µm in our study) above this value will ensure higher responses of the device with insensitivity towards deposition variations. Moreover, the large electrode area (~2.1 mm^2)—achieved by a meander pattern and small gap size—contributes to the observed sensitivity of the device, which resulted in a relatively high intrinsic capacitance (~22 pF).

For the synthesis of the composite films, Matrimid® 5218 was chosen as the polymer matrix (Figure S1 (page 97), S5 (page 99)). Its high thermal (T_g = ~300 °C) and mechanical stability, commercial availability and its well-studied compatibility with MOFs [25-26] make this polymer a logical candidate for proof-of-principle sensing studies. Further, the selected MOF, NH_2-MIL-53(Al) is one of the most well-characterized MOFs and has shown good

compatibility and selectivity enhancement in membrane separations, when dispersed in Matrimid® 5218[25].

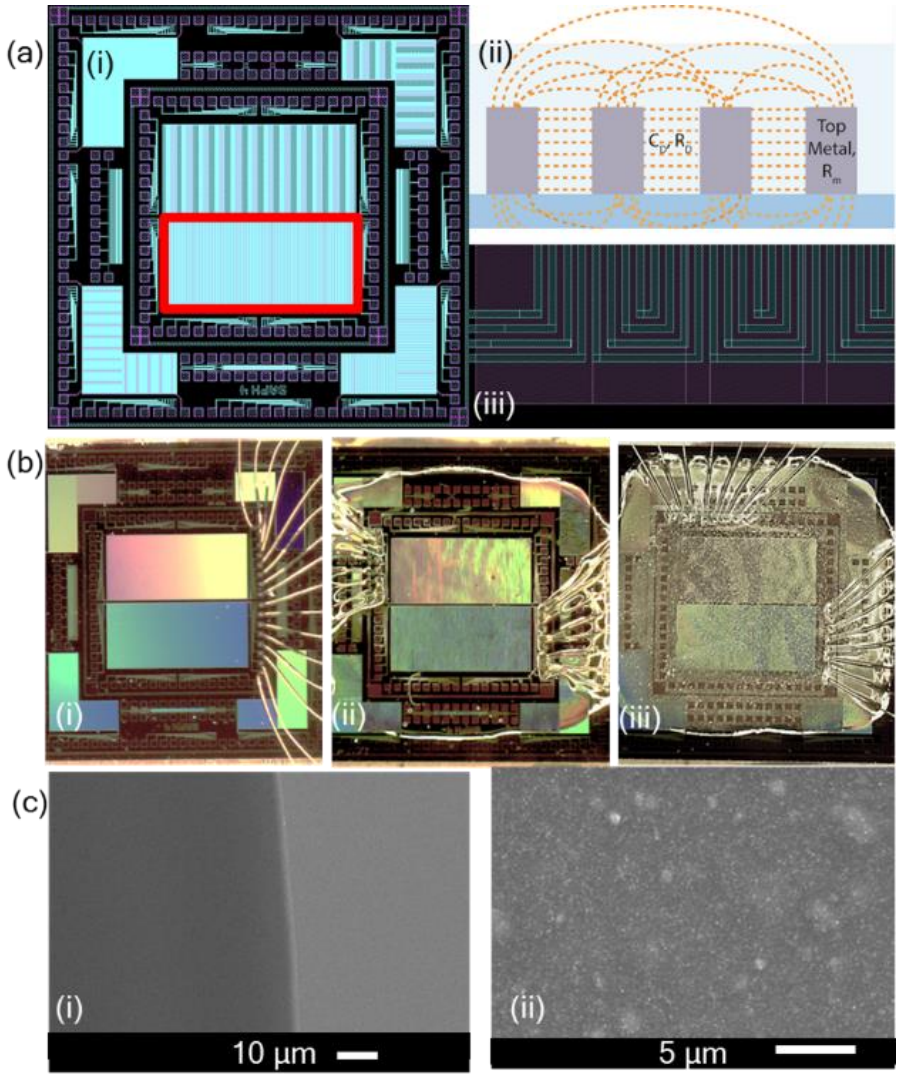

Figure 1*. (a, i) Top view optical image of showing the overall lay out of the bare device, highlighting the active area of sensing (red box); (a, ii) schematic cross section of 4 Al planar electrodes, including a qualitative field line pattern; (a, iii) detailed optical image showing the meander structure. (b) Optical images of the (i) bare device, and devices coated with (ii) Matrimid® polyimide and (iii) Matrimid® and MOF (20*

wt.%) showing good coverage of the sensing area. (c) SEM micrographs of coated layers on a silicon substrate: (i) polymer (dark area) and uncoated region of the Si substrate (light area), and (ii) MOF-Matrimid® composite layer casted on the Si substrate.

4.2. Experimental Details

Matrimid® 5218 Polyimide (Figure S1 (page 97)) was supplied by Huntsman Advanced Materials. All other chemicals, including solvents, were purchased from Sigma Aldrich and used as received.

4.2.1. Synthesis of NH_2-MIL-53(Al) MOF

NH_2-MIL-53(Al) nanoparticles were synthesized by conventional hydrothermal treatment: 1.902 g of 2-aminoterephthalic acid (99% purity) was dissolved in 10.5 mL of a 2.0 M aq. NaOH solution at room temperature and the volume was increased to 75 mL after dissolution. 3.935 g of $Al(NO_3)_3.9H_2O$ (99% purity) was dissolved in 75 mL of distilled water in a separate tube. Both solutions were mixed and the synthesis mixture was then treated at 393 K for 3 days under reflux conditions. The resulting material was filtered under vacuum and washed with ethanol. To efficiently remove the unreacted linker present in the MOF pores, the synthesized material was washed in DMF and methanol consecutively at 403 K and 363 K overnight, respectively. Finally, the powder was filtered and washed with ethanol and dried at 373 K in vacuum overnight.

4.2.2. Preparation of Coatings

Polyimide (PI) Matrimid® 5218 was pretreated at 453 K overnight under vacuum to remove the adsorbed water. 6 wt. % solution of 20 wt. % MOF and polymer in tetrahydrofuran (THF) was made to prepare the 10 µm thick coated films. First, 12 mg of MOF particles was dispersed in 940 mg of THF by ultrasonication for 15 min. Then 48 mg of PI was added to this suspension and stirred overnight, leading to a viscous solution. For MOF-free polyimide coatings, 60 mg of PI was dissolved in 940 mg of THF and stirred overnight. Before the deposition of the solutions over devices and reference silicon substrates, the solutions were subjected to three alternative cycles of ultrasonication and mixing of 15 min, each to ensure good dispersion of MOF particles. The dispersed solution was then cast over the reference substrate and transducer devices with 5 µl drops in a solvent-saturated environment in

order to slow down the natural evaporation of THF. This ensures that the formed coatings do not crack and remain uniform upon evaporation of THF. Once dried, the coated devices were treated at 453 K in vacuum for 4 h.

4.2.3. Device Fabrication

The short-loop structures consisted of a metal and dielectric stack to mimic the final layer of a typical CMOS14 back-end stack. Before processing the short-loop structures, Si_3N_4 was deposited on the back side of the p-doped Si wafer to avoid contamination of the Si during wet cleaning steps. A high-density plasma CVD silicon oxide (with a thickness of 3 µm) was deposited, mimicking the inter-metal dielectric, followed by the deposition of the metal stack. The bottom layers consisted of 25/25 nm Ti/TiN bilayer. It was followed by 800 nm thick aluminum layer and the 50 nm top layer of TiN. The bottom and top Ti/TiN and TiN layers were introduced to improve adhesion, decrease reflectivity and function as a stopping layer for etching processes. Afterwards, the Al metal layer for the device was patterned with lithography targeting 0.52 µm wide lines and a spacing of 1 µm (1.52 µm pitch). After resist patterning, the Al lines were dry etched to obtain 4 parallel meandering metal lines. Subsequently, a Ta_2O_5 liner of 40 nm is deposited by Chemical Vapor Deposition (CVD), serving as a moisture diffusion barrier for the dielectric (Figure S8 (page 100)). Finally, the prepared devices were diced and wire-bonded in a Dual In-Line (DIL-40) package to make electrical connections to perform measurements.

4.2.4. Impedance Measurements

Impedance spectroscopy and sensing measurements were carried out using an HP 4284A precision LCR meter at an applied voltage of 1 V in a four-probe method. Impedance spectra were measured with a frequency range of 20 Hz to 1 MHz. The obtained impedance spectra were fitted using a non-linear least-square fitting in Zview with normalized data (data weighted using Calc-Modulus mode)[27].

Sensing measurements were carried out at a frequency of 20 kHz in a four-probe method. The devices were kept in a controlled temperature at 28 ± 0.05 °C. Gas flows were controlled using Mass Flow Controllers (MFCs). During the measurements, a continuous stream of dry N_2 was passed over the devices

at a constant flow rate of 200 mL/min. Once a stable baseline response was obtained, different concentrations of methanol (or other analytes: water, ethanol and 2-propanol) in N_2 were applied to the gas chamber.

The desired concentrations were obtained by first passing the carrier N_2 gas through a series of two bubblers containing methanol at room temperature to obtain a saturated stream of methanol and then diluting it with a parallel stream of N_2 gas with a constant total flow rate. The saturated vapor pressure of methanol was calculated with the Antoine equation[28-29]. After stabilization under the flow of methanol in N_2, the sensors were recovered to the baseline by replacing the stream of N_2 with methanol by dry N_2 (Figure S10 (page 102)).

4.2.5. Material Characterization

XRD patterns were recorded with a Bruker D8 Advance diffractometer with Co-$K\alpha$ radiation (λ = 1.78897Å). The 2θ range of 5–60° was scanned with a step size of 0.02° and a scan speed of 0.2 s per step. The texture of the MOF powder was determined by CO_2 adsorption using a Tristar II 3020 Micromeritics instrument at 273 K. Prior to the measurement, the adsorbent was degassed at 180°C under vacuum for 16 h.

SEM micrographs of casted films were acquired in a JEOL JSM 6010LA microscope after sputtering the sample with a conductive Au layer. TEM images of MOF particles were acquired with a JEOL JEM-1400 microscope.

The TGA experiments were carried out in a Mettler Toledo TGA/SDTA851e equipment, using air flow of 100 mL/min and a heating rate of 5 K/min up to 1123 K.

The thickness of the coated films was determined using a DEKTAK 8 profilometer over reference silicon substrates with a force of 0.3 mg and a resolution of 0.5 µm.

Dynamic Light Scattering (DLS) experiments were carried out at room temperature with diluted suspensions of NH_2-MIL-53(Al) nanoparticles in ethanol (2 mg/L) in a Zetasizer nano-ZS equipment from Malvern, UK. Suspensions were ultra-sonicated for 15 min before the measurement.

4.3. Results and Discussion

NH_2-MIL-53(Al) particles were synthesized as nanoparticles with a high aspect ratio using a previously reported protocol (Experimental Details, Section 4.2.1). Morphology and dynamic light scattering studies show that the MOF particles were rod-like and nano-sized with length of 56 ± 18 nm and width of 17 ± 4 nm (Figs. S6 (page 99), S7 (page 100)). Adsorption and powder X-Ray Diffraction (PXRD) studies confirmed that the synthesized crystalline material was identical to the NH_2-MIL-53(Al) as reported in literature[25] (Figure S8 (page 100), S9 (page 101)). The material exhibited mainly a narrow-pore configuration[25] of the framework structure[30] (Figure S9 (page 101)).

Thin composite layers of polymer and 20 wt.% MOF were deposited over the capacitive devices in a similar fashion as the mixed matrix membranes[25]. In order to keep the majority of the electrical field lines within the polymeric layer, the thickness of these layers was kept at 10 µm (Figure S11 (page 103)), well above 0.5 times the electrode wavelength of ~3 µm (*vide supra*). To obtain the desired film thickness (*i.e.* 10 µm) dispersions of NH_2-MIL-53(Al) in a tetrahydrofuran (THF) solution of Matrimid® were optimized in terms of composition. The dispersions were first ultra-sonicated and subsequently drop-casted on the devices in an environment saturated with THF (Experimental Details, Section 4.2.2). After drying, the coated devices were inspected using an optical microscope to check optical uniformity and effective coverage of the complete electrode area (Figure 1b). The presence of the MOF nanoparticles made the film opaque in appearance, indicating the dispersed state (Figure 1b, ii and iii). The thickness, morphology and homogeneity of these layers were further studied with profilometer measurements (Figure S11 (page 103)) and SEM (Figure 1c).

Next, the devices were electrically characterized by impedance spectroscopy in a four-probe measurement over a frequency range of 20 Hz to 1 MHz (Figure 2). The electrical response of the bare device indicated mainly a capacitive behavior ($-90° < \theta < -85°$) up to a frequency of ~50 kHz. Above that frequency, a loss process (AC conductance) became clearly visible, which can be understood by the parasitic effects through the electrodes and connections

($tan\theta = -1/(2\pi fRC)$)[31]. Deposition of thin films of polymer and polymer-MOF composites provided a parallel path for the charges to move in the electric field, resulting in a decrease in the impedance of the film. Moreover, the films did not affect the capacitive nature of the device at frequencies up to ~50 kHz, as the phase angle (θ) remained constant near -90°. Based on this observation, the frequency for the remaining part of this study was selected to be 20 kHz.

To study the electrical effects of the added polymer films compared to those of the bare device, all measured impedance spectra were fitted to equivalent circuits (Figure 2a, inset), (Supporting Information, Section 4). For that, the impedance of the planar electrodes was divided into a capacitance effect of the SiO_2 layer ($C_{g,p}$) and the components, $R_{g,s}$ and $C_{g,s}$, indicating the resistance and capacitance of the electrodes through conductive p-doped Si ($R_{g,s}$) and capacitive SiO_2 layer ($C_{g,s}$), respectively (Figure 2b, inset). In the frequency domain below ~50 kHz, the device behaves as a pure capacitor as the loss feature, represented by $R_{g,s}$, contributes less significantly, resulting in a total bare device capacitance of ~22 pF (Table 1). The impedance of the polymeric layers can be modelled as R_{al} and C_{al} in parallel to the effects of the bare device.

Table 1 summarizes the characteristic modeling parameters. The total capacitance of the device was found to increase by ~15 pF upon the deposition of Matrimid®. This can be understood qualitatively by the higher dielectric constant of the polymer film compared to air. Next, upon the incorporation of MOFs in the polymer, C_{al} (as well as the total capacitance) drops. This can be rationalized by the low dielectric constant of MOF particles[13]. This is also reflected by the differences in the resistance (112 kΩ and 18 kΩ for composite and neat Matrimid® films, respectively).

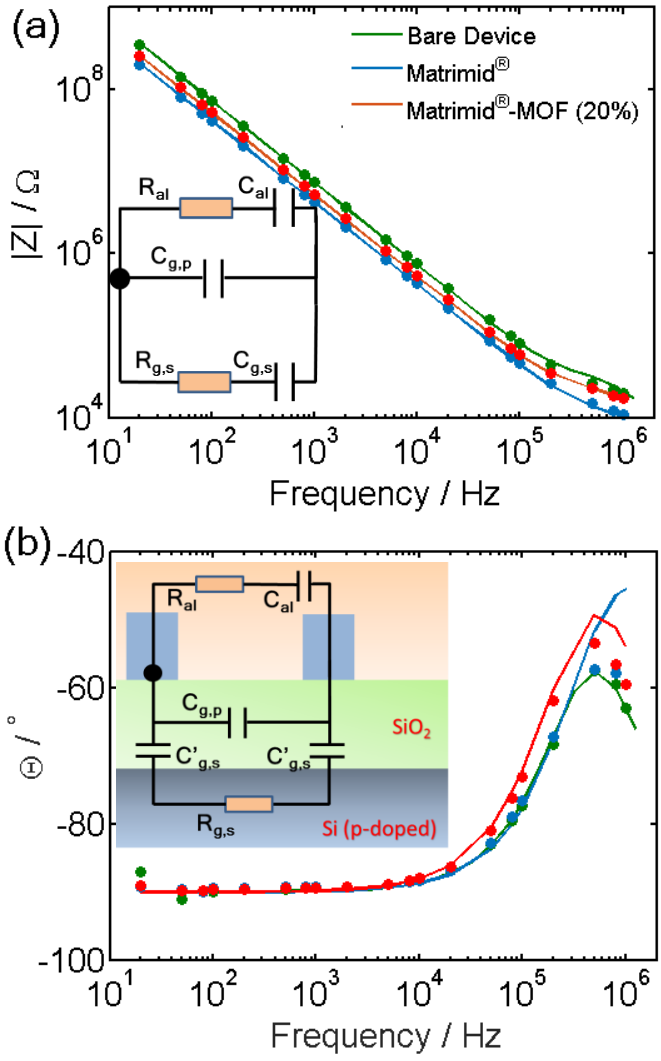

Figure 2. *Bode plots showing impedance spectra of prepared devices with and without coating of the affinity layer. Behavior of impedance (a) and phase angle, θ (b) with applied frequency indicate capacitive nature of devices. The spectra were modelled with an equivalent circuit (inset (a)) with components indicating physical contributions of the devices (inset (b)). Measured spectra (dots) and fitted data (lines) showed good agreement and the obtained circuit components are listed in Table 1.*

Table 1. *Circuit components of the equivalent circuits obtained via fitted impedance spectra*[*]*.*

	Bare Device	Matrimid®	Matrimid®-MOF
$R_{g,s}$ (kΩ)	37±1	37±1	37±1
$C_{g,s}$ (pF)	15.4±0.1	15.4±0.1	15.4±0.1
$C_{g,p}$ (pF)	6.1±0.3	6.1±0.3	6.1±0.3
R_{al} (kΩ)	-	18±2	112±8
C_{al} (pF)	-	15.5±0.5	8.2±0.2
C_{total} (pF)	~22	~37	~30

[*] *$R_{g,s}$, $C_{g,s}$ and $C_{g,p}$ represent the contribution of the bare device and R_{al} and C_{al} shows the affinity layer effects.*

For sensing measurements, the packaged devices were enclosed in a home-built gas flow chamber with controlled temperature (Figure S4 (page 98)). The electrodes of the coated devices were connected to the LCR equipment for a four-probe measurement to avoid any parasitic capacitance from the connecting wires. These devices were then measured for the changes in the overall impedance and capacitance with application of a fixed potential of 1 V for improved accuracy of the instrument. Lower potentials (<50 mV) result in very low currents in these high-impedance devices, which, in turn, results in reduced accuracy. Potentials higher than 1 V, however, damage the devices. The frequency of the measurement was kept at 20 kHz to reduce the AC conductance effect at high frequency and electrical interference at lower frequency regime.

Figure 3a shows the relative capacitive response of the three different sensor devices upon temporarily exposure to 5000 ppm of methanol (this is far below the saturation concentration, which is ~12.8% at 20°C). The bare device did not show any significant change over exposure to methanol, signifying the

importance of an affinity layer for detection. The exposure of the Matrimid®-coated device led to a sharp increase of the capacitance. The interaction of methanol with Matrimid® resulted in changes in the local dielectric properties of the film. This shows that Matrimid® has some affinity for methanol. Methanol and Matrimid® have dielectric constants (ε_r) of 32.7 and 3.5, respectively at 25°C, explaining these observations. Saturation of the Matrimid® polymer with methanol, showed a capacitance increase by 500 fF, which is an increase of ~1.5%.

Moreover, devices coated with a 20 wt % of NH_2-MIL-53(Al) in Matrimid® polymer, resulted in a capacitance increase by 750 fF, *i.e.* an increase of 2.5% upon exposure to 5000 ppm of methanol, which is significantly higher than the response obtained for the MOF-free, only Matrimid®-coated device. Clearly the added MOF shows affinity toward methanol[32], resulting in an increased uptake by the composite membrane. Even the response over independent measurements in these sensor devices was quite similar and resulted in a relative change of 2.49 ±0.30% and 1.28 ±0.18% for devices coated with 20 wt% MOF-Matrimid® and Matrimid® respectively upon exposure to 5000 ppm of methanol. This clearly indicates that addition of MOF particles to the polymer layer roughly doubles the affinity of the capacitive devices.

Removing the methanol from the applied gas flow, the sensor showed a complete recovery of the initial value, clearly clearly demonstrating the complete reversibility of the affinity process. The repeatability towards methanol response was studied further. The devices were exposed to 5000 ppm of methanol 3 times with intermediate regeneration steps and the signal response was monitored (repeated 6 times over two independent measurements). The 20 wt%-MOF-Matrimid® coated devices showed a reversible response as can be clearly seen in Figure 3a with no carry-over effect of the previous step (Figure S10 (page 102)). Moreover, it can be seen in Figure S12 (page 104) that the response increases with increasing concentrations of methanol, showing that it is a non-linear increase still below saturation.

Another important aspect for the sensor devices is cross-sensitivity upon exposure to different analytes. In order to study the selectivity properties, the devices coated with a 20 wt% MOF-Matrimid® film were exposed to 20000 ppm of water, methanol, ethanol and 2-propanol in a similar manner as previously described. The capacitive responses of the MOF-polymer coated device towards these analytes is depicted in Figure 3b.

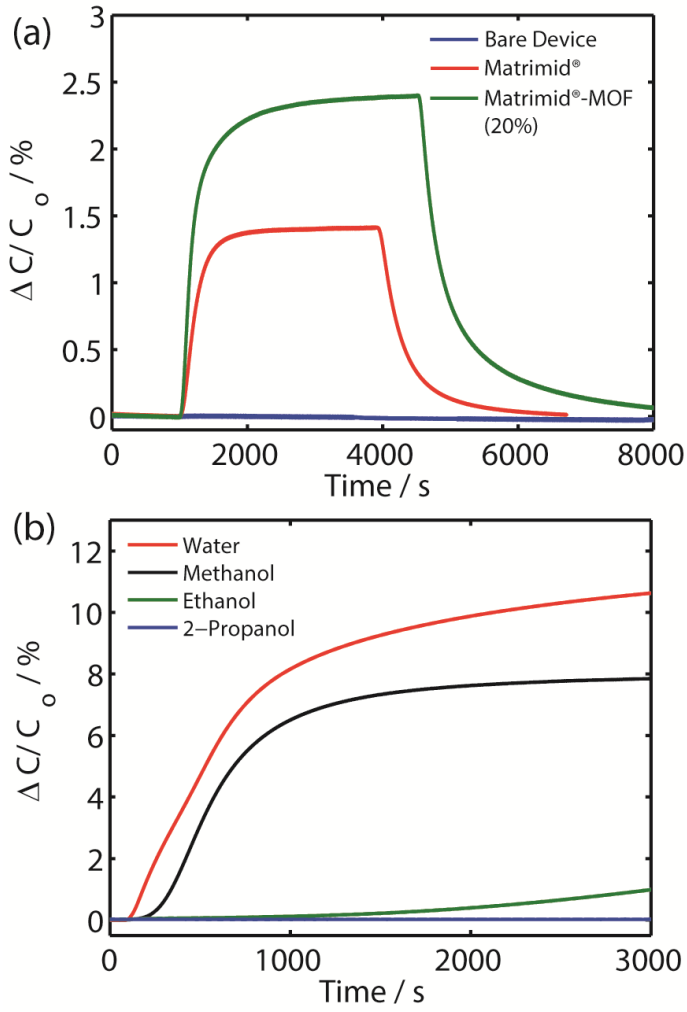

Figure 3. *(a) Response towards 5000 ppm methanol of bare device and devices coated with Matrimid® PI and Matrimid® PI-MOF (20 wt%) composite film. (b) Response of*

Matrimid®-MOF (20%) coated device towards 20000 ppm of water, methanol, ethanol and isopropanol at 28 °C.

It was clearly observed that the changes in capacitance on exposure to water and methanol were comparatively fast. Time taken for 50% of equilibrium response ($\tau_{0.5}$) was ~10 min at 40 mL/min flow rate. These molecules could easily diffuse into the film and the presence of NH_2-MIL-53(Al) inside the matrix enhances the overall adsorption capacity. Upon exposure to ethanol, a much slower capacitance increase was observed for neat Matrimid® ($\tau_{0.5}$ = ~50 min) and even slower for the MOF-Matrimid® system ($\tau_{0.5}$ = ~110 min) (Figure 3b, S13 (page 105)). Upon exposure to 2-propanol, hardly any capacitive response change was observed. These observations cannot be rationalized based on the polarity of the different analytes. Although the properties of the longer alcohols and Matrimid® are more likely to match[33-34], the opposite effect was observed. Thus not polarity, but the size of the alcohols plays a dominant role in the performance of the sensor system, as previously demonstrated for the diffusion of 2-propanol through the Matrimid® matrix[35] or in the separation of water-2-propanol mixtures using Matrimid® based polymeric membranes[36].

To compare the differences in response for water and methanol, it is important to emphasize that water has a dielectric constant (ε_r=78.3) that is ~2.5 times larger than that of methanol (ε_r=32.7). In all cases, the relative change of capacitance was enhanced by the presence of MOF particles dispersed in the polymer matrix (Figure 3b, S13 (page 105), S14 (page 105)). The initial response can be related to the affinity and sorption of the analyte within the Matrimid® matrix[37]. The microporosity and hydrophilic pores of NH_2-MIL-53(Al) provided additional adsorption sites for these polar analytes[32]. This adsorption leads to an additional concentration gradient through the Matrimid® matrix along with the additional changes in local polarity inside the polymeric layer. This enhanced uptake of an analyte inside the polymer matrix[38] allows the equilibrium capacitive response to increase. Possibilities to measure the sensor response near room temperature make these devices a

low-energy alternative to conventional metal oxide sensors, which require temperatures above 200 °C for operation.

4.4. Conclusions

In summary, we have reported the first example of MOF-polymer composites for capacitive sensor applications. Presence of NH_2-MIL-53(Al) nanoparticles inside the Matrimid® matrix significantly enhanced the intrinsic affinity of the polymeric thin film. The capacitive response doubled upon exposure to 5000 ppm of methanol for MOF-containing Matrimid® films (ca. 2.5 %) compared to that for Matrimid® (ca 1.3%), which leads to a reduction of the detection limit of Matrimid®-based sensors. The sensors perform completely reversible at 28 °C. Studies with different alcohols indicate faster response towards water and methanol ($\tau_{0.5} = 10$ min) with a higher affinity towards the less polar methanol. Adsorption of ethanol and 2-propanol resulted, despite the lower polarity, in a much slower response time, which is attributed to a strongly reduced diffusion as a result of the increased molecular size. The successful demonstration of MOF-Matrimid® films on capacitance transducers for sensing water and different alcohols opens avenues for further studies on different analytes. Combined with their compatibility with microelectronics industry and the great ease of measurement, these composite materials provide an interesting type of affinity layer, resulting in improved sensors properties. With a vast library of type of MOFs and polymers available, a variety of different parameters and materials can be optimized as well aiming to further improve sensitivity and selectivity.

References

[1] M. D. Allendorf, V. Stavila, *CrystEngComm* **2015**, *17*, 229-246.

[2] A. U. Czaja, N. Trukhan, U. Muller, *Chemical Society Reviews* **2009**, *38*, 1284-1293.

[3] J.-R. Li, R. J. Kuppler, H.-C. Zhou, *Chemical Society Reviews* **2009**, *38*, 1477-1504.

[4] L. E. Kreno, K. Leong, O. K. Farha, M. Allendorf, R. P. Van Duyne, J. T. Hupp, *Chemical Reviews* **2011**, *112*, 1105-1125.

[5] V. Stavila, A. A. Talin, M. D. Allendorf, *Chemical Society Reviews* **2014**, *43*, 5994-6010.

[6] Y. Cui, Y. Yue, G. Qian, B. Chen, *Chemical Reviews* **2012**, *112*, 1126-1162.

[7] D. J. Wales, J. Grand, V. P. Ting, R. D. Burke, K. J. Edler, C. R. Bowen, S. Mintova, A. D. Burrows, *Chemical Society Reviews* **2015**, *44*, 4290-4321.

[8] S. Achmann, G. Hagen, J. Kita, I. Malkowsky, C. Kiener, R. Moos, *Sensors* **2009**, *9*, 1574-1589.

[9] C. Sapsanis, H. Omran, V. Chernikova, O. Shekhah, Y. Belmabkhout, U. Buttner, M. Eddaoudi, K. Salama, *Sensors* **2015**, *15*, 18153-18166.

[10] P. Falcaro, R. Ricco, C. M. Doherty, K. Liang, A. J. Hill, M. J. Styles, *Chemical Society Reviews* **2014**, *43*, 5513-5560.

[11] A. A. Talin, A. Centrone, A. C. Ford, M. E. Foster, V. Stavila, P. Haney, R. A. Kinney, V. Szalai, F. El Gabaly, H. P. Yoon, F. Léonard, M. D. Allendorf, *Science* **2014**, *343*, 66-69.

[12] S. Han, S. C. Warren, S. M. Yoon, C. D. Malliakas, X. Hou, Y. Wei, M. G. Kanatzidis, B. A. Grzybowski, *Journal of the American Chemical Society* **2015**, *137*, 8169-8175.

[13] K. Zagorodniy, G. Seifert, H. Hermann, *Applied Physics Letters* **2010**, *97*, 251905.

[14] M. G. Campbell, D. Sheberla, S. F. Liu, T. M. Swager, M. Dincă, *Angewandte Chemie International Edition* **2015**, *54*, 4349-4352.

[15] M. G. Campbell, S. F. Liu, T. M. Swager, M. Dincă, *Journal of the American Chemical Society* **2015**, *137*, 13780-13783.

[16] Z. Guo, D. K. Panda, K. Maity, D. Lindsey, T. G. Parker, T. E. Albrecht-Schmitt, J. L. Barreda-Esparza, P. Xiong, W. Zhou, S. Saha, *Journal of Materials Chemistry C* **2016**, *4*, 894-899.

[17] B. Seoane, J. Coronas, I. Gascon, M. E. Benavides, O. Karvan, J. Caro, F. Kapteijn, J. Gascon, *Chemical Society Reviews* **2015**, *44*, 2421-2454.

[18] G. Dong, H. Li, V. Chen, *Journal of Materials Chemistry A* **2013**, *1*, 4610-4630.

[19] G. Harsányi, *Sensor Review* **2000**, *20*, 98-105.

[20] B. Adhikari, S. Majumdar, *Progress in Polymer Science* **2004**, *29*, 699-766.

[21] P. Gründler, *Chemical sensors: an introduction for scientists and engineers*, Springer Science & Business Media, **2007**.

[22] V. H. Nguyen, R. Daamen, A. Nackaerts, P. Bancken, Appl.No.: 13/438,716/US8779781 B2, July 15, 2014.

[23] R. Igreja, C. J. Dias, *Sensors and Actuators A: Physical* **2004**, *112*, 291-301.

[24] R. Igreja, C. J. Dias, *Sensors and Actuators B: Chemical* **2006**, *115*, 69-78.

[25] T. Rodenas, M. van Dalen, P. Serra-Crespo, F. Kapteijn, J. Gascon, *Microporous and Mesoporous Materials* **2014**, *192*, 35-42.

[26] T. Rodenas, M. van Dalen, E. García-Pérez, P. Serra-Crespo, B. Zornoza, F. Kapteijn, J. Gascon, *Advanced Functional Materials* **2014**, *24*, 249-256.

[27] G. Spinolo, G. Chiodelli, A. Magistris, U. A. Tamburini, *Journal of The Electrochemical Society* **1988**, *135*, 1419-1424.

[28] C. L. Yaws, *The Yaws handbook of vapor pressure: Antoine coefficients*, Gulf Professional Publishing, **2015**.

[29] G. W. Thomson, *Chemical Reviews* **1946**, *38*, 1-39.

[30] S. Couck, J. F. M. Denayer, G. V. Baron, T. Rémy, J. Gascon, F. Kapteijn, *Journal of the American Chemical Society* **2009**, *131*, 6326-6327.

[31] E. Barsoukov, J. R. Macdonald, *Impedance spectroscopy: theory, experiment, and applications*, John Wiley & Sons, **2005**.

[32] P. Serra-Crespo, E. Gobechiya, E. V. Ramos-Fernandez, J. Juan-Alcañiz, A. Martinez-Joaristi, E. Stavitski, C. E. A. Kirschhock, J. A. Martens, F. Kapteijn, J. Gascon, *Langmuir* **2012**, *28*, 12916-12922.

[33] A. F. M. Barton, *Chemical Reviews* **1975**, *75*, 731-753.

[34] L. Y. Jiang, H. Chen, Y.-C. Jean, T.-S. Chung, *AIChE Journal* **2009**, *55*, 75-86.

[35] L. Hesse, S. Naeem, G. Sadowski, *Journal of Membrane Science* **2012**, *415–416*, 596-607.

[36] S. Mosleh, T. Khosravi, O. Bakhtiari, T. Mohammadi, *Chemical Engineering Research and Design* **2012**, *90*, 433-441.

[37] M. Minelli, G. Cocchi, L. Ansaloni, M. G. Baschetti, M. G. De Angelis, F. Doghieri, *Industrial & Engineering Chemistry Research* **2013**, *52*, 8936-8945.

[38] S. Sorribas, A. Kudasheva, E. Almendro, B. Zornoza, Ó. de la Iglesia, C. Téllez, J. Coronas, *Chemical Engineering Science* **2015**, *124*, 37-44.

Polymer-Metal Organic Framework Composite Films as Affinity Layer for Capacitive Sensor Devices

Supporting Information

1. *Additional Material Details.*

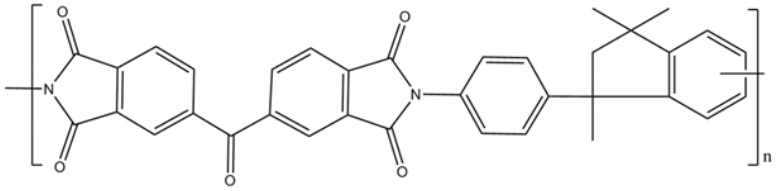

Figure S1. *Chemical structure of Polyimide Matrimid® 5218.*

2. *Sensor Device*

(a)

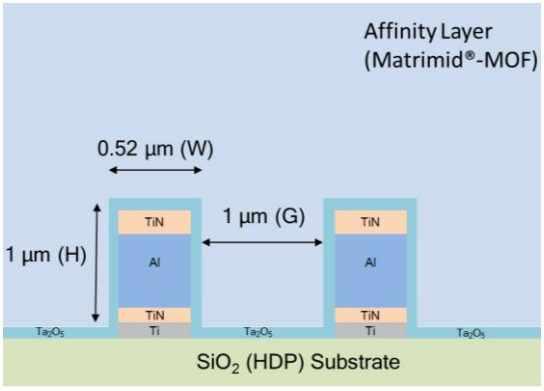

(b)

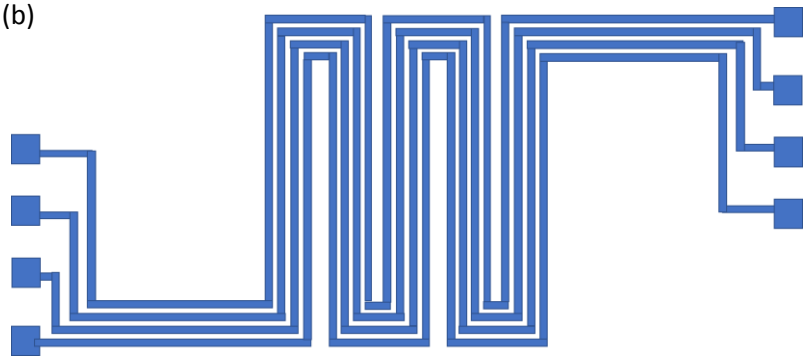

Figure S2. *Schematics of the sensor substrate (a) illustrating the dimensions and layout coated with the affinity layer and (b) illustrating the meander pattern of the electrodes.*

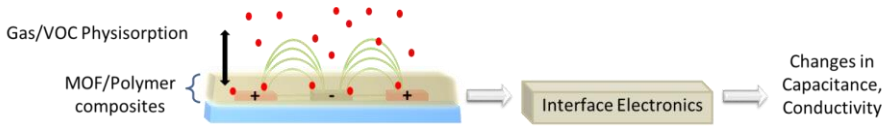

Figure S3. *Schematic of the working principle of an electrical sensor device containing planar electrodes as transducer devices. The green lines indicate the electric field lines. These electric field lines change on the presence of a MOF/polymer film as affinity layer. On adsorption/desorption of an analyte, the additional changes in field lines are converted to changes in parameters such as capacitance, which are monitored with help of electronics.*

3. Analysis Chamber

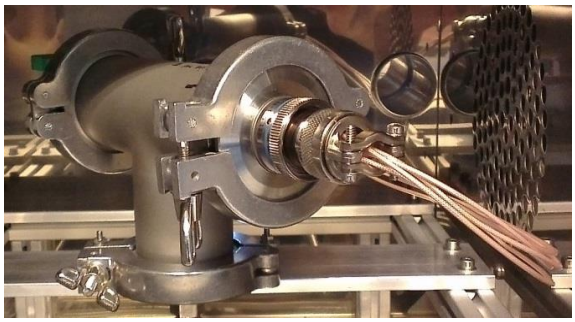

Figure S4. *Photograph of the home-built electrical measurement chamber with controlled gas flow and temperature.*

4. Explanation for Equivalent Circuit Fitting

The phase angle of the impedance spectra was close to −90°, which is typical for a capacitor. The overall capacitive behavior can be explained by the fitted equivalent circuit (Figure 2). Different components of the equivalent circuit can be related to the configuration of the device. First, the underlying SiO_2 layer acts as a dielectric layer and is usually represented as a capacitor. In the configuration, it is represented as $C_{g,p}$. Since the substrate below the SiO_2 layer is conductive p-doped Si, the semiconductor can be represented as a resistor ($R_{g,s}$) in the configuration which is in series with the capacitive effect of SiO_2 ($C_{g,s}$). Further, an affinity layer on top of the device will provide a parallel path for electrons to flow through. The affinity layer acts as another dielectric layer. It can be represented as a capacitance with some dielectric loss at higher frequencies due to AC conductance. This can be modelled as a resistor (R_{al}) and capacitor (C_{al}) in series.

5. *Additional Data*

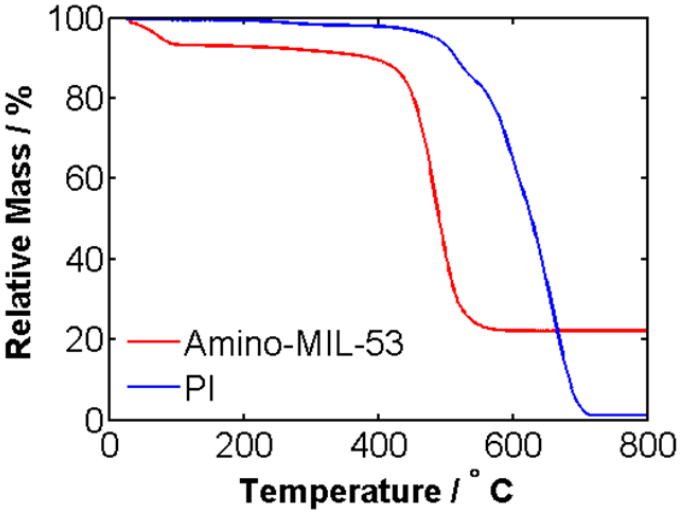

Figure S5*. Thermogravimetric Analysis (TGA) of MOF particles and the polymer carried out with air at a flow rate of 100 mL/min with a heating rate of 5 °C/min.*

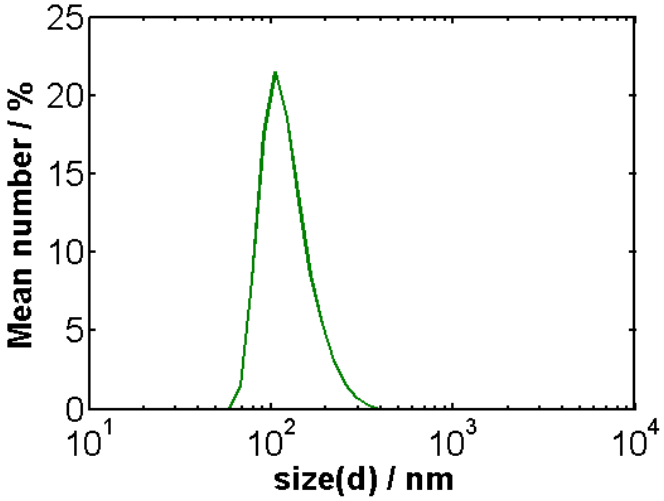

Figure S6. *Particle Size Distribution determined by dynamic light scattering.*

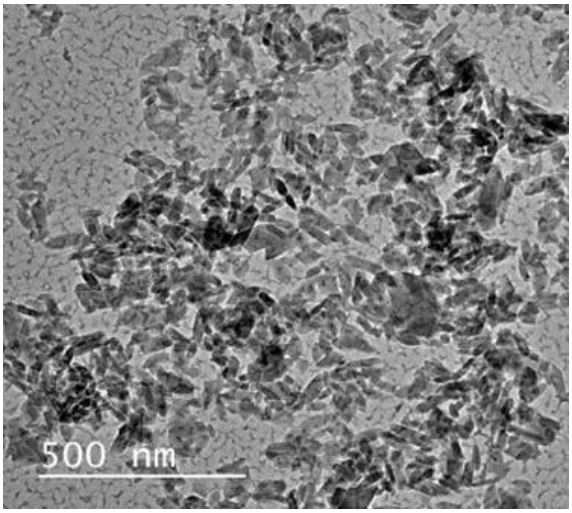

Figure S7. *TEM image of NH_2-MIL-53(Al) particles over a grid of Au.*

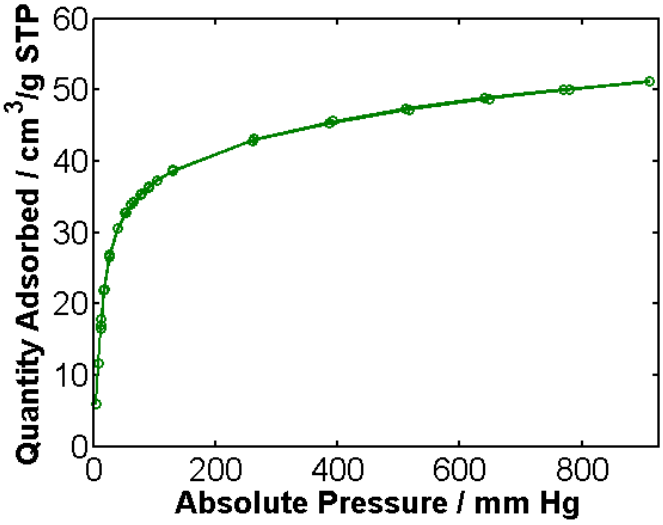

Figure S8. *CO_2 sorption isotherm of NH_2-MIL-53(Al) measured at 273 K. Samples were degassed at 180 °C in vacuum before measurement.*

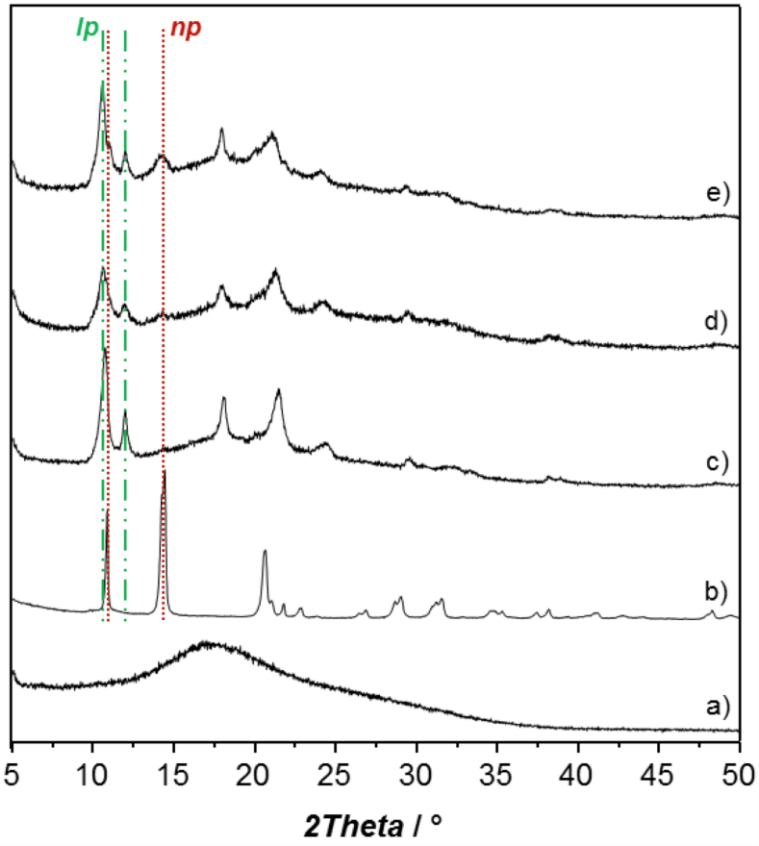

Figure S9. *X-ray diffraction patterns for the neat polyimide Matrimid® (a), the as-synthesized NH_2-MIL-53(Al) MOF (b) and composites containing a 25 wt% MOF loading, casted in a Petri dish (thickness 75-105 µm) and dried under free convection conditions at 273 K (c) and at room temperature (d), casted using a Doctor Blade system (thickness 35-75 µm) and dried under free convection conditions at room temperature (e). The most intense diffraction lines for the large pore (lp) and narrow pore (np) MOF configurations are indicated.*

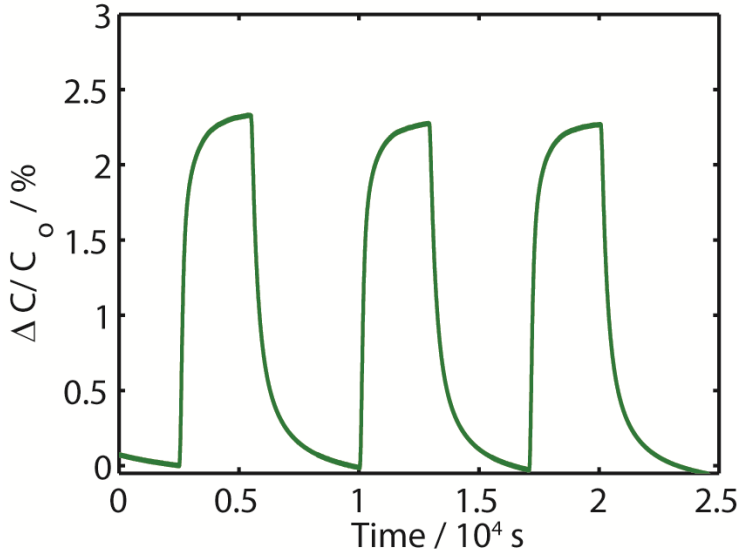

Figure S10. *Reversibility of the signal response of Matrimid®-MOF (20 wt%) device on the exposure to 5000 ppm of methanol at 28 °C.*

6. Thickness optimization

5 µl drops of different concentration of casting solutions were drop-cast on reference Si substrates to test for the adhesion properties and the thickness of the drop. Figure S11 shows the correlation of the obtained thickness and the starting solution concentration. 6% concentration was chosen for casting over the devices to obtain a 10 µm thick layer.

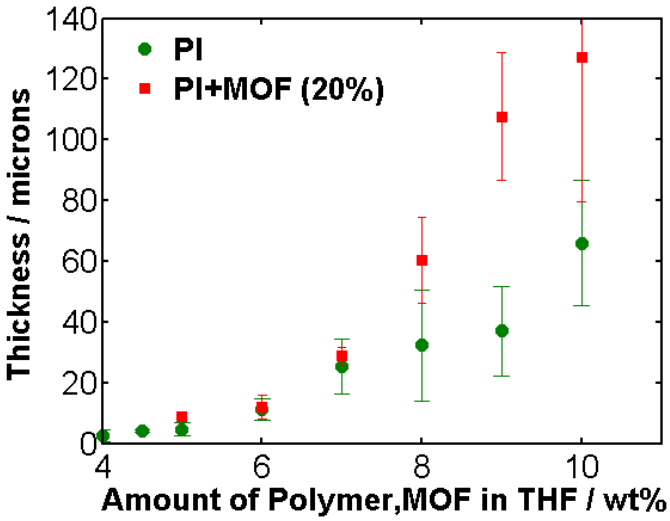

Figure S11. *Optimization profile between thickness and starting concentration of casting solutions for the preparation of the desired thick layers on reference Si substrates.*

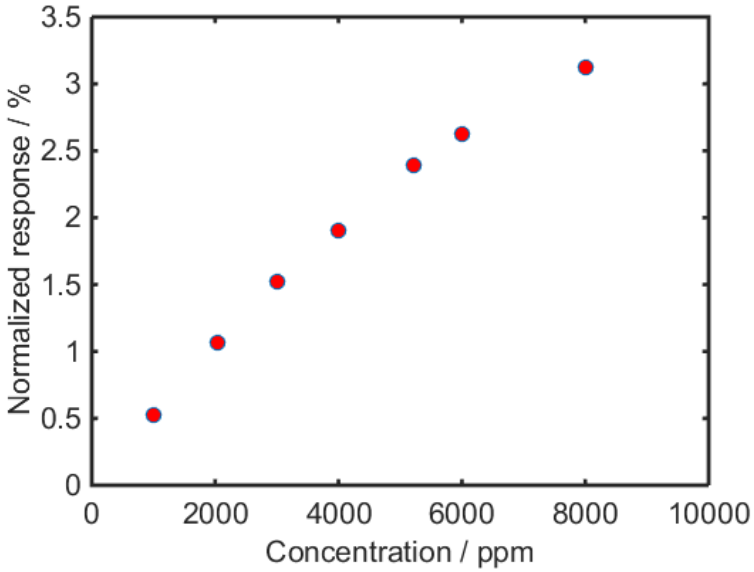

Figure S12. *Normalized sensor behavior ($\Delta C/C_o$) of 20% MOF-Polymer coated device on the exposure to different concentrations of methanol.*

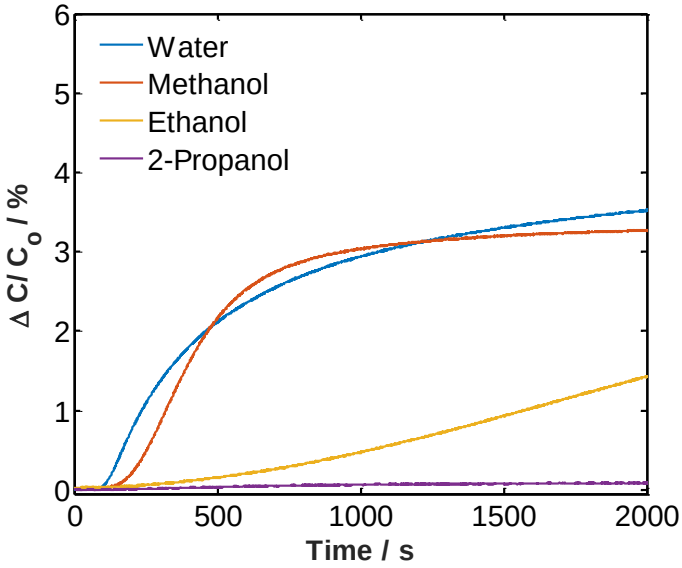

Figure S13. *Sensor response of Matrimid®-coated device to 20000 ppm of water, methanol, ethanol and 2-propanol at 28 °C.*

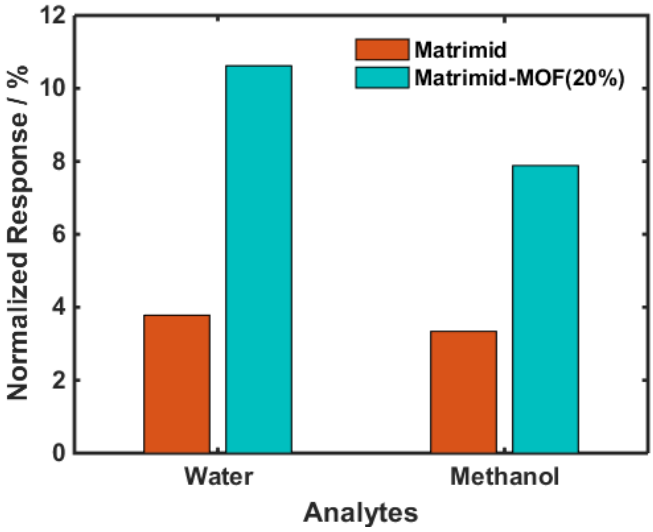

Figure S14. *Comparative normalized response (ΔC/C$_o$) of PI, PI-MOF(20%) devices towards 20000 ppm of water and methanol.*

Chapter 5

Gas Phase Sensing of Alcohols by Metal Organic Framework – Polymer Composite Materials

This chapter is based on the following work:

S. Sachdeva, S.J.H. Koper, A. Sabetghadam, D. Soccol, D. J. Gravesteijn, F. Kapteijn, E. J. R. Sudhölter, J. Gascon, L. C. P. M. de Smet, *Submitted*.

Abstract

Affinity layers play a crucial role in chemical sensors for the selective and sensitive detection of analytes. Here, we report the use of composite affinity layers containing Metal Organic Frameworks (MOFs) in a polymeric matrix for sensing purposes. Nanoparticles of NH_2-MIL-53(Al) were dispersed in a Matrimid® polymer matrix with different weight ratios (0 - 100 wt.%) and drop-casted on planar capacitive transducer devices. These coated devices were electrically analyzed using impedance spectroscopy and investigated for their sensing properties towards the detection of a series of alcohols and water in the gas phase. The measurements indicated a reversible and reproducible response in all the devices. Sensor devices containing 40 wt.% NH_2-MIL-53(Al) in Matrimid® showed a maximum response for methanol and water detection. The sensor response time slowed down with increasing MOF concentration till 40 wt.%. The half time of saturation response ($\tau_{0.5}$) increased by ~1.75 times for the 40 wt.% composition compared to only Matrimid® coated devices. This is attributed to polymer rigidification near the MOF/polymer interface. Higher MOF loadings (≥ 50 wt.%) resulted in brittle coating layers with a response similar to the 100 wt.% MOF coating. Cross-sensitivity studies showed the ability to kinetically distinguish between the different alcohols with a faster response for methanol and water compared to ethanol and 2-propanol. The observed higher affinity of the pure Matrimid® polymer towards methanol compared to water allows also for a higher uptake of methanol in the composite matrices. Also, as indicated by the sensing studies with the mixture of water and methanol, methanol uptake is independent of the presence of water up to 6000 ppm of water. The NH_2-MIL-53(Al) MOFs dispersed in the Matrimid® matrix show a sensitive and reversible capacitive response, even in the presence of water. By tuning the precise compositions, the affinity kinetics and overall affinity can be tuned, showing the promise of this type of chemical sensors.

5.1. Introduction

Detection of analytes in the gas phase is important in environmental, security, health, food and industrial processes requiring detection and quantification in a fast, accurate and reversible manner[1-3]. In recent years, studies have focussed on developing chemical coatings as a selective affinity layer in sensors using nanomaterials[1, 4-5] and polymeric films[6-7]. The uptake of analytes in the affinity layer leads to changes in the physical properties of the films which can be monitored by the transducer beneath. Often, metal oxides are used as the affinity layer which usually require high operation temperatures (>200°C) and do show a significant cross-sensitivity in most cases[8-9].

Metal organic frameworks (MOFs) are a new emerging class of materials of which their specific affinity properties can be attractive for the use as selective substrates in chemical gas phase sensors operating at low temperature[2, 10-11]. These materials consist of metal ions linked by organic ligand molecules forming porous, crystalline frameworks[11-12]. Their high porosity, tunability of their structure and selectivity make them promising for applications not only for sensing, but also for gas separation, storage, and catalysis[11-14].

Up to date, sensor studies using MOFs have focussed mainly on changing their luminescence properties[15-16]. Recent advances in the preparation of thin films of MOFs have opened their potential in the sensor industry beyond luminescence based sensors[13, 17]. Also, studies utilizing changes in the electrical properties of MOFs have shown promising application of MOFs as selective affinity layer for sensors[18-20]. Additionally, the use of polymeric composite materials with MOFs can combine the properties of both polymer and MOFs for obtaining superior sensing performance. This has also been exploited in gas separation applications[21-22]. The enhanced compatibility of polymer and MOF contribute also to their promising role in producing new sensor selector layers[21-23]. Studies with polymeric sensors containing filler molecules such as metal oxides, carbon nanotubes and graphene have already shown improvement of the intrinsic sensing properties of polymers[24-26]. Moreover, the use of composite materials can allow for easy and cost-effective integration with semiconductor technologies utilizing existing principles for synthesizing polymeric coatings[27-28].

Recently, we reported a simple methodology for developing polymer-MOF composite films using Matrimid® 5218 and NH_2-MIL-53(Al) for sensing applications[29]. Matrimid® 5218 belongs to the class of fully imidized polyimides with a high thermal and mechanical stability[30-31] and NH_2-MIL-53(Al) is one of the most well-studied MOFs with aluminium as the metal ion and amino-terephthalic acid as the organic ligand[31-32]. It was observed that incorporation of these MOF particles inside the Matrimid® polymer matrix enhances the sensitivity of the sensor devices. Matrimid® and NH_2-MIL-53(Al) have also shown significant compatibility during membrane separation studies leading to superior gas separation performances[31]. The presence of these MOF particles inside the polymeric matrix alter their physical and chemical properties[29, 31]. For example, it has been observed from membrane studies that variations of the concentration of MOF particles can lead to alterations in the gas transport and adsorption properties[31, 33]. Furthermore, upon blending the overall dielectric constant and hence the electrical polarizability changes[34]. These differences in the properties with varying MOF concentration can be quite significant for a pair of MOF and polymer.

In this study, we focused on developing sensor devices with composite films of Matrimid® and NH_2-MIL-53(Al) of different compositions and deposited on planar transducer devices. These devices are meander-patterned planar aluminium electrodes having a width (W) of 0.52 µm, a gap (G) of 1 µm, and an electrode area of ~2.1 mm^2 (Figure 1). About 95% of the electrical field lines stay within the distance equal to the sum of W and G in a perpendicular orientation[35-37]. Our bare electrodes show a bare capacitance of ~22 pF. After deposition of polymer-MOF affinity layers of 10 µm in thickness onto our electrode, the capacitance increases to 28-36 pF as a result of the higher dielectric constant of the deposited layer (ε_r = ~3.5-4.5) as compared to air (ε_r = 1), as previously discussed[29]. If analyte molecules are adsorbed in the polymer-MOF matrix, the overall dielectric constant will also change, resulting in a capacitance change[29]. We have performed such sensing experiments using methanol and water as the analyte, varying the polymer-MOF composition ratio. In addition, cross-sensitivity studies with ethanol and 2-propanol and temperature-dependent response studies were performed.

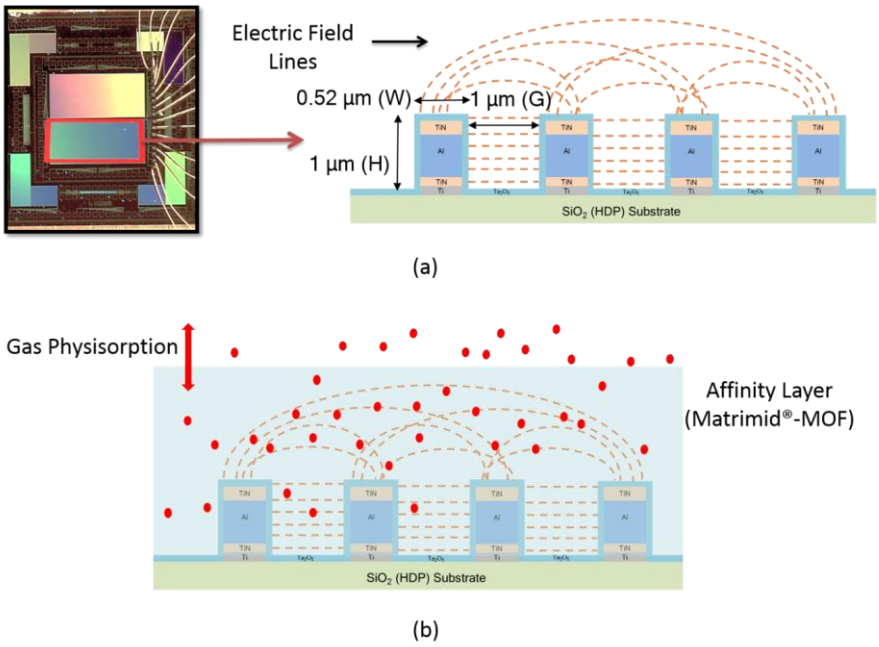

Figure 1. *(a) The sensor device consisting of meander-patterned electrodes with height (H), width (W) and gap (G) of 1 µm, 0.52 µm and 1 µm, respectively. (b) Schematic representation of the device with the higher dielectric affinity layer and gas physisorption within this layer.*

5.2. Experimental

5.2.1. Materials

The polyimide (PI) Matrimid® 5218 was obtained from Huntsman Advanced Materials and was used as the polymeric matrix. Methanol, ethanol and 2-propanol were obtained from Sigma Aldrich at highest purity. N_2 gas (99.99%) was obtained from Linde Gas and used as carrier gas in our sensor experiments. All other chemicals were obtained from Sigma Aldrich and used as received.

5.2.2. Device Fabrication

The fabrication of the devices was performed as described previously[29]. Briefly, the active electrode area consisted of aluminium metal stacked between TiN layers over underlying dielectric layer of SiO_2 to mimic the final layer of a typical 140 nm CMOS platform. Devices were processed to obtain meander-patterned planar aluminum (Al) electrodes by photo-lithography. These electrodes consist of 4 parallel electrodes with a meander pattern with line width (W) of 0.52 µm, a gap (G) of 1 µm and an electrode area of ~2.1 mm^2. First, Si_3N_4 was deposited on the back-side of the p-doped Si wafer to avoid contamination of the Si during the wet cleaning steps. A high-density plasma CVD silicon dioxide (with a thickness of 3 µm) was deposited to represent the inter-metal dielectric, followed by the deposition of the metal stack. This metal stack consists of a 25/25 nm Ti/TiN adhesion bilayer at the bottom and followed by a 800 nm thick layer of aluminum and a 50 nm layer of TiN at the top. The Ti/TiN and TiN layers were introduced to improve the adhesion, to decrease reflectivity and also to function as a stopping layer during the etching processes. Afterwards, the Al metal layer for the device was patterned by lithography targeting the required width and spacing dimensions. After photo-resist patterning, the Al lines were dry etched to obtain 4 parallel meander-patterned aluminium lines. Subsequently, a Ta_2O_5 line of 40 nm was deposited by CVD to serve as a moisture diffusion barrier.

5.2.3. Synthesis of the MOF nanoparticles

NH_2-MIL-53(Al) nanoparticles were synthesized by hydrothermal treatment using 2-aminoterephthalic acid as organic ligand and aluminum nitrate using the procedure previously described[22, 38]. Therefore, 1.902 g (= 10.5 mmol) 2-aminoterephthalic acid was dissolved in 10.5 mL 2 M aqueous NaOH solution after which the volume was increased to 75 mL using distilled water. 3.935 g $Al(NO_3)_3.9H_2O$ (= 10.5 mmol) was dissolved in 75 mL distilled water in a separate tube. Both solutions were mixed and stirred under reflux conditions (393 K) for 3 days. The formed MOF particles were filtered under vacuum and washed with 96% ethanol twice. The material was then washed in DMF (~100 mL) and methanol (~100 mL) consecutively at 403 K and 363 K overnight, respectively to efficiently remove any unreacted ligand. Finally, the

powder was filtered and washed with ethanol twice and dried at 373 K in vacuum overnight.

5.2.4. Preparation of the device affinity layers

The polyimide (PI) Matrimid® 5218 was pretreated at 453 K overnight under vacuum to remove any physically adsorbed water. Different loadings (0, 20, 40, 50, 60 wt. %) of NH_2-MIL-53(Al) in Matrimid® were prepared by dissolving the calculated amount of materials in tetrahydrofuran (THF) in such a way that the total weight of both components was 6 wt. % (5.5 wt.% for 50 and 60 wt.% loadings). First, the required amount of MOF particles for each concentration was dispersed in 940 mg of THF by ultrasonication for 15 min. Then, the remaining amount of polymer (for each desired concentration) was added to this dispersion and stirred overnight. In the case of MOF-free polyimide coatings, 60 mg of PI was dissolved in 940 mg of THF and stirred overnight. For the preparation of coatings containing pure MOF (100 wt.%, *i.e.* without PI), 22.5 mg of MOF nanoparticles were dispersed in 480 mg of THF. Before the deposition of the solutions over devices and reference silicon substrates, the solutions were subjected to three alternative cycles of ultrasonication and mixing of 15 min each to ensure good dispersion of MOF particles[22, 31]. The dispersed solution was then cast over the reference substrate and transducer devices with 5 µl drops under a solvent-saturated environment in order to reduce evaporation of the THF solvent. This ensures that the formed coatings do not crack and remain uniform. Once dried, the coated devices were treated at 453 K in vacuum for 4 h.

5.2.5. Materials Characterization

Scanning Electron Microscopy (SEM) images of the composite films were acquired using a JEOL JSM 6010LA microscope after sputtering the sample with a conductive gold layer. TEM images of MOF particles were acquired with a JEOL JEM-1400 instrument. XRD patterns were recorded with a Bruker D8 Advance diffractometer with Co-$K\alpha$ radiation ($\lambda = 1.78897$Å). The diffraction pattern was scanned with a step size of 0.02° and a scan speed of 0.2 s per step. A DEKTAK 8 profilometer was used to determine the thickness of the composite films over reference silicon substrates with a force of 0.3 mg and a horizontal and vertical resolution of 0.5 µm and 4 nm, respectively.

Impedance measurements of the sensor devices were carried out with a HP 4284A LCR meter in a four-probe configuration.

5.2.6. Gas Sensing Measurements

An automated gas mixing and detection setup has been designed and built for monitoring the behavior of gas sensor devices using impedance measurements on exposure to analytes and vapors in the gas phase[29]. Figure 2 provides a schematic lay-out. The major part of the equipment consists of a (i) gas mixing unit containing mass flow controllers for providing desired flow rates of the gases, (ii) vapor generation system with a series of bubblers for analysis of individual and mixtures of vapors, (iii) temperature-controlled measurement chamber to analyze the components in the gas phase using sensor devices under test, (iv) electrical measurement units for monitoring perturbations in the measurement chamber, and (vi) instrument controller and data logger system for controlling mass flow controllers, electrical instruments and recording data using LabVIEW® based software.

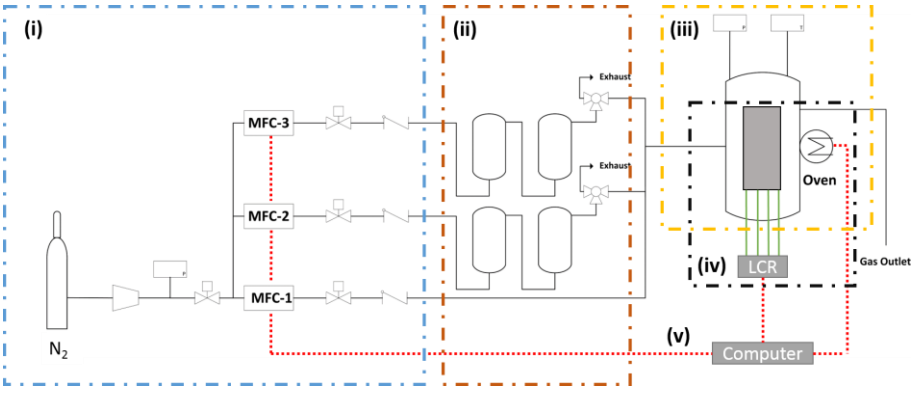

Figure 2. *Schematic of the measurement setup consisting of a (i) gas mixing unit with mass-flow controllers, (ii) vapour generation system with series of bubblers, (iii) temperature-controlled measurement chamber, (iv) electrical measurement unit and (v) instrument control and data logging using LabVIEW® and computer.*

The gas mixing units were connected with the calibrated gas bottles to provide gases with desired concentration and flow rates to the measurement chamber. The addition of vapors was achieved by passing the inert gas (N_2) at atmospheric pressure through a series of bubblers to generate a saturated

stream of N_2 with the vapor at room temperature. The vapor concentration was calculated with the Antoine Equation[39-40]:

$$\text{Log } P^{\circ} = A - \frac{B}{T+C} \quad (1)$$

where P° is the saturated vapor pressure of the analyte and T is the temperature of the bubbler. A, B, C are analyte-dependent constants.

Sensing measurements were carried out using a HP 4284A precision LCR meter at a frequency of 20 kHz and a voltage of 1 V in a four-probe arrangement. The devices were kept at a controlled temperature of 28 °C and a total flow of 200 mL/min. During the measurement, the desired concentration of an analyte component in dry N_2 was passed through the measurement chamber having a volume of ~400 ml. After stabilization and equilibration, the sensors were recovered to the baseline by replacing the stream of N_2 with the analyte by dry N_2 only.

The frequency analyzer and the gas mixing setup were automated using a custom-built LABVIEW® program to control the parameters such as flow rates, voltage, temperature and carry out the time-based and frequency-based measurements.

5.3. Results and Discussion

5.3.1 Sensing layer formation

The crystallinity of the synthesized NH_2-MIL-53(Al) MOFs nanoparticles was confirmed with powder X-ray Diffraction (XRD)[31] (Figure S1 (page 133)). The structure of the MOF consists of $AlO_4(OH)_2$ octahedra coordinated to 2-aminoterepthalic acid and mainly exhibited a narrow-pore (*np*) configuration[31]. The nanoparticles had a rod-shaped morphology and dimensions of 56 nm × 17 nm (Figure 4f, S2 (page 133)).

In order to investigate the role of the MOF particle concentration in the affinity layer for sensing, sensor devices were prepared with different filler ratios (0-60 wt.%) of NH_2-MIL-53(Al) in a matrix of Matrimid®. The polymer-MOF mixture in tetrahydrofuran (THF) was drop-casted in a solvent-saturated environment onto the sensor devices and reference silicon substrates

to obtain a 10 µm thick layer. The thickness was kept at 10 µm to ensure that the electrical field lines of the transducer stay inside the polymeric layer[29]. This is three times higher than the spatial wavelength (~3 µm) of the transducer and ensures that deposition variations do not influence the equilibrium sensor response. The coated region was kept larger than the central active region (Figs. 1 and 3) to maintain uniformity in the active region. The differences in the deposited layers can be seen with SEM (Figs. 3a and b) and optically (Fig. 3, insets) for inclusion of MOF in the polymeric layer. The surface coating turned slightly opaque due to the presence of agglomerated MOF particles. The roughness of the material was increased. At further increased MOF loadings, opacity also increased and the layer became brittle. At loadings above 50 wt. % the layer started to show cracks (Figs. 3d and e). For comparison, MOF particles (100 wt.%. *i.e.* in absence of polymer matrix) were also deposited over the sensor devices (Fig. 4f).

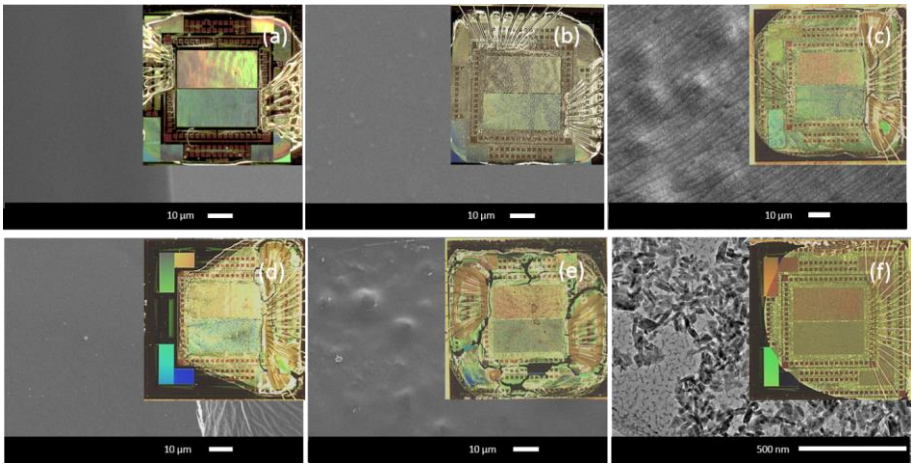

Figure 3*. SEM micrographs and optical images (inserts) of the casted layers of NH_2-MIL-53(Al)-Matrimid® composites with different MOF concentrations: (a) 0, (b) 20, (c) 40, (d) 50, and (e) 60 wt.%. (f) represents the TEM micrograph of NH_2-MIL-53(Al) nanoparticles along with the optical image of casted device with only MOF particles (100 wt.%).*

5.3.2 Quantitative Investigation of the Sensing Performance

Sensor devices coated with layers containing different MOF loadings were exposed to increasing concentrations of methanol in N_2 at 28 °C. Methanol was selected as the primary analyte due to the good sensitivity of NH_2-MIL-53(Al) and Matrimid® for this alcohol[29]. The capacitive changes on the exposure to methanol were monitored by using impedance spectroscopy with a frequency of 20 kHz and a voltage of 1 V. The sensor devices were first exposed to dry N_2 in the measurement chamber until a stable baseline was achieved. Next, methanol vapors were introduced at different concentrations using a series of two bubblers (see Section 2.6 for details). Figure 4a shows a typical response of a sensor device covered with a PI coating containing 40 wt.% of MOF nanoparticles towards different concentrations of methanol at 28°C.

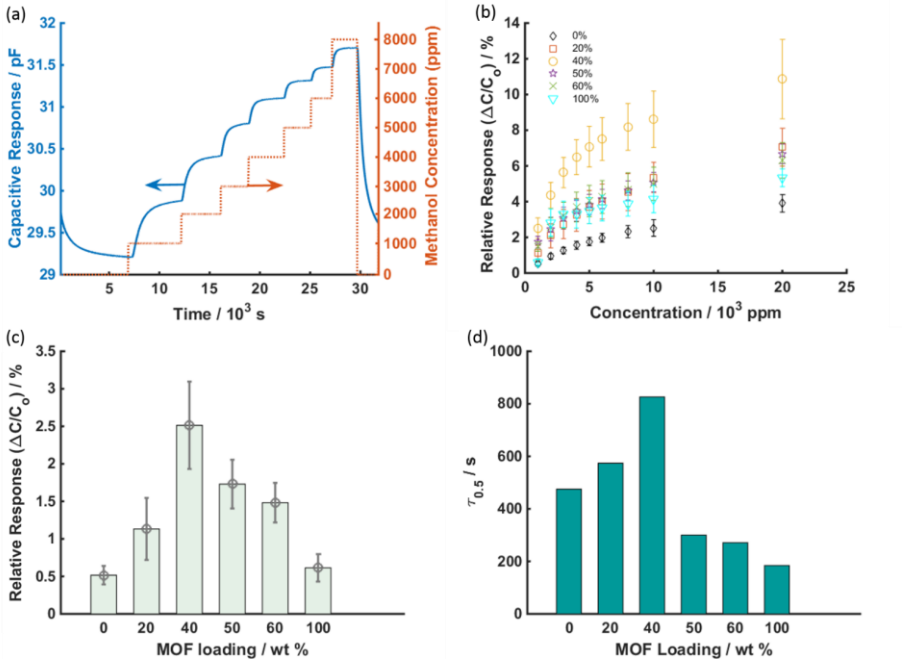

Figure 4. *(a) Quantitative, cumulative response towards methanol by the sensor device coated with a thin layer of 40 wt.% NH_2-MIL-53(Al) nanoparticles in Matrimid®. (b) Comparison of the sensor response by devices with different ratios of NH_2-MIL-53(Al) and Matrimid® to the exposure of different concentrations of methanol. (c) Comparison of the response of these sensor devices towards 1000 ppm of methanol. (d) The half-*

time for response saturation ($\tau_{0.5}$) for these sensor devices on the exposure to 20000 ppm of methanol.

The capacitive response of the sensor device increases on exposure to methanol in the measurement chamber (t = ~7000 s in Fig. 4a). The capacitive response further increased upon increasing methanol concentrations. Furthermore, the response was completely reversible as the initial baseline was recovered on replacing the methanol containing N_2 gas by dry N_2 (Figs. 4a, S3 (page 134)).

The sensitivity of our devices with different amounts of MOF in the polymer matrix towards methanol is plotted in Figure 4b. The response was normalized by C_0, the capacitance in dry N_2, yielding a relative change in capacitance ($\Delta C/C_0$) allowing easy and accurate comparison of the different sensor devices. The inclusion of these porous nanoparticles inside the polymer matrix enhances the overall signal response, e.g. the addition of 20 wt.% of MOF more than doubles the sensor response to methanol. This increase in the sensitivity is due to the additional adsorption sites introduced by the NH_2-MIL-53(Al) along with the intrinsic adsorption capacity of the Matrimid® [29, 38, 41]. The response increased further upon increasing amounts of MOF in the polymeric layer, resulting in a five-fold increase (over exposure to 1000 ppm methanol) for the 40 wt.% MOF loading as compared to the MOF-free Matrimid® layer (Fig. 4b and c). Further, the maximum capacitive response was observed at 40 wt.% (Fig. 4c). Moreover, in sensor devices with MOF loading above 40 wt.%, the equilibrium response became closer to the response observed with only MOF-coated device indicating a transition from a polymer-limited adsorption to MOF-limited adsorption (Fig. 4b and c).

We attribute this reduction in response to the decreased adhesion between the composite layers and transducer at loadings above 40 wt.%. Formation of brittle and cracked films at these loadings, as observed by SEM, supports this way of reasoning (Fig. 3). Additionally, this decreased signal transduction behavior is also clearly visible in the sensor response of 100 wt.% MOF devices as the high adsorption capacity of NH_2-MIL-53(Al) is not completely reflected in the sensor response (Fig. 4b, S4 (page 134)). Moreover, percolation of methanol molecules from MOF particle to MOF particle at such high loadings (above 40 wt.%) ensures that the adsorption process is directly determined by

the MOF[23]. The slightly higher response in these devices compared to that for the 100 wt.% MOF-coated device (Fig. 4b, 4c) can be explained by additional adsorption in the Matrimid® phase, which covers these nanoparticles partially.

The response kinetics provide further insights into the adsorption process. Interestingly, considering the time taken to reach half the saturation response ($\tau_{0.5}$), the $\tau_{0.5}$ is observed to increase (slower process) with increasing the amount of NH_2-MIL-53(Al) in the Matrimid® matrix for the lower concentration regime (0-40 wt.%) (Fig. 4d). The observed increase of $\tau_{0.5}$ is attributed to rigidification of the polymer matrix near the polymer-MOF interface[42-43]. The solvent evaporation can induce stress in the polymeric matrix around the filler molecules and reduce the relaxation of the polymeric chains close to the MOF surface while drying takes place. This would lead to a decrease in the free volume close to the surface and hence reduction in the permeability. This has also been observed before in membranes prepared by spin-coating layers of a glassy polymer (PSF-Udel®) with NH_2-MIL-53(Al)[43]. In addition, partial penetration of the Matrimid® polymer chains into the micropores of NH_2-MIL-53(Al) can also affect the transport of methanol to the MOF particles[43]. Also, as shown in Figure 4d, $\tau_{0.5}$ drops approximately 3 times (faster process) at a MOF loading of ≥ 50 wt.% when compared with devices containing 40 wt.% of MOF. The response time also became significantly closer to the MOF-coated device (100 wt.%) at loadings of 50 and 60 wt.%. This observation confirms the direct accessibility of the MOF particles to the exposed environment due to cracks and to a thin or partial coverage of NH_2-MIL-53(Al) particles with the (rigidified) Matrimid®.

Moreover, on assumption that the sensor response is proportional to the adsorbed concentration of the analyte in the composite matrix[29], the non-linear response of different devices with varying methanol concentrations (Fig. 4b) was fitted to the Langmuir adsorption model as shown in Equation 2:

$$v = v_{\max} \cdot \frac{K_{eq} \cdot p_{MeOH}}{1 + K_{eq} \cdot p_{MeOH}} \qquad (2)$$

where v, v_{max}, K_{eq} and p_{MeOH} indicate the observed response ($\Delta C/C_0$), maximal (saturation) response ($\Delta C_{max}/C_0$), adsorption equilibrium constant and partial pressure of the analyte, respectively. v and v_{max} are represented as normalized response (%) for accurate comparison between different devices as the C_0 varies in each device due to the differences in the dielectric properties of composite films. The fitting was carried out on the average response by devices with different MOF loadings in the polymer matrix (Fig. S5 (page 135)). The obtained parameters are listed in the Table 1, showing that there is a good agreement with the experimental data in all the polymer-MOF coatings ($R^2 \geq$ 0.978).

*Table 1: Langmuir parameters (K_{eq} and v_{max} ($=\Delta C_{max}/C_0$)) for sensor devices coated with Matrimid® layer containing different amounts of NH_2-MIL-53(Al) as function of different vapor concentrations of methanol. *Sensor devices with 100 wt.% MOF showed deviation from Langmuir behavior at low concentrations (1000-2000 ppm) of methanol*

MOF loading (wt.%)	K_{eq} (bar^{-1})	v_{max} (%)	R^2
0	120	4.8	0.996
20	132	8.9	0.999
40	241	12.9	0.995
50	368	6.1	0.978
60	264	7.1	0.998
*100**	860	4.4	0.947

The 100 wt.% coating devices showed a slight deviation from Langmuir behaviour at low methanol concentrations. This can be attributed to additional structural changes in the NH_2-MIL-53(Al) due to initial adsorption of methanol in freely accessible MOF,[38] which resulted in a significant transition in the response between 1000 and 2000 ppm of methanol in device coated with 100 wt.% MOF (Figure 4b).

Further, the equilibrium affinity constants of experiments using devices with a NH_2-MIL-53(Al) (100%) and Matrimid® coating show that both MOF and polymer have an intrinsic affinity towards methanol. MOF particles showed higher affinity as expected due to the hydrophilic nature of the pores and the high porosity. All composite-coated devices showed the affinity constants in-between these two extreme cases with 40 wt.% showing the highest saturation response with an increase of 12.9%, compared to 4.8% and 4.4% for the only Matrimid® (0 wt.%) and only-MOF (100 wt.%) coated devices, respectively.

Based on these saturation responses and mass fraction of MOF, the contribution of MOF towards the response ($\nu_{max,MOF}$) was calculated in these composite films. It was assumed that the adsorption contributions of both Matrimid® and NH_2-MIL-53(Al) are additive in the total response. Expectedly, the calculated contribution of MOF towards the relative response doubled over increase in loading from 20 wt.% ($\nu_{max,MOF} = 5.0\%$) to 40 wt.% ($\nu_{max,MOF} = 10.0\ \%$). From both cases, the saturation response (ν_{max}) of the MOF-only (100 wt.%) device was calculated to be 25% which is nearly 6 times higher than the observed response (4.4%). Such decrease in ν_{max} (also in case of devices with 50 wt.% and 60 wt.% MOF (Table 1)) can be associated, as discussed above, to the decreased adhesion in these highly-loaded devices.

In summary, from this comparative study it can be concluded that 40 wt.% showed highest capacitive change and there was a transition from polymer driven adsorption to a MOF-driven adsorption at MOF loadings above 40 wt.%.

5.3.3 Sensitivity and Selectivity

Next to sensor responses and kinetics, another important parameter to consider for a sensor device is its cross-sensitivity towards different analytes. The 40 wt.% MOF-modified sensor devices were exposed to water, methanol, ethanol and 2-propanol to study its cross-sensitivity (Figs. 5, S6 (page 136)). Upon exposure to 20000 ppm of each analyte, the equilibrium response decreased and $\tau_{0.5}$ increased with increase of molecular size of the analyte (water, methanol, ethanol, 2-propanol) (Fig. 5a). A 10-fold and 70-fold increase in $\tau_{0.5}$ for ethanol and 2-propanol, respectively, compared to methanol

and water clearly indicates slower uptakes, likely due to a slower diffusion through the Matrimid® polymer composite[29]. In order to correlate with the analyte concentration, the equilibrium responses were normalized to the relative dielectric constant ($\varepsilon_{r,\,Water} = 78.3$, $\varepsilon_{r,\,Methanol} = 32.7$, $\varepsilon_{r,\,Ethanol} = 24.5$, $\varepsilon_{r,\,Propanol} = 18$, Fig. 5b) Now, it can be seen that the uptake of analytes by the MOF-Matrimid® composite sensor increases from water to methanol to ethanol. This is well in line with the known higher affinity of Matrimid® towards ethanol and methanol than water[44-45]. Even though there was a higher affinity towards 2-propanol, it still resulted in a decrease in the normalized response. This decrease along with the slower uptake can be attributed to the size-exclusion effect of the Matrimid® as previously observed, with no response towards 2-propanol in only Matrimid® based sensors[29]. In contrast, the presence of a higher amount of MOF in the polymer matrix allowed some adsorption of this analyte.

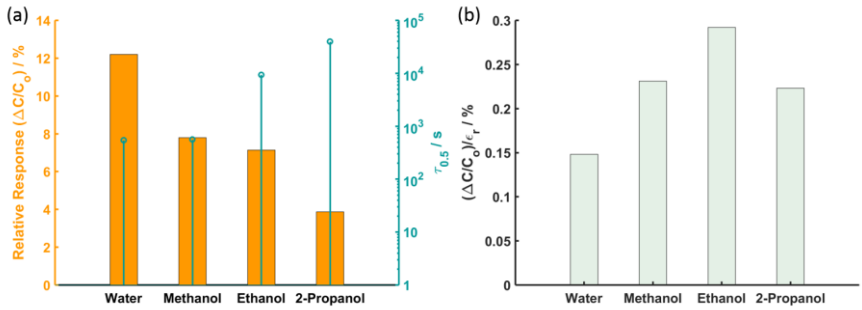

Figure 5. *(a) Relative response of a sensor device containing 40 wt.% MOF in a Matrimid® layer upon exposure to 20000 ppm of different analytes (orange) and the corresponding half-time for saturation, $\tau_{0.5}$ (blue). (b) Relative response normalized to relative dielectric constant.*

Moreover, with significant responses and similar $\tau_{0.5}$ towards water and methanol, these sensor devices show sensitivity towards both analytes. In order to study this cross-sensitivity further, the behavior of devices with different MOF loadings was compared on exposure to 1000 ppm of water and methanol at 28°C (Figure 6a).

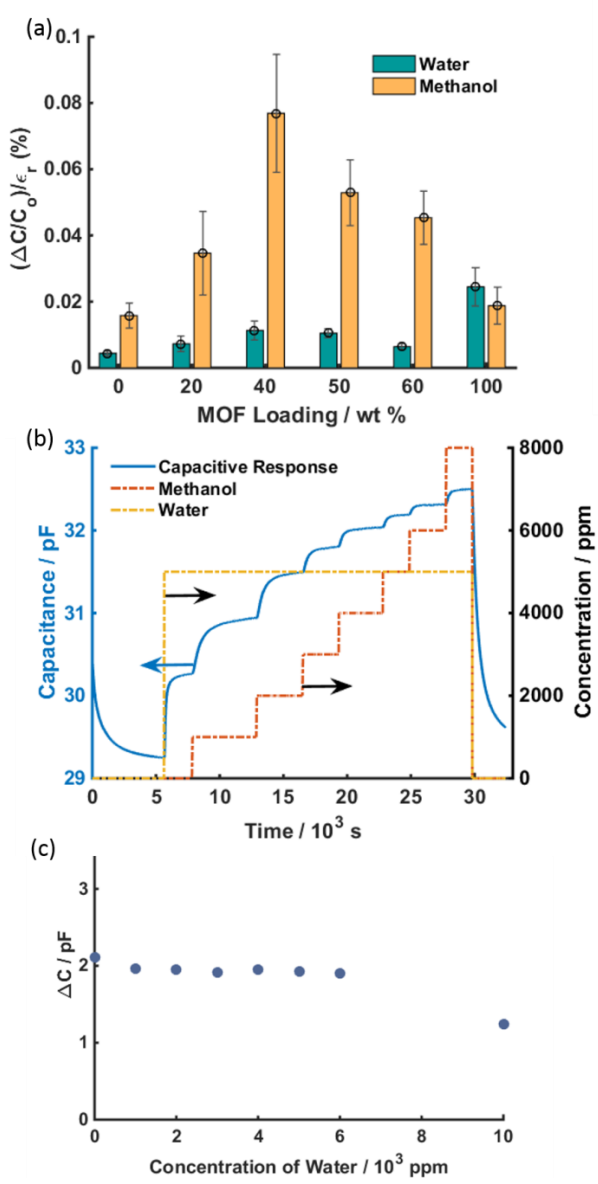

Figure 6*. (a) Relative response normalised to relative dielectric constant of sensor devices containing different loadings of NH_2-MIL-53(Al) in a Matrimid® layer upon exposure to 1000 ppm of water and methanol. (b) The sensor response of a device with 40 wt.% NH_2-MIL-53(Al) in Matrimid® towards different concentrations (1000 to 8000 ppm in steps of 1000 ppm, indicated by right axis) of methanol in the presence of 5000*

ppm of water. (c)) The capacitance change of a device with 40 wt.% NH_2-MIL-53(Al) in Matrimid® for a fixed methanol concentration of 5000 ppm at *different water concentrations. Temperature is always 28˚C.*

The change in the response was normalized with respect to the relative dielectric constant of the analyte to make interpretation in terms of change of concentrations in the affinity layer possible.

Figure 6a shows that sensors with only Matrimid® as affinity layer exhibit a higher response towards methanol than to water. This is due to the intrinsic higher affinity of Matrimid® towards methanol compared to water[29, 44]. For sensors having an affinity layer of pure MOF, the response towards water is slightly larger than towards methanol. This is attributed to the slightly hydrophilic nature of the MOF (certainly the MOF is more hydrophilic than the polymer). For the MOF-Matrimid® composite systems, the uptake of water and methanol is always higher than for the pure Matrimid® system, with a maximum response (uptake) observed around 40 wt.% MOF.

In Figure 6b the sensor response to varying methanol concentrations in the range of 1000 to 8000 ppm in steps of 1000 ppm in the presence of a fixed water concentration of 5000 ppm is presented. The sensor has an affinity layer containing 40 wt.% MOF in Matrimid®. The response is similar (after correction for the fixed contribution of water to the capacitive response) to the response observed in the absence of water (see Fig. 4a), indicating that there is no competition for water and methanol affinity, and both analytes do behave as if the other component is not present.

In Figure 6c the sensor response to a fixed concentration of methanol of 5000 ppm is shown in the presence of varying water concentrations (0-10000 ppm). In the investigated range till 6000 ppm of water, it is observed that the capacitance increase is independent to the water concentration, confirming that methanol and water adsorption is non-competitive. Deviation was observed at still higher water concentration, where condensation in the pores is likely to occur.

5.3.4 Effect of Temperature on Sensor Response

To get further insight into the sensing process, adsorption studies of methanol and water were also carried out at different temperatures. A sensor device with 40 wt.% NH_2-MIL-53(Al) in Matrimid® and a MOF-free Matrimid® (0 wt.%) were exposed to 1000 ppm of methanol and 1000 ppm of water at different temperatures (301-323 K). The effect of the operating temperature on sensing performance is clearly visible in Figure 7 and S7 (page 137), showing an Arrhenius plot of the relative response (v) (defined as $\Delta C/C_0$) versus the absolute temperature (T). At higher temperatures, the capacitance change ΔC decreases, indicating that less analyte is adsorbed by the affinity layer, as expected.

For the classical Arrhenius behavior applies:

$$v = v_0 e^{-\frac{\Delta H}{RT}} \qquad (3)$$

where v_0 and R indicate a pre-exponential constant and the gas constant, respectively. ΔH represents the difference in activation energy of adsorption and desorption and v represents the relative change in the capacitance ($\Delta C/C_0$). From the exponential fit of the Arrhenius plot (Fig. 7), we have deduced the value of ΔH.

The enthalpy of adsorption (ΔH) for devices with only Matrimid®-coated devices was calculated to be -44.4 ± 3.0 kJ/mol and -42.6 ± 9.2 kJ/mol for methanol and water, respectively. A negative value of ΔH confirms the exothermic nature of the process, with similar affinities for methanol and water. For devices with 40 wt.% MOF loading, the enthalpy of adsorption (ΔH) was found to be -44.1 ± 1.3 kJ/mol and -30.9 ± 1.5 kJ/mol for methanol and water, respectively clearly indicating higher affinity for methanol than for water.

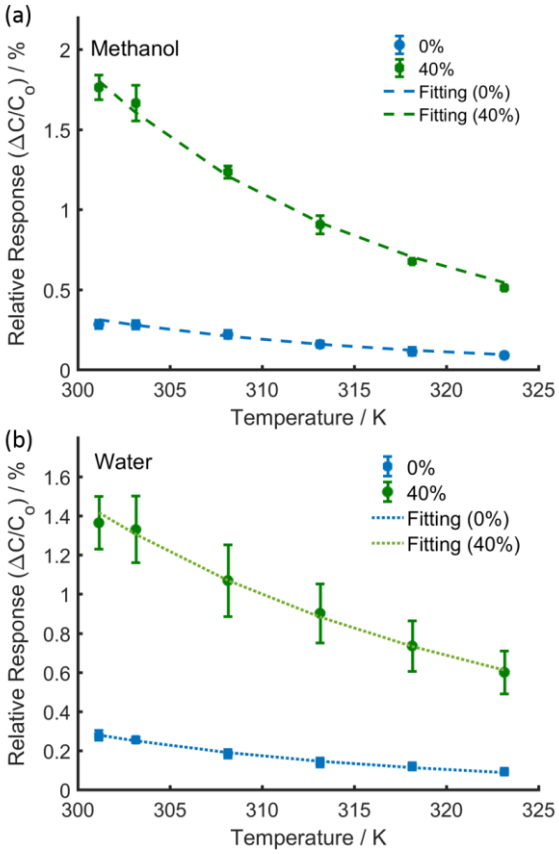

Figure 7. *Arrhenius relation between the relative response ($v = \Delta C/C_0$) and the temperature (T) for devices coated with 40 wt.%-NH_2-MIL-53(Al) in Matrimid® (green) and Matrimid® only (blue) on exposure to 1000 ppm of methanol (a) and 1000 ppm of water (b) at different temperatures.*

Moreover, ΔH has become less favorable by the addition of MOF to the polymer for adsorption of water. We tentatively suggest that these differences in ΔH can be related to polymer rigidification near the MOF interface[42-43]. This rigidification would result in a stronger barrier towards water than towards (the less polar) methanol.

5.4. Conclusions

In this study, we have investigated affinity layers composed of varying amounts of NH_2-MIL-53(Al) MOF mixed in a Matrimid® polymer and deposited on top of meander-patterned aluminium electrodes for capacitive sensing in the presence different analytes in the gas phase. As analytes, we have investigated water, methanol, ethanol and 2-propanol. The capacitive response towards methanol and water was enhanced by the incorporation of the MOFs in the polymeric matrix. The optimum composition was found at ~40 wt. % of MOF, showing an up to five-fold increase in equilibrium response for 1000 ppm of methanol compared with only Matrimid® coated devices. The response time also increased with increase in MOF concentration (up-to 40 wt.%), which is attributed to polymer rigidification near the MOF-polymer interface. Devices containing ≥ 50 wt.% MOF in Matrimid® resulted in brittle and cracked films. The equilibrium response and response time decreased in these devices compared to devices with 40 wt.% MOF and became closer to the equilibrium response and response time shown by a polymer-free MOF-coated sensor device. The decrease in the response behavior was attributed to the poor adhesion. Quantitative analysis of the sensor devices indicated Langmuir behavior showing a maximum affinity (K_{eq} = 860 bar^{-1}) for the polymer-free MOF coated devices. The affinity of all composite devices was found to be in-between those of 100% MOF and 100% Matrimid-coated devices, with the 40 wt.% devices showing a maximum saturation response. Cross-sensitivity studies showed the ability of the devices to kinetically distinguish between alcohols and water. This is based on the molecular size of the analyte resulting in a ~70 times increased $\tau_{0.5}$ for 2-propanol for the 40 wt.%-MOF-polymer sensor compared to methanol and water. Sensing studies with mixtures of water and methanol indicated that both molecules have independent contributions. For water this additive effect to the detection of methanol holds up to concentrations of 6000 ppm. The temperature dependency of the sensor devices showed an Arrhenius-type behavior with a stronger methanol adsorption than water adsorption, confirming a higher affinity towards methanol. With differences in response sensitivity and kinetics for devices coated with affinity layers with different MOF-polymer ratios, quantitative fingerprinting of various analytes is at reach by utilizing

sensor arrays with different MOF-polymer fractions and types at different operational temperatures.

References

[1] Y.-F. Sun, S.-B. Liu, F.-L. Meng, J.-Y. Liu, Z. Jin, L.-T. Kong, J.-H. Liu, *Sensors* **2012**, *12*, 2610.

[2] D. J. Wales, J. Grand, V. P. Ting, R. D. Burke, K. J. Edler, C. R. Bowen, S. Mintova, A. D. Burrows, *Chemical Society Reviews* **2015**, *44*, 4290-4321.

[3] X. Liu, S. Cheng, H. Liu, S. Hu, D. Zhang, H. Ning, *Sensors* **2012**, *12*, 9635.

[4] D. Jariwala, V. K. Sangwan, L. J. Lauhon, T. J. Marks, M. C. Hersam, *Chemical Society Reviews* **2013**, *42*, 2824-2860.

[5] J. Bai, B. Zhou, *Chemical Reviews* **2014**, *114*, 10131-10176.

[6] H. Bai, G. Shi, *Sensors* **2007**, *7*, 267.

[7] R. A. Potyrailo, C. Surman, N. Nagraj, A. Burns, *Chemical Reviews* **2011**, *111*, 7315-7354.

[8] D. R. Miller, S. A. Akbar, P. A. Morris, *Sensors and Actuators B: Chemical* **2014**, *204*, 250-272.

[9] R. Gosangi, R. Gutierrez-Osuna, *Sensors and Actuators B: Chemical* **2013**, *185*, 201-210.

[10] L. E. Kreno, K. Leong, O. K. Farha, M. Allendorf, R. P. Van Duyne, J. T. Hupp, *Chemical Reviews* **2012**, *112*, 1105-1125.

[11] A. U. Czaja, N. Trukhan, U. Muller, *Chemical Society Reviews* **2009**, *38*, 1284-1293.

[12] H. Furukawa, K. E. Cordova, M. O'Keeffe, O. M. Yaghi, *Science* **2013**, *341*.

[13] P. Falcaro, R. Ricco, C. M. Doherty, K. Liang, A. J. Hill, M. J. Styles, *Chemical Society Reviews* **2014**, *43*, 5513-5560.

[14] J. A. Mason, M. Veenstra, J. R. Long, *Chemical Science* **2014**, *5*, 32-51.

[15] V. Stavila, A. A. Talin, M. D. Allendorf, *Chemical Society Reviews* **2014**, *43*, 5994-6010.

[16] Z. Hu, B. J. Deibert, J. Li, *Chemical Society Reviews* **2014**, *43*, 5815-5840.

[17] O. Shekhah, J. Liu, R. A. Fischer, C. Woll, *Chemical Society Reviews* **2011**, *40*, 1081-1106.

[18] C. Sapsanis, H. Omran, V. Chernikova, O. Shekhah, Y. Belmabkhout, U. Buttner, M. Eddaoudi, K. Salama, *Sensors* **2015**, *15*, 18153.

[19] M. G. Campbell, D. Sheberla, S. F. Liu, T. M. Swager, M. Dincă, *Angewandte Chemie International Edition* **2015**, *54*, 4349-4352.

[20] S. Achmann, G. Hagen, J. Kita, I. Malkowsky, C. Kiener, R. Moos, *Sensors* **2009**, *9*, 1574.

[21] B. Seoane, J. Coronas, I. Gascon, M. E. Benavides, O. Karvan, J. Caro, F. Kapteijn, J. Gascon, *Chemical Society Reviews* **2015**, *44*, 2421-2454.

[22] A. Sabetghadam, B. Seoane, D. Keskin, N. Duim, T. Rodenas, S. Shahid, S. Sorribas, C. L. Guillouzer, G. Clet, C. Tellez, M. Daturi, J. Coronas, F. Kapteijn, J. Gascon, *Advanced Functional Materials* **2016**, *26*, 3154-3163.

[23] S. Shahid, K. Nijmeijer, S. Nehache, I. Vankelecom, A. Deratani, D. Quemener, *Journal of Membrane Science* **2015**, *492*, 21-31.

[24] H. J. Salavagione, A. M. Diez-Pascual, E. Lazaro, S. Vera, M. A. Gomez-Fatou, *Journal of Materials Chemistry A* **2014**, *2*, 14289-14328.

[25] D. W. Hatchett, M. Josowicz, *Chemical Reviews* **2008**, *108*, 746-769.

[26] S. Wang, Y. Kang, L. Wang, H. Zhang, Y. Wang, Y. Wang, *Sensors and Actuators B: Chemical* **2013**, *182*, 467-481.

[27] G. Harsányi, *Sensor Review* **2000**, *20*, 98-105.

[28] W. J. Lau, A. F. Ismail, N. Misdan, M. A. Kassim, *Desalination* **2012**, *287*, 190-199.

[29] S. Sachdeva, D. Soccol, D. J. Gravesteijn, F. Kapteijn, E. J. R. Sudhölter, J. Gascon, L. C. P. M. de Smet, *ACS Sensors* **2016**, *1*, 1188-1192.

[30] C. A. Scholes, W. X. Tao, G. W. Stevens, S. E. Kentish, *Journal of Applied Polymer Science* **2010**, *117*, 2284-2289.

[31] T. Rodenas, M. van Dalen, P. Serra-Crespo, F. Kapteijn, J. Gascon, *Microporous and Mesoporous Materials* **2014**, *192*, 35-42.

[32] S. Couck, J. F. M. Denayer, G. V. Baron, T. Rémy, J. Gascon, F. Kapteijn, *Journal of the American Chemical Society* **2009**, *131*, 6326-6327.

[33] B. Zornoza, C. Tellez, J. Coronas, J. Gascon, F. Kapteijn, *Microporous and Mesoporous Materials* **2013**, *166*, 67-78.

[34] Z.-M. Dang, C.-W. Nan, D. Xie, Y.-H. Zhang, S. C. Tjong, *Applied Physics Letters* **2004**, *85*, 97-99.

[35] R. Igreja, C. J. Dias, *Sensors and Actuators A: Physical* **2004**, *112*, 291-301.

[36] R. Igreja, C. J. Dias, *Sensors and Actuators B: Chemical* **2006**, *115*, 69-78.

[37] P. Van Gerwen, W. Laureyn, W. Laureys, G. Huyberechts, M. Op De Beeck, K. Baert, J. Suls, W. Sansen, P. Jacobs, L. Hermans, R. Mertens, *Sensors and Actuators B: Chemical* **1998**, *49*, 73-80.

[38] P. Serra-Crespo, E. Gobechiya, E. V. Ramos-Fernandez, J. Juan-Alcañiz, A. Martinez-Joaristi, E. Stavitski, C. E. A. Kirschhock, J. A. Martens, F. Kapteijn, J. Gascon, *Langmuir* **2012**, *28*, 12916-12922.

[39] C. L. Yaws, *The Yaws handbook of vapor pressure: Antoine coefficients*, Gulf Professional Publishing, **2015**.

[40] G. W. Thomson, *Chemical Reviews* **1946**, *38*, 1-39.

[41] M. Minelli, G. Cocchi, L. Ansaloni, M. G. Baschetti, M. G. De Angelis, F. Doghieri, *Industrial & Engineering Chemistry Research* **2013**, *52*, 8936-8945.

[42] T. T. Moore, W. J. Koros, *Journal of Molecular Structure* **2005**, *739*, 87-98.

[43] P. Burmann, B. Zornoza, C. Téllez, J. Coronas, *Chemical Engineering Science* **2014**, *107*, 66-75.

[44] A. F. M. Barton, *Chemical Reviews* **1975**, *75*, 731-753.

[45] L. Y. Jiang, H. Chen, Y.-C. Jean, T.-S. Chung, *AIChE Journal* **2009**, *55*, 75-86.

Gas Phase Sensing of Alcohols by Metal Organic Framework – Polymer Composite Materials

Supporting Information

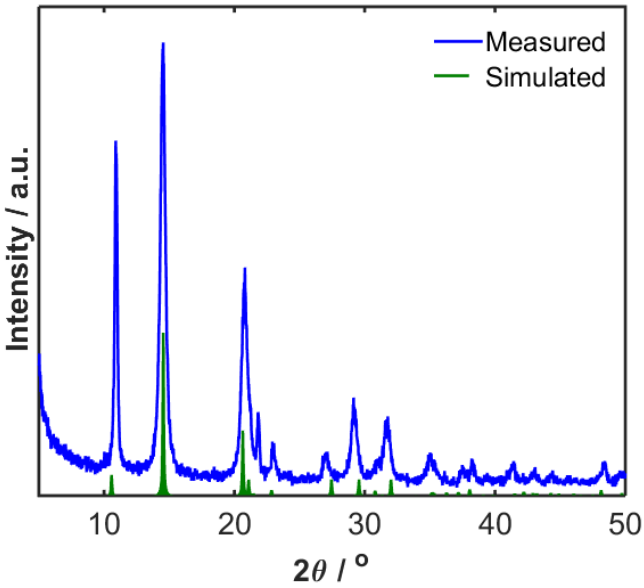

Figure S1*. Experimental and simulated X-ray Diffraction pattern of the as-synthesised NH_2-MIL-53(Al)*

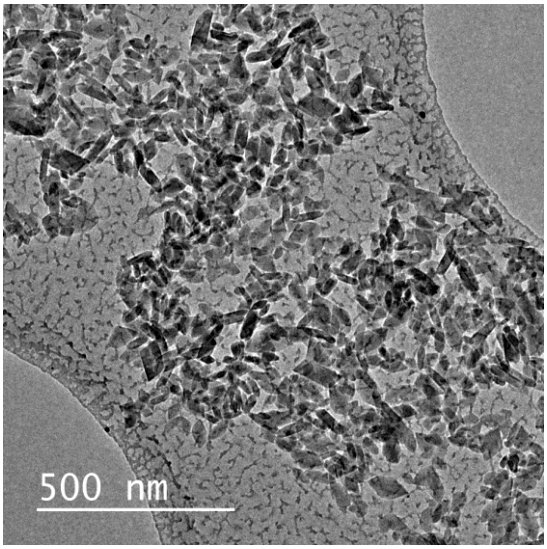

Figure S2. *TEM micrograph of the NH_2-MIL-53 (Al) nanoparticles.*

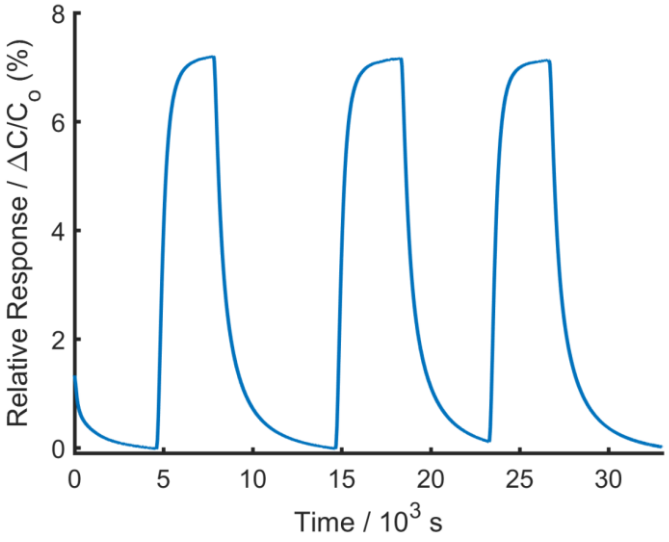

Figure S3. *Reversibility of the sensor response for MOF-polymer sensor device (40 wt.%) over repeated exposure to 5000 ppm of methanol at 28°C*

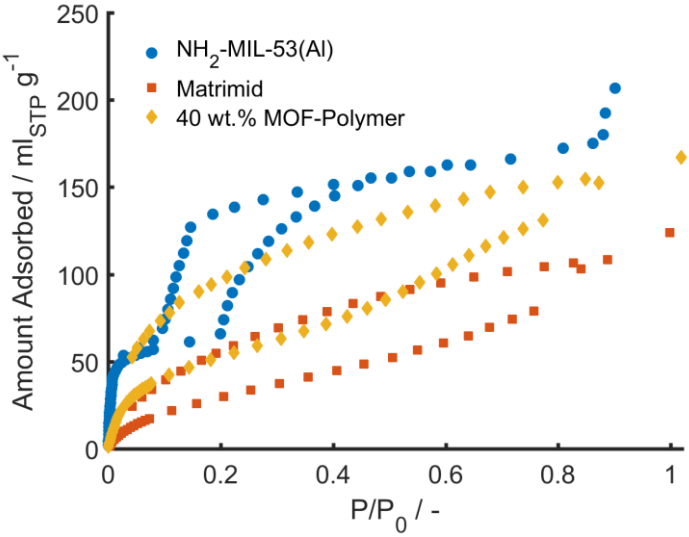

Figure S4. *Methanol Adsorption isotherm for NH_2-MIL-53(Al), Matrimid® and mixed matrix membrane containing 40 wt.% NH_2-MIL-53(Al) in Matrimid® at 25°C.*

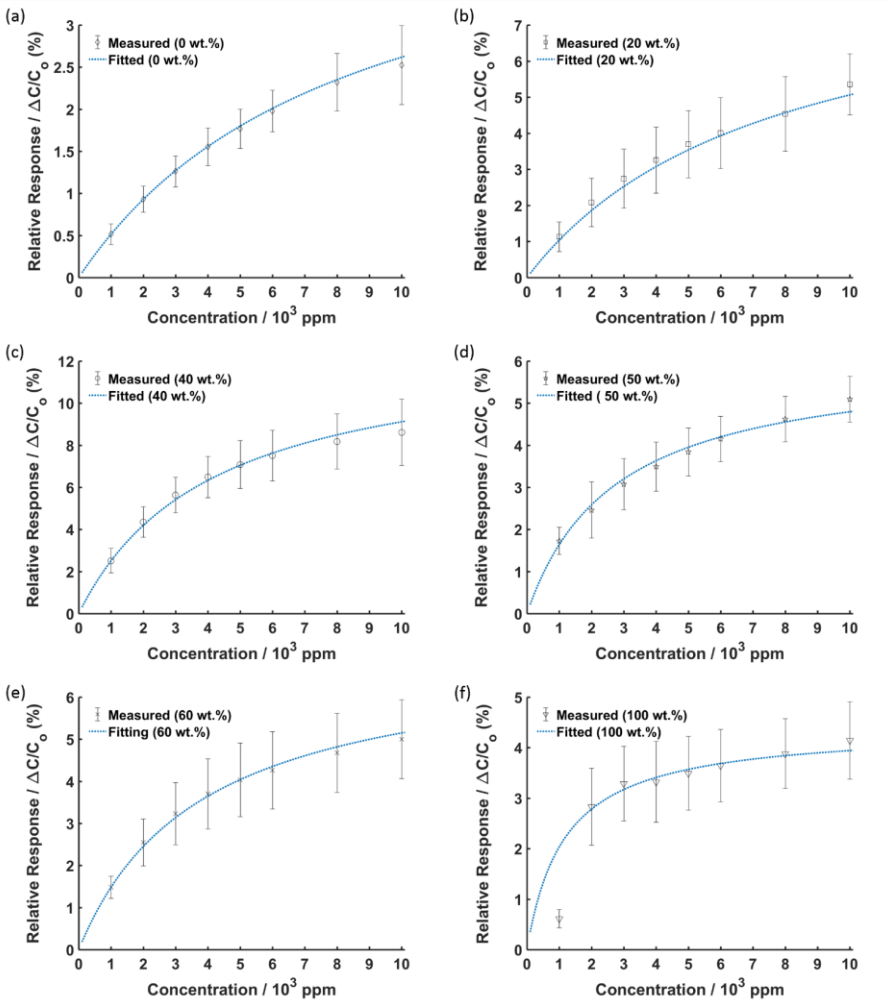

Figure S5. *Langmuir fitting (line) on the sensor response (symbols) towards varying concentrations of methanol for devices with 0 wt.% (a), 20 wt.% (b), 40 wt.% (c), 50 wt.% (d), 60 wt.% (e) and 100 wt.% (f) of NH_2-MIL-53(Al) in Matrimid®.*

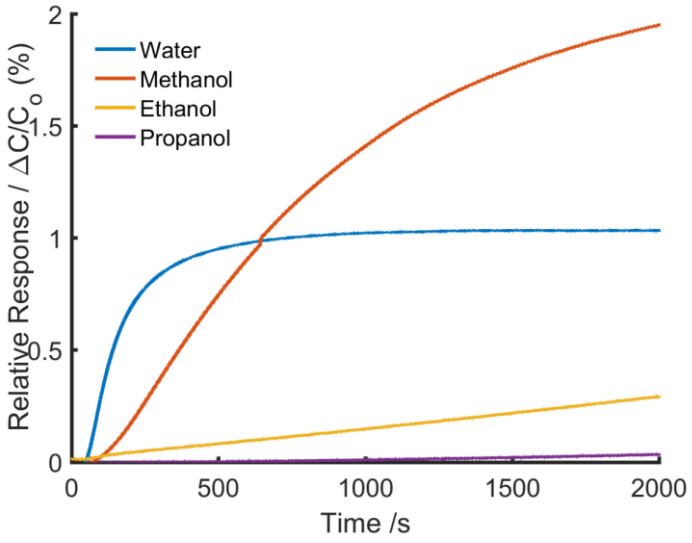

Figure S6. *Cross-sensitivity study of the device with 40 wt.% NH_2-MIL-53(Al)-Matrimid® towards 1000 ppm of water, methanol, ethanol and 2-propanol.*

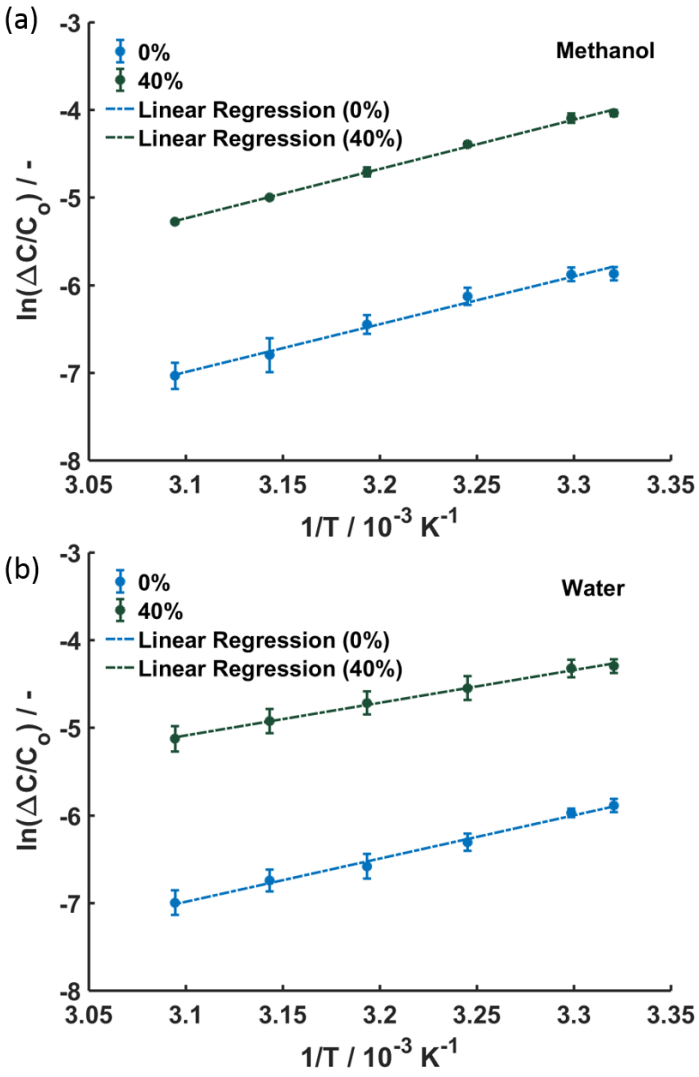

Figure S7. *Linearized Arrhenius relation between the natural logarithm of the relative response ($v = \Delta C/C_0$) and 1/T for devices coated with 40 wt.%-NH_2-MIL-53(Al) in Matrimid® (green) and Matrimid® only (blue) on exposure to 1000 ppm of methanol (a) and 1000 ppm of water (b) at different temperatures.*

Chapter 6

Summary and Outlook

6.1. Summary

This thesis describes a study on gas-phase sensing using capacitive transducers coated with selective affinity layers containing Metal-Organic Frameworks (MOFs). Gas sensing plays an important role in several industrial applications, medical diagnostics and environment monitoring. In order to improve the sensitivity and selectivity of existing sensor devices, MOF-based affinity layers can be potential candidates due to their selective and tunable nature. The capacitive transducers detect changes in the dielectric properties of the affinity layers as a result of interactions with the analyte. Transducers used in this study belong to the class of planar electrodes having a geometry as either interdigitated electrodes (Chapter 3) or as meander-patterned electrodes (Chapters 4 and 5). The precise geometry of these transducers determines the electrical field strength through the affinity layer, which, in turn, affects the sensitivity of the device. Such planar configurations of the transducer have certain advantages like ease of fabrication and performing the measurements. However, parasitic contributions from the supporting substrate reduce the sensitivity. Besides the transducer geometry, thermodynamics and kinetics of the interaction between the analyte and affinity layer also contribute to the sensitivity and selectivity of the sensor devices.

MOFs, being porous solid materials with tunable structural and functional properties, add gas sensitivity and selectivity when integrated with the transducer devices. The fabrication of such MOF-based affinity layers in this study was achieved following two different approaches: (i) *in-situ* electrochemical synthesis (Chapters 2 and 3) and (ii) deposition of MOF-polymer composites (Chapters 4 and 5).

Firstly, electrochemical synthesis was considered as a good approach for the surface growth of MOFs (Chapter 2). Copper-based MOFs were chosen because they show a high nucleation rate. Both CuBTC and CuTATB were synthesized having a benzene 1,3,5-tricarboxylic acid (H_3BTC) and 4,4',4''-s-triazine-2,4,6-triyl-tribenzoic acid (H_3TATB) organic linker, respectively. Differences in their morphology and adsorption properties as bulk powder

and surface-grown material (on flat Cu plates and Cu meshes) were observed for CuTATB. CuBTC on the other hand showed similar properties and morphology for surface-grown and bulk material. These differences between CuTATB and CuBTC originate from some interpenetration of the relatively long linker (H_3TATB), present in CuTATB, in the bulk material as deduced by structural refinement studies. For the surface-grown CuTATB, this interpenetration was less present. The smaller linker present in CuBTC does not allow such interpenetration to happen.

In Chapter 3, the electrochemical synthesis of MOFs over custom-fabricated interdigitated electrodes (IDEs) was successfully demonstrated for CuBTC. IDEs used in this study consisted of 100 finger electrodes having a width (W) and a gap (G) of both 50 µm. Capacitive sensing studies of these CuBTC-coated devices in the presence of methanol vapor (concentrations varying between 1000-8000 ppm) showed sensitive and reversible responses. The observed response times of 120-150 s indicated a diffusion-limited kinetics for the methanol affinity. Responses to equilibrium followed a Langmuir adsorption behavior (K_e = 174.8 bar^{-1}). These responses could be very well simulated by applying finite-element analysis methods. From the simulations, the relative dielectric constant of the CuBTC layer changed from ~1.5 to ~2.7 upon increasing the methanol vapor concentration from 0 to 8000 ppm. Preliminary sensing studies with CuTATB demonstrated also the versatility of this approach.

Another method for MOF integration on capacitive transducers makes use of mixed matrix membranes (Chapter 4). Such membranes are widely studied in gas separation. Composite mixtures of NH_2-MIL-53(Al) MOFs in Matrimid® polymers were chosen because of their good mutual compatibility and good performance in gas separation studies. The mixed matrix membranes were deposited on meander-patterned planar electrodes, having a width, W=0.52 µm and gap, G=1 µm. In comparison with the IDEs described earlier (Chapter 3), the current small dimensions and large electrode area (~2.1 mm^2) contribute to enhanced sensitivity.

MOF-polymer composite films containing 20 wt.% NH_2-MIL-53(Al) in Matrimid® deposited on these planar electrodes showed a reversible

capacitive response towards methanol vapor. Sensitivity of these devices was increased two-fold compared to MOF-free Matrimid® affinity layers. This was attributed to the additional adsorption by the presence of MOFs.

In Chapter 5, further investigation of NH_2-MIL-53(Al)-Matrimid®-based composite films is described for gas-phase sensing for a range of MOF-polymer mixtures (0-100 wt.% of MOF). For methanol vapor sensing, the maximal capacitive response was found for a 40 wt.% MOF composition. At this composition, the response was 5 times higher compared to pure Matrimid®. For 20 wt.% MOF composition, the observed increase was a factor of two. For MOF loadings >40%, the sensitivity was reduced. This was related to the brittleness of the composite polymer layer and the presence of cracks, which resulted in reduced adhesion and increased contact resistance. The response time showed a transition from polymer-limited to MOF-limited uptake. Upon increasing the MOF loadings to 40 wt.% the rate of methanol uptake reduced, due to rigidification of the polymer near the polymer-MOF interface. This rigidification comes from a fast solvent evaporation during the composite films preparation and results in a decrease of the free volume near the MOF interface, hence reducing the permeability to methanol.

For loadings ≥50 wt.% the response time becomes smaller because in that situation some MOF particles are accessible directly. Cross-sensitivity studies with water, methanol, ethanol and 2-propanol vapors clearly exhibited a selectivity, which can be attributed to the polymeric layer, promoting a higher uptake towards the smaller-sized water and methanol. Up to water vapor concentrations of 6000 ppm, the adsorption of water and methanol did not compete.

6.2. Outlook

MOFs as selective component in chemical sensors measuring the change of electrical capacitance upon binding certain analytes from the gas phase offer challenging possibilities for selective, sensitive and quantitative detection of a range of compounds by tuning their functional and morphological properties. MOFs can be *in-situ* synthesized and deposited in pure form

(CuBTC) on the capacitance transducer or can be deposited mixed with a suitable polymer (NH_2-MIL-53(Al) in Matrimid®), as has been successfully demonstrated in this study.

For the system with the pure (polymer-free) deposited MOFs, the porous structure is directly in contact with the environment to be sensed. Application of directly electrochemically grown MOF structures on the metal electrode surfaces, as we have studied in Chapter 3, offers fabrication methods which can easily be integrated with procedures to make the structured electrodes. This method can be easily extended to other electrode structures, to other metals and other organic linkers to tune the affinity properties and the overall detection sensitivity to the desired specifications.

Instead of using pure MOFs, these porous solids can also be mixed with suitable polymers, and the composite polymer can be deposited as the selective affinity layer on the capacitance transducer. The combination of MOF with polymer alters the overall affinity properties as we have demonstrated in Chapter 4 and 5.

Given the large number of MOFs and different polymers available, the use of such composite polymeric films extends the possibilities even further. For the latter system, useful knowledge can be obtained from the investigated mixed matrix membranes for selective gas separations, for the design of sensitive and selective chemical sensors. A wide range of well-developed deposition techniques are available, like spin coating, dip coating, and inkjet printing.

Functionalization of an array of (interdigitated) electrodes with different MOFs and different combinations of MOF-polymer composites allow the development of highly accurate chemical sensors of which the output signals are interpreted correlatively for qualitative and quantitative analysis. Mathematical algorithms and statistical approaches such as Principle Component Analysis (PCA) and Linear Discriminant Analysis (LDA) can be utilized for analyzing such complex data. If the adhesion of certain MOF-polymer composite is poor, adhesion promotors like silylating agents, might give the solution of such problems.

In this study, only chemical sensors for gas-phase applications have been investigated. It is challenging to develop chemical sensors for precise analysis in solution phase: detection of ions and/or volatile organic components (VOCs) in aqueous solution, but also the detection of specific analytes in non-aqueous solutions. In such situations, the stability of the applied MOFs becomes an important issue, especially in the aqueous phase. For the solution-phase chemical sensors, the adhesion of the affinity layer becomes even more important compared to the gas phase chemical sensors, since the solvent might concentrate at the transducer-affinity layer interface and delaminate that layer.

The geometry of the electrode structure is of influence on its detection sensitivities. Reduction of the gap size G and increase in the electrode width W, the number of finger electrodes and the overall electrode area will have a positive effect. These dimensions also dictate the optimal thickness of the affinity layer, which, as a general rule, should be thicker than or equal to the sum of the width (W) and the gap (G) dimensions to make sure that the electrical field lines are almost completely embedded by the affinity layer. On the other hand, too thick selector layers make the chemical sensor response time large. A challenge for future research is to reduce the parasitic contribution of the supporting substrate.

Finally, considering the complete system of measuring chamber/environment, affinity layer, transducer, and electronic read-out, it can be said that the accuracy we have obtained by using a HP4284A LCR Meter was 0.1 fF. On integration of our chemical sensors with CMOS compatible read-out systems, the accuracy can be improved by a factor of 1000. In conclusion, it can be said that the future of chemical sensors as described in this thesis has just begun.

Samenvatting

Gassensoren spelen een belangrijke rol in diverse industriële toepassingen, in medische diagnostiek en in milieuonderzoek. De gevoeligheid en selectiviteit van bestaande gassensoren laat echter vaak te wensen over. Een oplossing voor dit probleem is te vinden in het vervaardigen van sensoren op basis van *Metal-Organic-Frameworks* (MOFs), vooral interessant vanwege de hoge selectiviteit en de vele verschillende toepassingsmogelijkheden. Dit proefschrift handelt over de detectie van componenten (analieten) in de gasfase door middel van gecoate *capacitive transducers* waarvan de selectieve affiniteitslagen zijn voorzien van MOFs. Door veranderingen in de diëlektrische eigenschappen van deze affiniteitslagen bij interactie met een gas kunnen middels dergelijke sensoren componenten worden gedetecteerd. De *transducers* welke in dit proefschrift worden beschreven, behoren tot de klasse van de vlakke elektrodes, namelijk geïnterdigiteerde (z.g. vinger- of kam-) elektrodes (Hoofdstuk 3) en meandervormige elektrodes (Hoofdstuk 4 en 5). De precieze geometrie van deze elektroden bepaalt de sterkte van het elektrische veld door de affiniteitslagen en daarmee ook de gevoeligheid van de sensor. Een vlakke geometrie geeft voordelen wat betreft de fabricage en het uitvoeren van de metingen. Echter, parasitaire bijdragen van het onderliggende substraat kunnen de gevoeligheid reduceren. Naast de geometrie van de elektroden spelen ook de thermodynamica en de kinetiek van de component-affiniteitslaag interactie een grote rol in de gevoeligheid en selectiviteit van de sensor.

Metal-Organic-Frameworks zijn poreuze vaste stoffen waarvan de structurele en functionele eigenschappen kunnen worden aangepast. Door MOFs en transducers te combineren, kunnen sensoren met een zeer hoge gevoeligheid en selectiviteit worden verkregen. In deze studie zijn twee verschillende fabricageroutes gevolgd met betrekking tot de MOF-affiniteitslagen, namelijk i) in-situ elektrochemische synthese (Hoofdstukken 2 en 3) en ii) depositie van MOF-polymeer composieten (Hoofdstukken 4 en 5).

Elektrochemische synthese is overwogen als een goede methode voor het coaten van affiniteitslagen met MOFs (Hoofdstuk 2). In deze studie zijn

twee koper-bevattende MOFs (CuBTC en CuTATB) gebruikt vanwege hun hoge kiemvormingssnelheid. De synthese van deze MOFs is uitgevoerd middels respectievelijk, benzeen 1,3,5-tricarbonzuur (H_3BTC) en 4,4',4''-s-triazine-2,4,6-triyl-tribenzoezuur (H_3TATB) als organische *linkers*. Verschillen met betrekking tot de morfologie en de adsorptie-eigenschappen tussen beide MOFs in poedervorm en als coating op vlakke koperen gaasjes konden alleen worden waargenomen voor CuTATB. Middels *structural refinement* studies kon worden aangetoond dat de verschillen tussen CuTATB en CuBTC veroorzaakt worden door de interpenetratie (ook wel vervlechting) van de relatief lange organische linkers (H_3TATB) zoals gebruikt bij de synthese van CuTATB in poedervorm. Bij de oppervlaktecoating van CuTATB bleek deze interpenetratie minder aanwezig.

Hoofdstuk 3 handelt over de elektrochemische synthese van CuBTC-MOFs op geïnterdigiteerde elektroden (IDEs). De hier gebruikte IDEs zijn opgebouwd uit 100 vingerelektroden met een gelijke breedte en afstand tussen de elektroden (elk 50 μm). De studies in dit hoofdstuk laten zien dat deze sensoren een gevoelige en reversibele respons geven in contact met methanoldamp (1000-8000 ppm) met responstijden tussen 120 en 150 s. Deze waarden zijn indicatief voor een diffusie-gelimiteerde kinetiek met betrekking tot de methanolaffiniteit van de sensor. De sensorrespons verloopt volgens een Langmuir-isotherm (K_e = 174.8 bar^{-1}), welke kon worden gesimuleerd middels *finite-element* analysemethoden. Uit deze analyse bleek dat bij een stijgende methanoldampconcentratie (0 tot 8000 ppm) de relatieve diëlektrische constante van de CuBTC-laag toenam van ~1.5 naar ~2.7. Eerste sensor studies met CuTATB tonen de veelzijdigheid van deze aanpak aan.

Hoofdstuk 4 beschrijft een andere veel onderzochte aanpak voor het aanbrengen van MOFs op *capacitive transducers*, namelijk MOF-coatings door middel van *mixed matrix membranen*. In deze studie is gekozen voor

composieten van NH_2-MIL-53(Al) MOFs in Matrimid® polymeren, vanwege de wederzijdse compatibiliteit en goede prestaties in het scheiden van gassen. De mixed matrix membranen zijn aangebracht op meandervormige, platte elektroden (breedte: 0.52 μm, afstand tussen de elektroden: 1 μm). Vergeleken met de IDE zoals beschreven in Hoofdstuk 3 dragen vooral de kleine afmetingen en het grote elektrode-oppervlak (~2.1 mm^2) van dit type sensor bij aan een hogere gevoeligheid. Uit deze studie is gebleken dat een reversibele respons (methanoldamp) kan worden verkregen met 20% (g/g) NH_2-MIL-53(Al) MOFs in Matrimid®. Ten opzichte van methoden waarbij alleen Matrimid® wordt gebruikt, werd voor deze mixed matrix aanpak een tweemaal zo grote gevoeligheid waargenomen. Deze verhoging is toe te schrijven aan het extra adsorberende vermogen door de toegevoegde MOFs.

Hoofdstuk 5 vormt een vervolg op bovenstaande aanpak en beschrijft studies van verschillende verhoudingen MOF/polymeer mengsels (0-100% (g/g)). Ten aanzien van de detectie van methanoldamp blijkt uit deze studies dat een 40% (g/g) NH_2-MIL-53(Al) MOFs in Matrimid® een maximale respons geeft. Deze respons was vijf keer hoger in vergelijking met alleen Matrimid® en twee keer hoger dan de 20% (g/g) MOF-variant. Voor MOF-polymeer mengsels > 40% (g/g) werd een afname in gevoeligheid waargenomen. Dit is te wijten aan de brosheid van deze polymeerlaag en de aanwezigheid van scheurtjes, wat resulteert in een afname in hechting en een toename van de contactweerstand. De responstijd van dit type sensoren laat een overgang zien van een polymeer-gelimiteerde naar een MOF-gelimiteerde respons. Tot een gehalte van 40% (g/g) MOF-polymeer mengsel kon een afname van de methanol opnamesnelheid worden waargenomen. De oorzaak van dit fenomeen ligt in de verstarring van het polymeer nabij de polymeer-MOF overgang. Deze verstarring is het gevolg van de snelle verdamping van het oplosmiddel tijdens de bereiding van de mixed matrix membranen en zorgt voor een afname van het vrije volume nabij de polymeer-MOF overgang en dus een afname in permeabiliteit ten aanzien van methanoldamp. Bij gehalten ≥ 50% (g/g) MOF-polymeer mengsel worden de responstijden korter, omdat nu de MOFs bloot komen te liggen en direct toegankelijk zijn.

Cross-gevoeligheid studies met dampen van water, methanol, ethanol en 2-propanol laten duidelijk selectiviteit zien, welke toegeschreven kan worden aan de polymeerlaag die een hogere opname bevordert van kleinere moleculen als water en methanol. Bij waterdampconcentraties tot 6000 ppm is de adsorptie van water en methanol niet competitief.

Samenvattend, MOFs als selectieve laag in chemische sensoren bieden aantrekkelijke mogelijkheden voor de selectieve, gevoelige en kwantitatieve detectie van een aantal verbindingen door precieze afstemming van de structuur, waardoor functionele en morfologische eigenschappen worden afgestemd. Met dit werk is succesvol aangetoond dat MOFs in situ kunnen worden gesynthetiseerd en daarbij in zuivere vorm (CuBTC) worden gedeponeerd op *capacitive transducers*. Ook kunnen MOFs worden gemengd met een geschikt polymeer (NH_2-MIL-53(Al) in Matrimid®) en kan dit mengsel worden aangebracht op de *capacitive transducers*. Beide methoden leiden tot stabiele, gevoelige en reversibele werkende chemische sensoren. Met de grote diversiteit van structureel verschillende MOFs en een breed pallet van beschikbare polymeren, kan gesteld worden dan de toekomst van chemische sensoren, zoals beschreven in dit proefschrift, net is begonnen.

List of Publications

1. **S. Sachdeva**, A. Pustovarenko, E.J.R. Sudhölter, F. Kapteijn, L.C.P.M. de Smet, J. Gascon. *"Control of interpenetration of copper-based MOFs on supported surfaces by electrochemical synthesis"* CrystEnggComm, **2016**, 18(22), 4018-4022 (Inside Front Cover).

2. **S. Sachdeva**, D. Soccol, D.J. Gravesteijn, F. Kapteijn, E.J.R. Sudhölter, J. Gascon, L.C.P.M. de Smet. *"Polymer-Metal Organic Frameworks based capacitive sensors for gas sensing"* ACS Sensors, **2016**, 1(10), 1188–1192.

3. **S. Sachdeva**, M.R. Venkatesh, B. El Mansouri, J. Wei, A. Bossche, F. Kapteijn, G.Q. Zhang, J. Gascon, L.C.P.M. de Smet, E.J.R. Sudhölter. *"Sensitive and Reversible Detection of Methanol and Water Vapor by in-situ Electrochemically Grown CuBTC MOFs on Interdigitated Electrodes"* (submitted, 2017).

4. **S. Sachdeva**, S.J.H. Koper, A. Sabetghadam ,D. Soccol, D.J. Gravesteijn, F. Kapteijn, E.J.R. Sudhölter, J. Gascon, L.C.P.M. de Smet et al. *"Gas Phase Sensing of Alcohols by Metal Organic Framework – Polymer Composite Materials"* (submitted, 2017).

5. L. Chu, A.V. Korobko, A. Cao, **S. Sachdeva**, Z. Liu, L.C.P.M. de Smet, E.J.R. Sudhölter, S.J. Picken, N.A.M. Besseling. *"Mimicking an Atomically-thin 'Vacuum Spacer' to Measure the Hamaker Constant between Graphene Oxide and Silica"* Advanced Materials Interfaces, **2016** (DOI: 10.1002/admi.201600495).

6. P. Ngene, R.J. Westerwaal, **S. Sachdeva**, W. Haije, L.C.P.M. de Smet, B. Dam. *"Polymer-Induced Surface Modifications of Pd-based Thin Films Leading to Improved Kinetics in Hydrogen Sensing and Energy Storage Applications."* Angewandte Chemie, **2014**, 53(45), 12081-12085.

7. V. Seshan, D.H.K. Murthy, A. Castellanos-Gomez, **S. Sachdeva**, H.A. Ahmad, S.D. Janssens, W. Janssen, K. Haenen, H.S.J. van der Zant, E.J.R. Sudhölter, T.J. Savenije, L.C.P.M. de Smet. *"Contactless photoconductance study on undoped and doped nanocrystalline diamond films"* ACS Applied Materials & Interfaces, **2014,** 6(14), 11368-11375.

8. P.Á. Szilágyi, E. Callini, A. Anastasopol, C. Kwakernaak, **S. Sachdeva**, R. van de Krol, H. Geerlings, A. Borgschulte, A. Züttel, B. Dam. *"Probing hydrogen spillover in Pd@MIL-101(Cr) with a focus on hydrogen chemisorption"* Physical chemistry chemical physics, **2014**. 16(12) 5803-5809.

9. V. Seshan, D. Ullien, A. Castellanos-Gomez, **S. Sachdeva**, D.H.K. Murthy, T.J. Savenije, H.A. Ahmad, T.S. Nunney, S.D. Janssens, K. Haenen, M. Nesládek, H.S.J.v.d. Zant, E.J.R. Sudhölter, L.C.P.M. de Smet. *"Hydrogen termination of CVD diamond films by high-temperature annealing at atmospheric pressure*" The Journal of Chemical Physics*,* **2013**. 138(23), 234707.

Prior to the thesis

10. A. Li, **S. Sachdeva**, J.H. Urbanus, P.J. Punt. *"In-Stream Itaconic Acid Recovery from Aspergillus terreus Fed-batch Fermentation"* Industrial biotechnology, **2013**, 9(3):139-145.

Acknowledgments

This thesis has been a great learning experience for me and efforts of several people have contributed in not only completion of this work but also in my growth as a researcher.

First of all, I would like to thank my supervisors, Ernst, Louis, Jorge and Freek for providing me the opportunity to do this research. Their supervision, regular feedback and thoughtful discussions have really helped in improving the quality of the work. I really appreciate the support and exposure I got from them during the course of these years. Working with them was quite helpful in both improving my technical knowledge and developing the personal skills.

During my PhD research, I worked in close collaboration with people from NXP and EWI, TU Delft. I would like to thanks Dirk Gravesteijn and Dimitri Soccol for providing me the transducer devices. Thank you, Dimitri for answering my endless queries about the devices and discussions of the results. I would also like to thank Manjunath and Jia Wei from EWI for fabricating additional devices for me.

Being part of two groups, Organic Materials and Interfaces (OMI) and Catalysis Engineering (CE), I got the opportunity to interact with quite a lot of people. Such discussions with the colleagues within ChemE has really broadened my knowledge and provided me a friendly environment at the

workplace. I am thankful to all my former and current friends and colleagues in ChemE. Thank you Venkatesh, Aldo, Daniela, Anping, Marleen, Laura, Lukasz, Naveen, Sander, Rajeev, Stijn, Pierre, Nick, Mohammad, Hamid, Sneha, Judith, Liangyong, Zhen, Arun, Sipeng for the lovely time at OMI. Thank you Anping for listening to all my stories. Thank you Wolter, Marcel and Klaas for your guidance and discussions during last years. Sander, you were a good student. It was fun working together with you. Also, I would like to thank my colleagues from CE: Maria, Tania, Alla, Beatriz, Alexey, Maxim, Abrar, Anastasiya, Sonia, Eduardo, Anahid, Dmitrii, Tim, Vijay, Xiaohui, Pablo, Jara, Yixiao, Emmanuel, Meixia, Canan, Lide, Alma, Martijn, Maarten, Rupali, Jana, Mallesh, Rob. It was great to share experiences with you all even though I was missing many times. It is difficult to be in 2 offices at same time.

I would like to thank all the technical and support staff who have helped me throughout my PhD. A special thanks to Astrid, Marian, Karin, Caroline and Els for answering all my questions and quickly sorting all the administrative problems. Also, I would like to thank Duco for his help in the lab, gas sensing setup and SEM. A special thanks to Piet Droppert for dielectric spectroscopy experiments and discussions. Thank you, Ben for your help with XRD. I am sure dealing with small amount of my materials was quite challenging at times. I would like to thank Willy as well for always incorporating all my special requests for gas adsorption. I also acknowledge the support I received from Bart van der Linden, Harrie Jansma, Ruben Abellon, Bart Boshuizen, Lars van der Mee and John Suijkerbuijk. I also appreciate all the members of the gas team of ChemE especially Erwin Jansen for taking care of timely arrangement of gas cylinders for my measurements. Thank you.

Delft has been an important part of my life and a lot of people have made it wonderful during my stay here during my Master's and PhD. Thank you the Busy Pencils team: Shreyas and Gunjan for awesome time, nature trips especially cold ones, lot of discussions and support during difficult times. Thank you Lalit, Purvil, Rajat, Bhaskar, Trinath for being great housemates. Each one of you have taught me something and I cherish the time I shared with you guys and also you Rupali and Mohini. Bhuvana,

Brhamesh, Amit, even though you guys are far in India, thanks for caring for me. Also, thank you Soumya for everything you did for me. Also, a special thanks to you Vasu. Maulik, Kartik, Emma, Karolis, Durgesh, Ashish, Roman, Marco, Shaurya, Kai, Manas, Hrushikesh, Sandeep, Nishchay, Wuyuan, Caroline, Florian, Prashant, Peter, Sudeep, Aditya, Vaishnavi, Abhay, Murthy, Thanks for sharing good time in ChemE. I would also like to thank Deepak bhai, Sushil, Sriram, Ajith, Aditya TT, Choka, Ashish, Prashad, Ron, Shreyas, JK, Prashant, Aarthi, Nadeem. Thank you Juhi for all the inquiries about me from Sheffield.

Thank you, Krishna bhai. You have been a great inspiration and support. Your dedication and helpful nature is just commendable. Together with you, Venkatesh, Murthy and Abrar have helped me a lot in the initial years of my PhD. I really appreciate it.

I have also been lucky to enjoy good support from my old friends as well. Thank you Kshitiz, Akshay, Prateek, Ashish, Ritesh for the support when I needed the most. Thank you Jolly bhai, Manas for accompanying my journey to Netherlands and being great friends.

This thesis would not have been possible without the support of my family. More than my own efforts, this thesis is a result of hard work and sacrifices of my father and mother. Papa, I know you would have been so happy and proud seeing this completed. Thank you, Mom for everything you did for me. I am sorry for the endless wait you had to go through. Also, my brother, Piyush, all the unconditional support and trust I get from you, is really appreciated. Thank you for taking care of everything else when it was needed the most.

Finally, I would also like to thank all other people who has contributed either positively or negatively in my PhD. My current social, personal and scientific development is a result of all these small or big contributions.

Sumit Sachdeva

March 2017

Biography

Sumit Sachdeva was born in New Delhi (India) on December 5. He completed his Bachelor's degree (B.Tech) in Biotechnology from VIT University (India) in 2008. In 2009, he joined Delft University of Technology (The Netherlands) for Master's degree and graduated with a degree in Biochemical Engineering in 2011. During his Masters, he carried out the internship at TNO (Delft and Zeist) and the Master's thesis at Biocatalysis and Organic Chemistry group at TU Delft. In 2012, he joined the Department of Chemical Engineering, TU Delft as a Ph.D. researcher to investigate Metal-Organic Frameworks as potential candidate for gas-phase capacitive sensing.